00 EPXX0055

ÉCOLE POLYTECHNIQUE
BIBLIOTHÈQUE CENTRALE
22.08.01
COTE : C1A 120/2000/SOL
b
usuel

THESE

pour obtenir le grade de

DOCTEUR de l'Ecole POLYTECHNIQUE

Spécialité: Physique

ÉCOLE POLYTECHNIQUE
MAGASIN
THÈSES
BIBLIOTHÈQUE CENTRALE

présentée par

Andrei SOLODOV

Titre de la thèse:

Interaction d'impulsions laser ultra-courtes et ultra-intenses avec des plasmas sous denses

soutenue le 21 Décembre 2000 devant le jury composé de:

M. Pierre BERTRAND Président, Rapporteur
M. Patrick MORA
M. Alexander LITVAK
M. Nikolai ANDREEV Rapporteur

ECOLE POLYTECHNIQUE
6007484

153296

Contents

1 Introduction **5**

1.1 Main aspects of interaction of ultra-short ultra-intense laser pulses with underdense plasmas 6

1.2 Laser acceleration of electrons in plasma 9

1.3 Notation about the structure of the thesis 12

2 Description of the code used for numerical simulation of the laser pulse propagation in plasma **14**

2.1 Equation for high-frequency field 15

2.2 Equations for low-frequency (plasma) fields 16

2.3 Equations for electrons 19

2.4 Ions 22

2.5 Notations about the structure of the numerical scheme 22

2.6 Acceleration of test electrons 24

3 Investigation of propagation of ultra-short ultra-intense laser pulses in underdense plasmas **27**

3.1 Photon acceleration in a plasma wake 27

3.1.1 Review of the results obtained before 28

3.1.2 Photon acceleration in the 1D case in a stationary plasma wake 29

3.1.3 Photon acceleration in the 1D case in a nonstationary plasma wake 33

3.1.4 Photon acceleration in the axially symmetrical 2D case 38

3.1.4.1 Analytical estimation of the frequency and phase shift of the probe pulse in the case of small refraction 39

3.1.4.2 Simulation of photon acceleration 42

3.1.5 Discussions 50

3.2 Phase velocity of the plasma wave in the scheme of Self-Modulated Laser Wake-Field Accelerator and electron acceleration. Relativistic self-focusing and self-similar laser pulse structures. 52
3.2.1 Phase velocity of the plasma wave in the scheme of Self-Modulated Laser Wake-Field Accelerator 52
3.2.2 Relativistic channeling. Self-similar laser pulse structures. . . 59
3.3 Ion dynamics in the plasma wake of a short laser pulse 66
3.3.1 Longitudinal ion momentum in the plasma wake 67
3.3.1.1 Basic equations and quasistatic approximation 67
3.3.1.2 The energy and momentum of the plasma wake . . . 70
3.3.1.3 Numerical simulations 73
3.3.1.4 Discussions 74
3.3.2 Transverse ion momentum in the plasma wake 77
3.3.2.1 Analytical description of ion channel formation . . . 77
3.3.2.2 Remarks about numerical simulations using the hydrodynamic code 80
3.3.2.3 Numerical simulation of ion channel formation and plasma wave breaking with the code Wake 81
3.3.2.4 Discussions and conclusion 90

4 Investigation of ultra-short ultra-intense laser pulse propagation in underdense plasma in application to laboratory experiments 92
4.1 Acceleration of injected electrons in a laser wakefield experiment . . . 92
4.2 Propagation of a laser pulse in plasma in the self-modulated regime . 100
4.3 Electron acceleration by the laser field and plasma wave in the experiment on laser-driven electron acceleration in plasma 110

5 Main results of the thesis 118

Bibliography 128

Chapter 1

Introduction

During a few last ten years an essential progress has been achieved in generation of ultra-short ultra-intense laser pulses. This progress is associated with a development of compact solid-state lasers in the middle of 80-th, using chirped pulse amplification technique [1]. The development of such systems is comparable by importance with the invention of lasers themselves. Using the chirped pulse amplification it has become possible to achieve intensities 4 orders of magnitude larger than before. By focussing such pulses with powers up to hundreds of terrawatt and higher, the intensity at the focus is achieved in the range of 10^{18} W/cm^2 and higher and electric field amplitude 10^{10} V/cm and higher. These fields greatly exceed the atomic Coulomb electric fields that results in direct colisionless ionization of atoms without tunneling. For such intensities and laser wavelength of the order of 1 μm (that is characteristic for lasers) plasma electrons oscillate with relativistic velocities. It opens absolutely new regimes of interaction of laser radiation with matter that have not been studied yet. At the same time the pulses have very small duration: from 10 fs to 1 ps. It is less than characteristic time of hydrodynamic motion and plasma thermalisation. Therefore, creation of non-equilibrium plasmas with densities up to solid state densities becomes possible.

These revolutionary achievements in laser pulse generation technology enhanced and in essential degree caused an interest to the questions of their interaction with matter. The combination of high intensities and short pulse duration makes the interaction of such pulses with matter unique.

1.1 Main aspects of interaction of ultra-short ultra-intense laser pulses with underdense plasmas

In the present thesis the problems of interaction of ultra-short ultra-intense laser pulses with underdense plasmas (with densities much less than critical $N_c = m\omega_0^2/4\pi e^2$) are studied. The study of this interaction is necessary for different applications. It was suggested to use relativistically fast plasma waves, excited by short intense laser pulses in underdense plasma for electron acceleration [2, 3]. The advantages of this method of acceleration are associated with a possibility of producing accelerating fields in plasmas a few orders of magnitude larger than presently achievable in conventional radio-frequency linacs. Different applications exist in which a propagation of ultra-short intense laser pulses over large distances in underdense plasmas is required. It includes applications in which interaction with a more dense plasma represents the main interest, if it is preceded by a region of underdense plasma. These applications include nuclear fusion with fast ignition [4], X-ray lasers [5], high order harmonic generation [6], and initiation of nuclear reactions when ultra-short intense laser pulses interact with solid-state target plasma [7, 8].

When short intense laser pulses propagate in underdense plasma the main effects that determine their interaction are generation of relativistically fast plasma waves, Raman scattering, and self-focusing. Ponderomotive forces, associated with longitudinal and transversal gradients of laser pulse intensity, excite electron Langmuir waves in plasma. The amplitude of the excited plasma wave is maximum if the laser pulse duration is of the order of a plasma period. In particular, in the case of a Gaussian laser pulse with an intensity profile $a^2 = a_0^2 \exp(-r^2/\sigma_r^2 - \xi^2/\sigma_z^2)$, $\xi = v_{gr}t - z$ (the pulse group velocity $v_{gr} \approx c$) the amplitude of electron density perturbations in the plasma wake [2, 9, 10]

$$n_1 = \frac{\Delta N}{N_0} = \frac{\sqrt{\pi}}{4} a_0^2 e^{-(r/\sigma_r)^2} \left[1 + \frac{4}{(k_p\sigma_r)^2}\left\{1 - \left(\frac{r}{\sigma_r}\right)^2\right\}\right]\left[k_p\sigma_z e^{-(k_p\sigma_z)^2/4}\right], \quad (1.1)$$

this result is obtained for the case of $a_0^2, n_1 \ll 1$, $a = eA/mc^2$ is the amplitude of the laser field vector potential, N_0 is the value of electron density in plasma. The phase velocity of the plasma wave is close to the pulse group velocity and, consequently, to the speed of light. Due to this fact such plasma waves are called relativistically fast. Relativistically fast plasma waves are also excited in result of forward Raman scattering and Raman scattering at very small angles with respect to the propagation direction of laser pulses with duration larger than a plasma period. We will speak

about this later.

Raman scattering takes place in a plasma with a density less than a quarter of the critical density [11, 12]. In the general case Raman scattering is a decay of the laser field with a frequency and a wave vector (ω_0, $\mathbf{k}_0$) in an electron plasma wave (ω, $\mathbf{k}$) and two daughter waves, Stokes ($\omega_0 - \omega$, $\mathbf{k}_0 - \mathbf{k}$) and anti-Stokes ($\omega_0 + \omega$, $\mathbf{k}_0 + \mathbf{k}$). Typically, $\omega \simeq \omega_p + i\Gamma$, where Γ is the instability rate that is obtained from a linear analysis. If the amplitude of the Stokes wave is much larger than the amplitude of the anti-Stokes one, the process is a 3-wave process; if these amplitudes are comparable one speaks about a 4-waves process. Depending on the direction of the wave vector of the scattered radiation Raman scattering at different angles is considered. One distinguishes forward, backward Raman scattering, Raman scattering at large and small angles with respect to the laser radiation propagation direction.

The particularities of Raman scattering for short ultra-intense laser pulses were studied first in Refs. [12, 13, 14]. In Ref. [12] a dispersion equation was obtained for Raman instability taking into account relativistic effects. Convective and absolute nature of the instability and its particularities for ultra-short pulses were investigated in Ref. [14], where the dependence of the instability rate on the size and duration of the pulse was analyzed. 2 characteristic regimes of Raman instability for short laser pulses were obtained, corresponding to relatively large and small angles of scattering. For the case of a large angle scattering the instability has a convective nature in the frame moving with the pulse and the instability rate increases with the angle of scattering. If a noise level in plasma is high, backward Raman scattering is the strongest. At the same time, if one considers seed perturbations in the spectrum of a Gaussian laser pulse, forward and near-forward scattering becomes more important. The pulses that pass through a limited aperture before their propagation in plasma, contain harmonics in the spectrum with large transversal wave numbers, that can be strongly reinforced in plasma due to the scattering at large angles. Backward Raman scattering and Raman scattering at large angles with respect to the propagation direction lead to the depletion of the backward part of the pulse. At large intensity and pulse duration the forward part of the pulse is scattered as it is shown by numerical simulations [15, 16, 17] and experiment [18].

Forward Raman scattering and Raman scattering at small angles with respect to the direction of the laser pulse propagation correspond to the absolute instability in the frame, connected with the pulse. For relativistically strong laser pulses the rate of this instability increases in the presence of relativistic self-focussing. Due to this instability longitudinal modulation of the pulse intensity develops with a plasma period. Simultaneously a relativistically fast plasma wave is excited with

the phase velocity close to the pulse group velocity and, consequently, to the speed of light. The amplification factor of this instability, which is also called resonant modulational instability (or self-modulation), increases with the pulse amplitude and duration. On the one hand, this instability developing at the times of self-focusing makes impossible a stable propagation of laser pulses with duration longer than a plasma period. On the other hand, relativistically fast plasma waves, excited in result of the instability, can be used for acceleration of charged particles (electrons) to high energies.

From the practical point of view the measurement of the Raman spectrum can be used for obtaining an information about the value of plasma density. If the rate of Raman instability is not too large (less than ω_p) one can observe harmonics in the Raman spectrum with a frequency interval equal to ω_p. If the plasma frequency becomes known, one can determine the plasma density. At the same time at large intensities of the laser radiation an essential broadening of the Raman spectrum is possible. In particular, very wide spectra of the scattered radiation were observed for backward Raman scattering, when it was impossible to determine picks at the combinational frequencies [18, 19].

When Langmuir waves are excited by ultra-intense laser pulses in plasma a loss of their regular structure is very simply achieved [20, 21, 22, 23]. In result of breaking of large amplitude plasma waves, bunches of fast electrons are produced that move at different angles with respect to the laser axis. A part of electrons are trapped by the plasma wave and accelerated to higher energies. As a rule, plasma thermalization has not time to occur on the pulse duration. Correct description of the phenomenon of the plasma wave breaking requires using a kinetic approach.

Relativistic self-focusing of laser beams in plasmas was investigated first in Refs. [24] and [25]. Relativistic increase of electron mass in a high-frequency laser field leads to an increase of the plasma refractive index as:

$$\eta \simeq 1 - (\omega_p^2/2\omega_0^2)\gamma^{-1} \simeq 1 - (\omega_p^2/2\omega_0^2)(1+a^2)^{-1/2}. \tag{1.2}$$

If the amplitude of the laser field (a) has maximum on the beam axis, refraction leads to an additional focusing. The analysis of the paraxial wave equation with a refractive index in the form (1.2) shows, that if the radiation power is larger that a threshold value [26]:

$$P_c[\mathrm{GW}] = 16.2\frac{\omega_0^2}{\omega_p^2},$$

relativistic effects compensate diffraction and self-channeling of the beam is possible. The full analysis of self-focusing requires an account of the ponderomotive effects

as well. Inside the laser beam a transverse ponderomotive force acts on plasma electrons: $F \sim \partial|a|^2/\partial r$, that pushes electrons out from the field region. The redistribution of electron density leads to an increase of the refractive index in the beam region and to an additional focusing. Thus, in general case the self-focusing is relativistic and ponderomotive. According to Refs. [26, 27], the ponderomotive mechanism does not change the value of the critical power P_c, that was found for pure relativistic self-focusing neglecting the transverse redistribution of electron density. Numerical simulations that were done, show also that if the power of the beam is already 10 % larger than critical, a total electron cavitation is observed. In these numerical simulations the profile of the beam at the beginning was Gaussian with a plane transverse phase front. It is evident, that after a total electron cavitation in the region of the field a further growth of the refractive index becomes impossible and a quasi-stationary structure can form, that means self-channeling of the laser beam. Relativistic self-channeling of the laser radiation in plasma was observed in numerous experiments, in particular in Refs. [28, 29, 30, 31, 32, 33, 34]. For powers of the beam $P \gg P_c$ formation of a few (or several) filaments was observed with power in each filament larger than critical.

Finally, a finite duration of the pulse introduces its corrections in the process of self-focusing of relativistically strong laser pulses in underdense plasma. Pulses with a characteristic time of the intensity variation less than a plasma period, excite plasma waves. Linear theory of the plasma wave excitation [9, 10] predicts an increase of electron density at the forward slope of the pulse, if the intensity changes on a time scale of the order of a plasma period. It is related either to the laser pulses with duration of the order of a plasma period or to longer pulses with a sharp forward edge. Electron density increase makes self-focusing of such short pulses or forward edges of longer pulses essentially more difficult or impossible [35, 36, 37]. We will return to this problem of self-focusing of short pulses in our investigation in paragraph 3.2.

1.2 Laser acceleration of electrons in plasma

Currently the most interesting application that stimulates studies of ultra-short ultra-intense laser pulses interaction with underdense plasma is laser-driven electron acceleration in plasma. Electrons can be accelerated to large energies by the longitudinal electric fields of the plasma waves, excited by intense laser pulses in plasma. For the first time this idea of electron acceleration was discussed by Tajima and Dawson in 1978 [2]. The main advantage of this scheme of electron acceleration

with respect to the conventional one, with high-frequency linacs, is associated with a possibility of production of essentially larger accelerating fields in plasmas. In the modern radio-frequency linacs the maximum accelerating fields that are used are limited first of all by a breakdown on the walls of the chamber and do not exceed 100 MV/m. At the same time accelerating (longitudinal) fields of the plasma waves can be 4 orders of magnitude higher – of the order of a nonrelativistic plasma wave breaking field [20] $E_0 = cm\omega_p/e$ or

$$E_0[\mathrm{V/cm}] \simeq 0.96 n_0^{1/2}[\mathrm{cm}^{-3}], \tag{1.3}$$

where $\omega_p = (4\pi n_0 e^2/m)^{1/2}$ is the Langmuir frequency and n_0 is the electron density in plasma.

Up to now several schemes of laser-driven plasma-based electron accelerators were proposed. These schemes differ by the method of the plasma wave excitation. In the Laser Beat-Wave Accelerator two long laser pulses are used with frequencies ω_1 and ω_2. If plasma density is chosen so that $\omega_p = \omega_1 - \omega_2$, resonant plasma wave excitation takes place on the beating of high-frequency fields of these pulses. The main drawback of this scheme is the necessity of the plasma production with a precise value of electron density, that is not a simple technical problem. Resonant excitation of the plasma waves due to beating of the fields of two laser pulses was already investigated both theoretically and experimentally [2, 38, 39, 40, 41, 42, 43, 44, 45].

In another, so-called standard scheme of electron acceleration or Laser Wake-Field Accelerator [2, 9, 10, 35, 36, 46, 47, 48] the plasma wave is excited by a laser pulse with a duration of the order of a plasma period. In this scheme plasma electrons experience two pushes in the longitudinal direction, associated with the ponderomotive force of the laser pulse, with an interval equal approximately to half a plasma period, and a push in the transversal direction. In the case of a laser pulse with a Gaussian shape the dependence of the plasma wave amplitude on the duration and width of the pulse has been given above (1.1). Depending on the width of the pulse the relation between the amplitudes of the longitudinal and transverse components of the electric field in the wake changes: the longitudinal electric field $E_z \sim \exp(-r^2/\sigma_r^2)$ and the transversal field $E_r \sim (2r/k_p\sigma_r^2)\exp(-r^2/\sigma_r^2)$; at the same time the oscillations of the longitudinal and transverse fields are shifted in phase by $\pi/2$. Typically, for electrons accelerated in the plasma wave and deflected from the axis a phase interval exists $k_p|\Delta\xi| = \pi/4$, where they experience longitudinal accelerating and radial focusing forces, simultaneously. In this thesis we report on the first sufficiently reliable observation of electron acceleration in this scheme (see paragraph 4.1 and Refs. [49, 50]).

In one more scheme a fast plasma wave is excited in result of self-modulation instability (SMI) of the laser pulse with a duration larger than a plasma period [11, 12, 14, 15, 51, 52, 53, 54, 55, 56, 57, 58, 59]. In result of SMI longitudinal modulation of the pulse intensity develops with a plasma period. Simultaneously a large amplitude plasma wave is excited that can be used for electron acceleration. The plasma wave excited due to the longitudinal inhomogeneity of the pulse intensity profile acts as an initial seed perturbation for SMI. The SMI rate is high if the pulse power is larger than the critical power for relativistic self-focusing. Many experiments have been already performed on the observation of electron acceleration in this scheme [32, 33, 60, 61, 62, 63, 64].

The last two schemes can be considered as more attractive than the first one which requires using two laser pulses and a production of plasma with the precise value of electron density. At the same time, comparing the last two schemes, one can mention some advantages and disadvantages of both of them. The main advantage of the standard scheme of electron acceleration is a possibility of a better control of the process of the plasma wave excitation and, therefore, electron acceleration. At the same time in the scheme with self-modulation (Self-Modulated Laser Wake-Field Accelerator) one can reach larger amplitudes of the plasma wave due to the resonant character of its excitation by intensity modulations. Also the laser pulse amplitude increases in the modulations due to the effect of self-focusing. In the scheme with self-modulation the plasma wave breaking is reached simpler, in the process of wavebreaking fast electrons are produced that can be trapped by the plasma wave and, therefore, the electron injector can be unnecessary.

The main factors limiting the electron acceleration in these schemes are the following. Diffraction of the laser pulse limits the length of the pulse propagation in plasma and, consequently, the length of the region where the plasma wave is excited, to two Raleigh lengths $z_R = \pi w^2/\lambda$, where w is the pulse width. Relativistic self-channeling allows to overcome diffraction if the pulse power is larger than critical power for relativistic self-focusing, $P > P_c$. Plasma channels allow to overcome diffraction of the laser pulses with $P < P_c$. In the plasma channels with a density minimum on the axis the radial profile of the refractive index is produced with a maximum on the axis. Therefore, diffraction can be compensated by refraction.

Another factor that limits electron acceleration is a loose of the synchronism between an accelerated electron and the plasma wave. In the process of acceleration the electron outruns the plasma wave and comes from the accelerating phase do the decelerating one. Corresponding maximum acceleration length (dephasing length) can be found from simple considerations. It is a length when relativistic electron

(moving with a velocity approximately equal to the speed of light) outruns the plasma wave by a half of its period [2]:

$$l_d = \lambda_p \gamma_{ph}^2. \tag{1.4}$$

Here $\gamma_{ph} = (1 - v_{ph}^2/c^2)^{-1/2}$ is the relativistic factor of the plasma wave. Often in the determination of the dephasing length one substitutes the group velocity of the laser pulse $v_{gr} = c(1 - \omega_p^2/\omega_0^2)^{1/2}$ instead of v_{ph}. In result, one obtains that $\gamma_{ph} = \gamma_g \approx \omega_0/\omega_p$ and

$$l_d \approx \lambda_p(\omega_0/\omega_p)^2 = \lambda_0(\omega_0/\omega_p)^3. \tag{1.5}$$

As we will see in paragraph 3.2, such an approximation is not always acceptable and can lead to incorrect results for the dephasing length and the maximum electron energy in the scheme of Self-Modulated Laser Wake-Field Accelerator. One more factor that limits electron acceleration is depletion of the laser pulse itself due to loosing of its energy during the excitation of the plasma wave.

Recently it has also become known that when an ultra-intense laser pulse propagates in underdense plasma, electrons can be effectively accelerated not only by the plasma wave but also directly by the laser radiation. Such an acceleration takes place at the betatron resonance of electrons oscillating in a relativistic plasma channel produced due to self-focusing of the laser pulse [65, 66, 67]. It is necessary to mention that this mechanism of electron acceleration is not studied completely enough yet. In particular, reliable estimations of the maximum electron energy gain in result of this acceleration are absent. We will return to the discussion of this mechanism in paragraph 4.3. We only note here that this mechanism can play an additional role in the scheme of electron acceleration with self-modulation of the laser pulse. In this scheme laser pulses are used with duration larger than a plasma period, for which self-focusing is effective, and the plasma wave is excited inside the laser pulse. Acceleration of electrons by the plasma wave in this scheme can take place simultaneously with the acceleration directly by the laser field.

1.3 Notation about the structure of the thesis

The present thesis consists of 4 Chapters (besides Introduction). In Chapter 2 the description of the code is presented, that was used for modeling laser pulse propagation in plasma, and its improvements in the process of work on the thesis. The problems of ultra-short ultra-intense laser pulses interaction with plasma are divided in the thesis into two groups and presented in Chapters 3 and 4. Chapter 3 includes investigations of problems that have a general physical and applied

interest and are not related to particular experiments. These are (i) investigation of photon acceleration by a plasma wave excited by a laser pulse; (ii) study of the phase velocity of the plasma wave excited during the laser pulse self-modulation and consequences for electron acceleration; study of self-similar solutions describing self-focusing of short laser pulses in plasma; (iii) study of ion motion during the plasma wave excitation by laser pulses with duration of the order of a plasma period. In Chapter 4 we report on the numerical simulations of 3 experiments on the laser pulse propagation in plasma and electron acceleration in the laboratories Laboratoire pour l'Utilisation des Lasers Intenses (LULI) and Laboratoire d'Optique Appliquee (LOA), Ecole Polytechnique, France. In Chapter 5 we formulate the main results of the thesis.

Chapter 2

Description of the code used for numerical simulation of the laser pulse propagation in plasma

For numerical simulation of the processes, studied in the present thesis we used the code Wake [68, 69, 70]. This code was developed for modeling an ultra-short ultra-intense laser pulse propagation in underdense plasma with $N \ll N_c$. Actually another more strict condition is necessary: $\epsilon \equiv \omega_p/\omega_0 = (N/N_c)^{1/2} \ll 1$. This condition permits to separate two characteristic time scales of the evolution of the electromagnetic field and plasma: the period of the high-frequency field $T_0 \sim \omega_0^{-1}$ and the period of the plasma wave $T_p \sim \omega_p^{-1}$. If the characteristic transversal size of the laser field structure is much larger than the laser wavelength and the time of evolution is much larger than the field period, the electron motion in plasma is oscillations with the frequency of radiation and a low-frequency motion under the influence of the ponderomotive force of the laser field and plasma fields. It is possible to use averaged (ponderomotive) equations for electrons and equations for the low-frequency plasma field for the determination of the low-frequency plasma response.

The plasma response is found in the code using the method of particles, that means that trajectories of particular electrons and ions in plasma are calculated. The method of particles, that represents a kinetic description of the plasma dynamics, has apparent advantages compared with the hydrodynamic description. In the application to the propagation of short laser pulses in plasma it permits to describe correctly such phenomena as plasma wave breaking, fast electrons generation, total electron cavitation in plasma, that can not be described by the hydrodynamic

approach. The fact that the ponderomotive equations for particles are simulated in our code permits to reduce the simulation time comparing to the case when full equations are used, like it is in standard codes using the Particle-in-Cell method. The economy of time and computer resources becomes especially effective in the case of very underdense plasma.

The paraxial wave equation for the complex amplitude of the vector potential including the field dispersion is used for the description of the dynamics of high-frequency field. The code Wake is two-dimensional (2D). The dynamics of the field and plasma can be investigated in axially symmetrical and plane geometry.

2.1 Equation for high-frequency field

We present the vector potential of the high-frequency laser field in the form:

$$\widetilde{\mathbf{A}}_\perp = \hat{\mathbf{A}}_\perp(z, \mathbf{x}_\perp, t) \exp[-ik_0\xi] + \text{c.c.}, \tag{2.1}$$

where $k_0 = \omega_0/c$ and $\xi = ct - z$. It is possible to obtain the following equation for the complex envelope of the vector potential $\hat{\mathbf{A}}_\perp$ if one substitutes (2.1) in the wave equation:

$$\left[\frac{2}{c}\frac{\partial}{\partial t}\left(ik_0 - \frac{\partial}{\partial \xi}\right) + \nabla_\perp^2\right]\hat{\mathbf{A}}_\perp = k_{p0}^2 \frac{\overline{n}}{\overline{\gamma}}\hat{\mathbf{A}}_\perp, \tag{2.2}$$

here $k_{p0} = \omega_{p0}/c$, $n = N/N_0$ is the electron density in plasma normalized to its background value; bar over the quantities, here and below, signifies their averaging over the high-frequency period. The left-hand side of this equation represents the wave operator in new variables $(\mathbf{x}_\perp, \xi, t)$ in which we neglect, however, the term with $(1/c^2)\partial^2/\partial t^2$. The right-hand side includes the plasma response (current density with a coefficient $4\pi/c$) neglecting harmonics generation.

We explain our approximations in this equation in more detail. We assume always in the code, that the characteristic transversal size of the pulse structure is plasma wavelength and, therefore, the characteristic diffraction length (Rayleigh length) is much larger than $(k_0\epsilon)^{-1}$. We also assume that a characteristic distance on which the pulse profile changes due to nonlinear effects is much larger than $(k_0\epsilon)^{-1}$. In particular, this is valid for the nonlinear length of interaction in one-dimensional (1D) theory [48]: $L_{nl} \sim (k_0\epsilon^2)^{-1}$. Thus, as in paraxial approximation we neglect the term with $\partial^2/\partial t^2$ in Eq. (2.2). Although, we keep the term with mixed derivative in the left-hand side in Eq. (2.2). This permits us to take into account dispersion in plasma and not to be limited to the case of a quasi-monochromatic field. Eq. (2.2) is valid for radiation with a wide spectrum, in which, however, harmonics

with $0 < \omega < \omega_p$ must be absent. Keeping the term with mixed derivative is also necessary for an account of the laser pulse energy depletion during the plasma wave excitation. Besides, this term is important for modeling pure forward Raman scattering. Eq. (2.2) as paraxial one assumes, strictly speaking, absence of plane waves in the angular spectrum that propagate at large angles with respect to the longitudinal axis.

Neglecting generation of harmonics of laser radiation is usually also justified in underdense plasma. It is possible to show that this effect in underdense plasma is much weaker than in dense plasma. Harmonics generation becomes noticeable and essential for the description of the laser pulse dynamics only if sharp gradients of the refractive index in underdense plasma appear $|\nabla\eta| \sim \eta/\lambda_0$. It is not typical for underdense plasmas, where the characteristic size of the plasma-field structures, arisen in the result of self-focusing and plasma waves generation, is k_p^{-1}.

We do not precise the polarization of the laser radiation. As we will see below, our algorithm is applicable for an arbitrary polarization of the radiation. In numerical simulations we usually assumed linear polarization, for definiteness.

2.2 Equations for low-frequency (plasma) fields

In this and the next three paragraphs we will limit ourselves by considering the case of plane symmetry, for simplicity. The equations for fields and charged particles in plasma for the case of axial symmetry can be obtained by analogy. Let us suppose that the fields in plasma depend only on the coordinates z and x (longitudinal and transversal coordinates, respectively), the motion of particles along y coordinate is absent. The fact that the characteristic transversal size of the plasma-field structure is plasma wavelength permits to simplify the equations for low-frequency fields and particles essentially. In the first order with respect to the small parameter ϵ longitudinal and transversal components of the quasi-stationary electric field $\overline{E}_z$ and $\overline{E}_x$ and only one component of the quasi-stationary magnetic field $\overline{B}_y$ exist in plasma. In this case Maxwell equation for the excited quasi-stationary fields

$$\nabla \times \overline{\mathbf{B}} = \frac{4\pi}{c}\bar{j} + \frac{1}{c}\frac{\partial \overline{\mathbf{E}}}{\partial t}$$

can be rewritten in the projection on the x and z axis as

$$-\frac{\partial}{\partial z}\overline{B}_y = \frac{4\pi}{c}\bar{j}_x + \frac{1}{c}\frac{\partial \overline{E}_x}{\partial t}, \tag{2.3}$$

$$\frac{\partial}{\partial x}\overline{B}_y = \frac{4\pi}{c}\bar{j}_z + \frac{1}{c}\frac{\partial \overline{E}_z}{\partial t}, \tag{2.4}$$

respectively.

Another important approximation in the code Wake is quasistatic approximation [35, 36]. It supposes that the laser pulse amplitude does not change during the time when the pulse passes its own length. This condition allows us to transfer to the variable $\xi = ct - z$ instead of t and z in the equations for the quasi-stationary fields and particles. Here we neglect also the difference between the pulse group velocity and the velocity of light. On the one hand, apparently, this quasistatic approximation is not valid for electrons, that can be trapped by the plasma wave. On the other hand, neglecting the difference of the pulse group velocity and the velocity of light we, in fact, exclude such electrons from consideration making their trapping by the plasma wave field impossible [20, 21, 71]. Strictly speaking, this approximation is applicable only in the absence of electrons in plasma with longitudinal velocities close to the pulse group velocity, which can be trapped by the plasma wave. As we will note in the next paragraph for such electrons the approximation of ponderomotive force is not valid either. It is necessary to make sure in the absence of such fast electrons each time in the simulations. Eqs. (2.3) and (2.4) can be rewritten in the quasistatic approximation:

$$\frac{\partial}{\partial \xi}\left(\overline{B}_y - \overline{E}_x\right) = \frac{4\pi}{c}\overline{j}_x, \tag{2.5}$$

$$\frac{\partial}{\partial x}\overline{B}_y - \frac{\partial}{\partial \xi}\overline{E}_z = \frac{4\pi}{c}\overline{j}_z. \tag{2.6}$$

Then we introduce scalar and vector potentials for the quasi-stationary fields in the gauge $\nabla_\perp \cdot \overline{\mathbf{A}}_\perp = 0$, we consider this gauge as the most convenient. In this gauge in plane symmetry we can take the transversal component of the vector potential equal to zero and write $\overline{\mathbf{A}} = A\mathbf{e}_z$. Then we have for the components of the quasi-stationary fields:

$$\overline{E}_x = -\frac{\partial \Phi}{\partial x},$$

$$\overline{B}_y = -\frac{\partial A}{\partial x},$$

$$\overline{E}_z = -\frac{\partial \Phi}{\partial z} - \frac{1}{c}\frac{\partial A}{\partial t} = \frac{\partial \Phi}{\partial \xi} - \frac{\partial A}{\partial \xi} = \frac{\partial}{\partial \xi}(\Phi - A).$$

Substituting these expressions in Eqs. (2.5) and (2.6), we obtain the equations for potentials

$$\frac{\partial^2}{\partial \xi \partial x}(\Phi - A) = \frac{4\pi}{c}\overline{j}_x, \tag{2.7}$$

$$-\frac{\partial^2}{\partial x^2}A - \frac{\partial^2}{\partial \xi^2}(\Phi - A) = \frac{4\pi}{c}\overline{j}_z. \tag{2.8}$$

Differentiating Eq. (2.7) with respect to ξ and x, we obtain

$$\frac{\partial^2}{\partial x^2}\frac{\partial^2}{\partial \xi^2}(\Phi - A) = \frac{4\pi}{c}\frac{\partial^2}{\partial x \partial \xi}\bar{j}_x. \tag{2.9}$$

Combining this equation with Eq. (2.8) we get (here $k_p^2 = \omega_p^2/c^2$)

$$\left(\frac{\partial^2}{\partial x^2} - k_p^2\right)\frac{\partial^2}{\partial \xi^2}(\Phi - A) = \frac{4\pi}{c}\frac{\partial^2}{\partial x \partial \xi}\bar{j}_x + k_p^2\frac{\partial^2 A}{\partial x^2} + \frac{4\pi}{c}k_p^2\bar{j}_z. \tag{2.10}$$

We introduce an auxiliary function

$$G = \frac{\partial^2}{\partial \xi^2}(\Phi - A). \tag{2.11}$$

Substituting Eq. (2.11) in Eqs. (2.10) and (2.8), we obtain the equations for functions G and A:

$$\left(\frac{\partial^2}{\partial x^2} - k_p^2\right)G = \frac{4\pi}{c}\frac{\partial^2}{\partial x \partial \xi}\bar{j}_x + k_p^2\frac{\partial^2 A}{\partial x^2} + \frac{4\pi}{c}k_p^2\bar{j}_z, \tag{2.12}$$

$$\frac{\partial^2}{\partial x^2}A = -\left(G + \frac{4\pi}{c}\bar{j}_z\right). \tag{2.13}$$

We introduce then dimensionless quantities:

$$a = \frac{eA}{mc^2}, \qquad \phi = \frac{e\Phi}{mc^2}, \qquad g = \frac{G}{4\pi n_0 e},$$

$$\mathbf{e} = \frac{e\overline{\mathbf{E}}}{m\omega_p c}, \qquad b_y = \frac{e\overline{B}_y}{m\omega_p c}, \qquad \tilde{\mathbf{j}} = \frac{\bar{\mathbf{j}}}{n_0 e c},$$

$$\tilde{\xi} = k_p\xi, \qquad \tilde{x} = k_p x.$$

In this case Eqs. (2.11), (2.12), and (2.13) can be rewritten as

$$g = \frac{\partial^2}{\partial \tilde{\xi}^2}(\phi - a), \tag{2.14}$$

$$\left(\frac{\partial^2}{\partial \tilde{x}^2} - 1\right)g = \frac{\partial^2}{\partial \tilde{x}\partial \tilde{\xi}}\tilde{j}_x + \frac{\partial^2 a}{\partial \tilde{x}^2} + \tilde{j}_z, \tag{2.15}$$

$$\frac{\partial^2}{\partial \tilde{x}^2}a = -\left(g + \tilde{j}_z\right). \tag{2.16}$$

Let us introduce one more function

$$\psi = \phi - a; \tag{2.17}$$

note that the expression for the component of magnetic field has the form

$$b_y = -\frac{\partial a}{\partial \tilde{x}}. \tag{2.18}$$

Then we can rewrite Eqs. (2.14), (2.15), and (2.16) as

$$\frac{\partial^2}{\partial\tilde{\xi}^2}\psi = g, \tag{2.19}$$

$$\left(\frac{\partial^2}{\partial\tilde{x}^2} - 1\right) g = \frac{\partial^2}{\partial\tilde{x}\partial\tilde{\xi}}\tilde{j}_x - \frac{\partial b_y}{\partial\tilde{x}} + \tilde{j}_z, \tag{2.20}$$

$$\frac{\partial}{\partial\tilde{x}} b_y = \left(g + \tilde{j}_z\right). \tag{2.21}$$

In the code Wake we simulate Eqs. (2.19)-(2.21) for b_y and auxiliary functions ψ and g together with equations for particles (to find the quasi-stationary currents). We will speak about the equations for particles in the next paragraph. The components of the quasi-stationary electric field can be expressed through the component of the quasi-stationary magnetic field b_y and function ψ in the following way:

$$e_x = -\frac{\partial}{\partial\tilde{x}}\phi = -\frac{\partial}{\partial\tilde{x}}\psi + b_y, \tag{2.22}$$

$$e_z = \frac{\partial}{\partial\tilde{\xi}}\psi. \tag{2.23}$$

2.3 Equations for electrons

The expression for the averaged Hamiltonian and the low-frequency equation for electrons in plasma have the form (here $q = -e$):

$$\overline{H} = \left[m^2c^4 + \left(\overline{\mathbf{P}} - \frac{q\overline{\mathbf{A}}}{c}\right)^2 c^2 + q^2\overline{\widetilde{\mathbf{A}}^2}\right]^{1/2} + q\Phi, \tag{2.24}$$

$$\frac{d\overline{\mathbf{p}}}{dt} = q\left(\overline{\mathbf{E}} + \frac{\overline{\mathbf{v}}}{c} \times \overline{\mathbf{B}}\right) - \frac{q^2}{2\overline{\gamma}mc^2}\nabla\overline{\widetilde{\mathbf{A}}^2}, \tag{2.25}$$

where

$$\overline{\gamma} = \left(1 + \frac{\overline{p}^2}{m^2c^2} + \frac{q^2}{m^2c^4}\overline{\widetilde{\mathbf{A}}^2}\right)^{1/2} \tag{2.26}$$

and

$$\overline{\mathbf{p}} = \overline{\mathbf{P}} - \frac{q\overline{\mathbf{A}}}{c}. \tag{2.27}$$

The ponderomotive force approximation used in these equations is valid only for electrons with longitudinal velocity that is not high enough: $1 - v_z/c \geq \omega_p/\omega_0$ [68] (it is necessary to make sure in the absence of such fast electrons in the simulations). In the quasistatic approximation the Hamiltonian $\overline{H}$ depends on z and t only through

their combination $\xi = ct - z$. In this case we can obtain from the Hamiltonian equations:

$$\frac{d\overline{P}_z}{dt} = -\frac{\partial \overline{H}}{\partial z} = \frac{\partial \overline{H}}{\partial \xi}, \tag{2.28}$$

$$\frac{d\overline{H}}{dt} = \frac{\partial \overline{H}}{\partial t} = c\frac{\partial \overline{H}}{\partial \xi}. \tag{2.29}$$

Therefore, an integral of motion (quasistatic) exists:

$$\overline{H} - c\overline{P}_z = mc^2 \tag{2.30}$$

or

$$mc^2\overline{\gamma} + q\Phi - c\overline{p}_z - qA = mc^2. \tag{2.31}$$

Let us introduce dimensionless momentum, velocity and time:

$$\tilde{\mathbf{p}} = \frac{\overline{\mathbf{p}}}{mc}, \qquad \beta = \frac{\overline{\mathbf{v}}}{c} = \frac{\tilde{\mathbf{p}}}{\overline{\gamma}}, \qquad \tau = \omega_p t.$$

Then Eqs. (2.25), (2.26), and (2.31) can be rewritten as

$$\frac{d}{d\tau}\tilde{\mathbf{p}} = -\left(\mathbf{e} + \beta \times \mathbf{b}\right) - \frac{1}{2\overline{\gamma}}\widetilde{\nabla}\overline{\tilde{\mathbf{a}}^2}, \tag{2.32}$$

$$\overline{\gamma} = \left(1 + \tilde{\mathbf{p}}^2 + \overline{\tilde{\mathbf{a}}^2}\right)^{1/2}, \tag{2.33}$$

$$\overline{\gamma} - \tilde{p}_z - \psi = 1. \tag{2.34}$$

It is possible to resolve Eqs. (2.33) and (2.34) with respect to $\overline{\gamma}$ and $\tilde{p}_z$:

$$\overline{\gamma} = \frac{1 + \tilde{p}_x^2 + \overline{\tilde{\mathbf{a}}^2} + (1+\psi)^2}{2(1+\psi)}, \tag{2.35}$$

$$\tilde{p}_z = \frac{1 + \tilde{p}_x^2 + \overline{\tilde{\mathbf{a}}^2} - (1+\psi)^2}{2(1+\psi)}. \tag{2.36}$$

Taking into account that

$$\frac{d\xi}{dt} = c - \frac{dz}{dt} = c\left(1 - \frac{\tilde{p}_z}{\overline{\gamma}}\right) = c\frac{1+\psi}{\overline{\gamma}},$$

we can rewrite the x component of Eq. (2.32) taking into account (2.22) as

$$\frac{d\tilde{p}_x}{d\tilde{\xi}} = \frac{1}{1+\psi}\left(\gamma\frac{\partial}{\partial\tilde{x}}\psi - \frac{1}{2}\frac{\partial}{\partial\tilde{x}}\overline{\tilde{\mathbf{a}}^2}\right) - b_y. \tag{2.37}$$

For the determination of the electron motion we can use the x component of Eq. (2.32) in the form (2.37) and the expressions for the electron relativistic factor and longitudinal momentum Eqs. (2.35) and (2.36). These equations are convenient for

the determination of the plasma response using the method of particles. For small ξ (before the laser pulse coming) all electrons move in the reference frame (ξ, x) with the speed of light in the positive direction of the ξ axis. When the laser pulse comes the electron trajectories are determined by the action of the ponderomotive force of the laser pulse and quasi-stationary fields that arise in plasma. Eq. (2.37) determines the evolution of the transversal electron momentum along the coordinate ξ, Eqs. (2.35) and (2.36) determine then the longitudinal momentum and relativistic factor.

Knowledge of the trajectories of particular electrons gives us the information about the currents in plasma. In general case the expression for the electron current density has the form

$$\bar{\mathbf{j}}_e = \sum_k q_k \overline{\mathbf{v}}_k \delta(\mathbf{r} - \overline{\mathbf{r}}_k) = -e \sum_k \overline{\mathbf{v}}_k \delta(\mathbf{r} - \overline{\mathbf{r}}_k),$$

where we sum with respect to all electrons in a unity of volume. Dimensionless current density

$$\tilde{\mathbf{j}}_e = \frac{\bar{\mathbf{j}}_e}{n_0 e c} = -\frac{1}{n_0} \sum_k \beta_k \delta(\mathbf{r} - \overline{\mathbf{r}}_k).$$

In numerical simulations we deal with a limited number of particles, much less than the number of electrons in real plasma. The region of plasma is divided in the transversal direction into cells with a size coinciding with the mesh size Δx of the grid, on which the values of currents and fields are determined in the simulation. The nodes of the grids for different grid functions are located on the boundaries or in the centers of the cells. To find the values of current in the nodes we summarize the contributions of particles in the nearest cells to the current. If initially (at $\xi = 0$) there were n_p particles per each cell, their contributions to the current must by summarized with weights $p = 1/n_p$. Also, each particle spends a time

$$\Delta t = \frac{\Delta \xi}{c - \overline{v}_z} = \frac{\overline{\gamma}}{1 + \psi} \frac{\Delta \xi}{c}$$

in the interval $\Delta\xi$. "Density", associated with each particle equals $p\overline{\gamma}/(1 + \psi)$. In the method Cloud-in-Cell each particle contributes to the currents in the two nearest nodes, proportional to $\delta_k = 1 - |\Delta x_k|/\Delta x$, where $|\Delta x_k|$ are the distances to these nodes. The resulting expression for the current density in the node is:

$$\tilde{\mathbf{j}}_e = -p \sum_k \frac{\delta_k \overline{\gamma_k} \beta_k}{1 + \psi_k} = -p \sum_k \frac{\delta_k \tilde{\mathbf{p}}_k}{1 + \psi_k},$$

where we summarize with respect to the particles that are at a distance less than one mesh size from the node of the grid in the positive and negative direction of the x axis. This current together with ion current (we will speak about it in the next paragraph) we substitute in the equations for low-frequency fields (2.19)-(2.21).

2.4 Ions

Due to the large difference of electron and ion masses ion motion is not essential, as a rule, for the study of a propagation of sufficiently short laser pulses, shorter than a period of ion Langmuir oscillations $2\pi(\omega_{pi})^{-1}$, $\omega_{pi} = (4\pi q_i^2 N_i/m_i)^{1/2}$, here q_i, N_i, and m_i are charge, density and mass of ions, respectively. Really, at radiation intensities of the order of 10^{18} W/cm^2 (and a few orders of magnitude higher) it is possible to neglect the oscillatory motion of ions in the high-frequency laser and quasi-stationary plasma fields due to small amplitudes of oscillations. At the same time the oscillatory motion of electrons in these fields is already relativistic. But ion motion can be important for longer pulses as well as for the study of the plasma wake evolution behind short pulses. Simple estimations show that in the presence of quasi-stationary electric fields in plasma $E \sim m\omega_p c/e$ with a characteristic time of evolution of the order of ω_{pi}^{-1} and larger, an essential redistribution of ion density can occur. Besides, on the times of such an order the modulation instability of electron Langmuir waves in plasma develops. So the ion motion is included in the code "Wake". For the non-relativistic ion motion in the quasistatic approximation it is simple to obtain the following equations:

$$\frac{d\widetilde{p}_{ix}}{d\widetilde{\xi}} = e_x = -\frac{\partial\psi}{\partial\widetilde{x}} + b_y,$$

$$\widetilde{p}_{iz} = \psi,$$

here the dimensionless momentum $\widetilde{\mathbf{p}}_i$ is connected with the dimensional one $\overline{\mathbf{p}}_i$ as $\widetilde{\mathbf{p}}_i = \overline{\mathbf{p}}_i/mc$. The ion contribution to the current density ($\overline{\mathbf{j}}_i$) is taken into account similar to the electron contribution and the total current $\overline{\mathbf{j}} = \overline{\mathbf{j}}_e + \overline{\mathbf{j}}_i$ is substituted in Eqs. (2.19)-(2.21).

2.5 Notations about the structure of the numerical scheme

In the system of equations for high-frequency field, low-frequency fields and particles the explicit dependence on time t is present only in the equation for high-frequency field (2.2). This fact allows us to solve the full system of equations numerically in the following order. At each time step (at the moment t) for the known distribution of the complex amplitude of high-frequency field in space we find the plasma response, solving the equations for low-frequency fields and particles. Then we find a new distribution of the complex amplitude of the high-frequency field at

the next time step (at the moment of time $t + \delta t$). Each moment of time t all the fields are absent and the particles are at rest (in the laboratory frame) at small ξ. This circumstance allows us in the simulations at each time step consequently, in the positive direction of the ξ axis to find the solutions of all the equations for the fields in space (x, ξ) and equations for particles, starting from known values at small ξ.

It is necessary to mention that the equations for the fields must be supplemented by boundary conditions at $x = 0$ and some large $x = x_0$, corresponding to the boundary of the region in which we calculate the fields. At $x = 0$ the boundary conditions come from the transverse symmetry of the problem. At $x = x_0$ for the high-frequency fields the condition of absence of the reflected wave is used that was discussed in Ref. [14]; for the low-frequency fields the condition of their smallness is used. Finally, the particles that intersect the symmetry axis are reflected from it and the particles that leave the interaction region in the transversal direction (first of all, these are electrons) are supposed to be on the boundary $x = x_0$. The last condition, obviously, is an approximation, but it permits, at least, to interrupt the further leaving the interaction region by the particles with the same sign of charge.

For the complete problem statement we must also precise the distribution of the complex amplitude of the laser pulse vector potential in space at the initial moment of time. This distribution depends on the particular problem statement, in particular, in most our simulations we supposed the laser pulse to be Gaussian at the initial moment of time with respect to the longitudinal and transversal coordinates and focused in plasma.

In developing this algorithm we assumed a scheme in which the distribution of high-frequency field in space $(x, \xi = ct - z)$ evolves with time t. One can mention that this algorithm does not change if we consider the evolution of the high-frequency field in space $(x, \tau = t - z/c)$ with coordinate z and the code Wake does not need any modification or rewriting. At the same time, the second problem statement is often more convenient from the point of view of experimental observation, where a measuring device measures usually the characteristics of the processes that take place in a particular place in space and evolve with time.

We did not speak so far about the mechanism of the plasma generation in which the laser pulse propagates, in other words, we considered the plasma as preformed. Although the code contains a part that permits to simulate gas ionization using the ADK formula for tunnel ionization [72, 73]. We will not speak about this part of the code in more detail, referring the persons who are interested to Ref. [70]. We mention only that the simulation of ionization in different gases is possible: in

hydrogen, helium, and argon.

2.6 Acceleration of test electrons

As we discussed in the introduction one of the most interesting applications of short intense laser pulses propagation in underdense plasma is electron acceleration. In the frame of work on this thesis an additional part to the code Wake was developed by the author of the thesis that permits to study acceleration of test electrons in the plasma fields calculated with the code and in the high-frequency fields. In this part of the code the motion of an electron beam is simulated, these electrons are injected in plasma at some moment of time. The electrons are assumed to be non-interacting and they do not change the fields in plasma. The laser pulse is assumed to be axially symmetric and linearly polarized in x direction (z is the longitudinal direction). We remember also that high-frequency field has a small longitudinal component that is important to take into account in the equations for the electrons of the beam.

In the code Wake the equation for the transversal component of the complex envelope of the laser field vector potential (2.1) is simulated. We suppose that the characteristic scale of the transversal structure of the laser pulse is of the order of $(\epsilon k_0)^{-1}$ and larger and the characteristic time scale of the variation is of the order of $(\epsilon^2\omega_0)^{-1}$ and larger. In this case it is possible to write an approximate expression for the longitudinal and transversal components of the high-frequency field in the first order with respect to the parameter ϵ on the basis of the solution of Eq. (2.2) for the transversal component of the vector potential. From the Coulomb gauge condition $\mathrm{div}\widetilde{\mathbf{A}} = 0$ we obtain:

$$\mathrm{div}_\perp \hat{\mathbf{A}}_\perp - \frac{\partial \hat{A}_z}{\partial \xi} + ik_0 \hat{A}_z = 0. \tag{2.38}$$

Taking into account Eq. (2.38) and that $\widetilde{\mathbf{E}} = -\partial\widetilde{\mathbf{A}}/\partial(ct)$, $\widetilde{\mathbf{B}} = \mathrm{rot}\widetilde{\mathbf{A}}$, $\widetilde{\mathbf{A}}$ has x and z components only, it is possible to obtain expressions for the high-frequency fields up to the terms of the first order in ϵ:

$$\widetilde{\mathbf{E}} = \left[\left(i\hat{A}k_0 - \frac{\partial \hat{A}}{\partial \xi}\right)\mathbf{x}_0 - \mathbf{z}_0 \frac{\partial \hat{A}}{\partial x}\right] e^{-ik_0\xi} + c.c., \tag{2.39}$$

$$\widetilde{\mathbf{B}} = \left[\left(i\hat{A}k_0 - \frac{\partial \hat{A}}{\partial \xi}\right)\mathbf{y}_0 - \mathbf{z}_0 \frac{\partial \hat{A}}{\partial y}\right] e^{-ik_0\xi} + c.c., \tag{2.40}$$

where we take into account that $\hat{\mathbf{A}}_\perp = \hat{A}\mathbf{x}_0$.

In the axially symmetric case quasi-stationary fields in plasma have in the first order with respect to the parameter ϵ the following components: electric field has

longitudinal and radial components, $\overline{\mathbf{E}} = \overline{E}_z \mathbf{z}_0 + \overline{E}_r \mathbf{r}_0$, and magnetic field has a component directed along the azimuth $\overline{\mathbf{B}} = \overline{B}_\theta \theta_0$.

For each electron injected in plasma we simulated its motion according to Newton equation:

$$\frac{d\mathbf{p}}{dt} = -e\left(\mathbf{E} + \frac{\mathbf{v}}{c} \times \mathbf{B}\right), \tag{2.41}$$

where $\mathbf{E} = \widetilde{\mathbf{E}} + \overline{\mathbf{E}}$, $\mathbf{B} = \widetilde{\mathbf{B}} + \overline{\mathbf{B}}$. We pass to the dimensionless fields:

$$\tilde{\mathbf{e}}(\mathbf{e}) = \frac{e\widetilde{\mathbf{E}}(\overline{\mathbf{E}})}{m\omega_p c}, \qquad \tilde{\mathbf{b}}(\mathbf{b}) = \frac{e\widetilde{\mathbf{B}}(\overline{\mathbf{B}})}{m\omega_p c},$$

$$\tilde{\mathbf{a}}(\hat{a}, \mathbf{a}) = \frac{e\widetilde{\mathbf{A}}(\hat{A}, \overline{\mathbf{A}})}{mc^2}, \qquad \phi = \frac{e\overline{\Phi}}{mc^2}, \qquad \psi = \phi - a_z.$$

We also introduce dimensionless momentum, electron coordinate, and time:

$$\frac{\mathbf{p}}{mc} \to \mathbf{p} = \gamma\beta, \qquad k_p \mathbf{r} \to \mathbf{r}, \qquad \tau = \omega_p t, \qquad k_p \xi \to \xi.$$

Eq. (2.41) has the following form in coordinates:

$$\frac{dp_x}{d\tau} = \left[\frac{\partial\psi}{\partial r} - (1 - \beta_z)\, b_\theta\right] \frac{x}{r} + q\beta_y \frac{y}{r} - f(1 - \beta_z), \tag{2.42}$$

$$\frac{dp_y}{d\tau} = \left[\frac{\partial\psi}{\partial r} - (1 - \beta_z)\, b_\theta\right] \frac{y}{r} - q\beta_x \frac{y}{r}, \tag{2.43}$$

$$\frac{dp_z}{d\tau} = -\frac{\partial\psi}{\partial\xi} - (\beta_x x + \beta_y y)\frac{b_\theta}{r} + q\frac{x}{r} - \beta_x f, \tag{2.44}$$

where

$$f = \left(\frac{i\hat{a}}{\epsilon} - \frac{\partial\hat{a}}{\partial\xi}\right) e^{-i\xi/\epsilon} + c.c.,$$

$$q = \frac{\partial\hat{a}}{\partial r} e^{-i\xi/\epsilon} + c.c.$$

Eqs. (2.42)-(2.44) were used for the simulation of test electrons motion. It was supposed that all test electrons have the same energy γ at the moment of injection. The following procedure was used to determine their coordinates and velocities at initial moment of time. The coordinates of each test electron were set initially in the focal plane of the beam as if the electrons move freely in the absence of laser and plasma fields. At the same time the focal plane of the beam and the plane of injection may be different, generally speaking. The electron distribution with respect to the transversal coordinate and angle between the velocity vector and the beam axis in the focal plane was assumed to be Gaussian. The probability density that $r_\perp$ is a distance of a particular electron from the beam axis in the focal plane is

$$P(r_\perp) = \frac{1}{\pi\sigma_e^2} \exp\left(-\frac{r_\perp^2}{\sigma_e^2}\right),$$

where $\sigma_e = \langle r_\perp^2 \rangle^{1/2}$ is a root mean square (r. m. s.) value of the position from the beam axis. Similarly, the probability that α is an angle between the velocity vector of a particular electron in the focal plane and the longitudinal axis is

$$P(\alpha) = \frac{1}{\pi \alpha_e^2} \exp\left(-\frac{\alpha^2}{\alpha_e^2}\right),$$

where $\alpha_e = \langle \alpha^2 \rangle^{1/2}$ ($\alpha_e \ll 1$). Both these probabilities are independent. The transversal position and momentum are determined then by two angles $\phi_\perp$ and ϕ_α, that are chosen randomly in the interval of $[0, 2\pi]$,

$$x = r_\perp \cos\phi_\perp,$$

$$y = r_\perp \sin\phi_\perp,$$

$$p_x = p \sin\alpha \cos\phi_\alpha,$$

$$p_y = p \sin\alpha \sin\phi_\alpha,$$

$$p_z = p \cos\alpha,$$

where $p = mc\sqrt{\gamma^2 - 1}$ is the absolute value of the momentum of the particle. As the coordinates of a particular electron are determined in the focal plane of the beam, it is simple to recalculate them to the plane of injection that can be, for instance, a long distance before the focus outside the plasma. One more parameter of the electron beam is its duration, the probability of different longitudinal positions of electrons inside the beam was chosen to be the same.

After the simulation of test electrons motion we determined the variation of different characteristics of the beam. We calculated the electrons energy spectra; maximum electron energy in the result of acceleration, the dependence of the energy on the phase of injection in the plasma wave; change of the space size of the beam and of the angular divergence. To identify the mechanism of acceleration we studied the characteristic electron trajectories. In the investigations that we report in the present thesis we performed numerical simulations of test electron acceleration in paragraphs 3.2, 4.1, and 4.3.

Chapter 3

Investigation of propagation of ultra-short ultra-intense laser pulses in underdense plasmas

3.1 Photon acceleration in a plasma wake

As it is known, the frequency of radiation changes when it propagates in a medium with dielectric properties varying in time. If refractive index in the medium increases the frequency of radiation decreases and when the refractive index decreases the frequency increases. The frequency of radiation increases during gas ionization. Both the frequency of intense radiation that ionizes the gas or the frequency of low-intensity radiation that propagates through the ionization front can be shifted. The theory describing the frequency shift (photon acceleration) in this scheme is already developed (see Ref. [74] and references therein) and laboratory experiments were done. Both the frequency shift of ionizing radiation and of probe pulses propagating through the ionization front (co-propagating or counter-propagating with the ionization front) were observed in experiments [75, 76, 77].

Another scheme of photon acceleration was also proposed – by relativistically fast plasma waves excited by short intense laser pulses in plasma. In this scheme the frequency shift is due to non-stationarity of the refractive index in the plasma wave. Generally speaking, both the frequency of the pulse exciting the plasma wave and the frequency of a probe pulse propagating in the plasma wave can be changed. The frequency of the pulse (ω) exciting the plasma wave down-shifts. It leads from the conservation laws of energy and photons (see, for instance, Ref. [68]): the pulse energy decreases due to the plasma wave excitation, but the number of photons

is conserved; as the energy of photon is $\hbar\omega$ the frequency down-shifts. Another explanation is possible. During the plasma wave excitation either by a laser pulse with duration less than half a plasma period or by a longer laser pulse modulated with a plasma period (either in the Self-Modulated Laser Wake-Field Accelerator or in the Plasma Beat-Wave Accelerator), the laser pulse or its modulations are in the phase of growth of the refractive index in the plasma wave and, consequently, their frequency decreases. When a probe pulse propagates in the plasma wake the frequency shift of different signs can take place, depending on the phase of the plasma wave in which the pulse propagates.

In a narrow sense the frequency shift of the probe pulse is called as photon acceleration (as in the scheme with ionization or in the scheme with a plasma wave). In this thesis we studied the frequency shift of probe pulses in the plasma wave. We considered an intense laser pulse with duration of the order of a half plasma period as the main source of the plasma wave excitation. Our results can be useful for other schemes of plasma wave excitation as well. Everywhere below we will speak about photon acceleration only as a frequency shift of probe laser pulses.

3.1.1 Review of the results obtained before

The possibility of photon acceleration by plasma waves excited by ultra-intense laser pulses was first suggested in 1989 by Wilks *et al.* [78]. They performed one-dimensional (1D) numerical simulation confirming the possibility of photon acceleration and discussed the limits for the acceleration in this scheme. The theory of photon acceleration in a plasma wave in the 1D case was developed by Esarey *et al.* [79], who proposed a simple model describing modification of the laser pulse parameters in this process: frequency, duration, energy. In Refs. [80] and [81] an analogy between ultra-short laser pulse propagation and motion of a charged particle in a plasma wave was discussed. The theory of photon acceleration including the Hamiltonian formalism based on the equations of geometrical optics was developed. The self-sustained interaction of a short laser pulse with a plasma wave was studied in the approximation of a weak relativistic nonlinearity in Ref. [82]. The energy depletion of the plasma wave due to photon Landau damping was found in Ref. [83].

The frequency shift of a short probe pulse propagating in a plasma wave can be used as a plasma diagnostic tool. Because the frequency shift depends on the probe pulse position in the plasma wave (the shifts are of the opposite sign in the regions where the electron density increases or decreases) this allows a simple way of plasma wave profiling: only the "center of mass", or centroid, difference of the probe

pulse power spectra, measured before and after the interaction with the plasma, must be calculated [88]. Although this possibility has been widely discussed, the measurement of the probe pulse frequency shift in experiments and plasma wave profiling in this way has not yet been reported. However, plasma wave profiling has been performed in Refs. [84, 85, 86, 87, 88] by measurement of "dc" phase shift of a probe pulse in the plasma wave. In these experiments a time-domain shift in optical phase of the probe pulse was recorded using frequency-domain interferometry. In this technique multiple temporally separated coherent probe laser pulses are used. The relative phase shift of these pulses is recovered from their frequency domain interference spectra. In the experiments of Refs. [84] and [87] only the dc phase shift was recorded. The longitudinal dependence of the recovered phase responsible for frequency shift was not resolvable because of the small value of the frequency shift and high level of the detector limited phase noise. The method of plasma wave mapping based on frequency-domain interferometry has some advantages over the centroid-based method concerning issues of stray light, leakage of the pump pulse into the probe spectrum (if the spectra are overlapped), and detector defects [88]. On the other hand, this method is complicated by using multiple coherent probe pulses. The practical advantage of the centroid-based method is the simplicity and speed, with which the power spectrum of the probe pulse can be measured.

In this thesis the study of photon acceleration in 1D plasma wave is continued (sections 3.1.2 and 3.1.3). 1D numerical simulations confirm the results of the theory, developed earlier, and show new particularities in dynamics of a probe pulse in the process of its acceleration by the plasma wave. The most attention is given to two-dimensional (2D) axially symmetrical case that was not studied before (section 3.1.4). An analytical formula is obtained describing photon acceleration in the conditions close to the experimental ones. Numerical particle simulations show new particularities of the probe pulse dynamics that have not been discussed and studied yet.

3.1.2 Photon acceleration in the 1D case in a stationary plasma wake

In this section we neglect the plasma wave profile dynamics caused by the evolution of the plasma wave source (laser pulse or electron beam). This can be a reasonable approximation if the time scale for evolution of the plasma wave source is much greater than that for the accelerated laser pulse. Investigating photon acceleration in such a stationary plasma wake can also help us to understand better

the photon dynamics in a realistic nonstationary plasma wake. In our simulations the plasma wave profile is taken to be the instantaneous profile of a plasma wake excited by a short intense laser pulse propagating in plasma. As the phase velocity of the plasma wave we take the group velocity of this pulse in the linear approximation $v_{ph} = c(1 - \omega_{p0}^2/\omega_0^2)^{1/2}$, where $\omega_{p0} = (4\pi e^2 N_0/m)^{1/2}$ is the plasma frequency corresponding to the undisturbed density and ω_0 is the frequency of the pulse.

Ray tracing equations describing the evolution of a wave packet in such a stationary plasma wave predict the photon trajectories similar to the trajectories of charged particles moving in the presence of a plasma wave [80, 81]. These trajectories correspond to trapped and untrapped (moving backward and forward in the plasma wave frame) laser pulses. In the 2D phase space (as the canonical variables one must take a wave number and a coordinate in the plasma wave frame) these trajectories are separated by a separatrix. The frequency of the photon Ω in the plasma wave frame obtained by a Lorentz transformation from the laboratory frame is constant:

$$\gamma_p(\omega - v_{ph}k) = \Omega = \text{const.} \tag{3.1}$$

Here $\gamma_p = (1 - v_{ph}^2/c^2)^{-1/2}$ is the relativistic factor of the plasma wave, and $k = (1 - \omega_p^2(\xi)/\omega^2)^{1/2}\omega/c$ is the photon wave number in the laboratory frame. In writing the last expression for k we have assumed the cold plasma dispersion relation, which is valid for plasma waves with phase velocities much larger than the electron thermal velocity. The plasma frequency $\omega_p = (4\pi e^2 N/m\gamma)^{1/2}$ depends on the coordinate in the plasma wave frame $\xi = v_{ph}t - z$ through both the electron density N and the electron relativistic factor γ. On differentiating Eq. (3.1) with respect to time, and taking into account that the laser pulse in the Wentzel-Kramers-Brillouin (WKB) approximation propagates with its group velocity, we obtain equations describing the evolution of the pulse frequency and coordinate in the plasma wave frame:

$$\begin{aligned} \frac{d\omega}{dt} &= \frac{v_{ph}}{2\omega}\frac{d\omega_p^2}{d\xi}, \\ \frac{d\xi}{dt} &= v_{ph} - c\left(1 - \frac{\omega_p^2}{\omega^2}\right)^{1/2}. \end{aligned} \tag{3.2}$$

The validity of the WKB approximation underlying this approach is limited to the case of small radiation wavelength compared with the space scale of the plasma density inhomogeneity. Further, the laser pulse is supposed to be short in the time and narrow in the frequency domain in order to be characterized by definite values of coordinate and frequency (wave number) and for the effects of the group velocity dispersion to be negligible. In our simulations these conditions

are not always fulfilled leading to some differences in the pulse dynamics from the predictions of Eqs. (3.1) and (3.2). In Figs. 3.1-3.3 we present the results of a simulation where the background plasma density is $N_0 = 1.74 \times 10^{17}$ cm^{-3}. The profile of the plasma wake is shown in Fig. 3.1 (a). This is the instantaneous profile of the wake behind a 0.4 μm laser pulse (for which $\omega_{p_0}/\omega_0 = 0.005$) with a Gaussian temporal profile and a full width at half-maximum in intensity (FWHM) of 30 fs. The maximum amplitude of the vector potential $a_0 = eA_0/mc^2 = 1.8$. We have simulated the dynamics of probe pulses with initial wavelengths of 0.133 μm, 0.2 μm, 1.33 μm and duration of 30 fs (FWHM). The pulses were "loaded" in the first two cases in the minima and in the last case in the maximum of the plasma wave. The averaged frequency of the probe pulse spectrum

$$< \omega >= \frac{\int \omega |E_\omega|^2 d\omega}{\int |E_\omega|^2 d\omega},$$

is shown as a function of the pulse position in the plasma wave frame,

$$< \xi >= \frac{\int \xi |E|^2 d\xi}{\int |E|^2 d\xi},$$

in Fig. 3.1 (b), where we use the dimensionless coordinate $\zeta = (\omega_{p_0}/c) < \xi >= k_p < \xi >$. The averaged frequency is plotted as a function of time in Fig. 3.2, where we use the dimensionless time $\tau = (\omega_{p_0}^3/\omega_0^2)t$. The dotted lines in Fig. 3.1 (b) correspond to the phase space trajectories obtained as solutions to Eqs. (3.1) and (3.2).

The trajectory 2 shown in Fig. 3.1 (b) corresponds to a trapped laser pulse. In Fig. 3.3 the corresponding pulse vector potential profiles and spectral compositions are shown at different times during one oscillation. The other two trajectories correspond to untrapped laser pulses: moving forward and backward (with respect to the direction of the plasma wave propagation) in the plasma wave frame. The difference between the "model" curves [solutions to Eqs. (3.1) and (3.2)] and the results of our direct simulations is caused first of all by the finite length of the pulse (leading to different frequency shifts of the parts of the pulse and to variation of the group velocity through its length) and group velocity dispersion. The untrapped pulse moving backward in the plasma wave frame quickly becomes elongated and the oscillations of the averaged frequency saturate when the pulse length becomes of the order of one plasma wavelength. The trapped pulse broadens when it passes backward at the bottom of the plasma density profile (Fig. 3.3). The central part of the pulse is frequency shifted differently from the front and rear parts and the averaged frequency of the pulse spectrum becomes greater than that predicted by

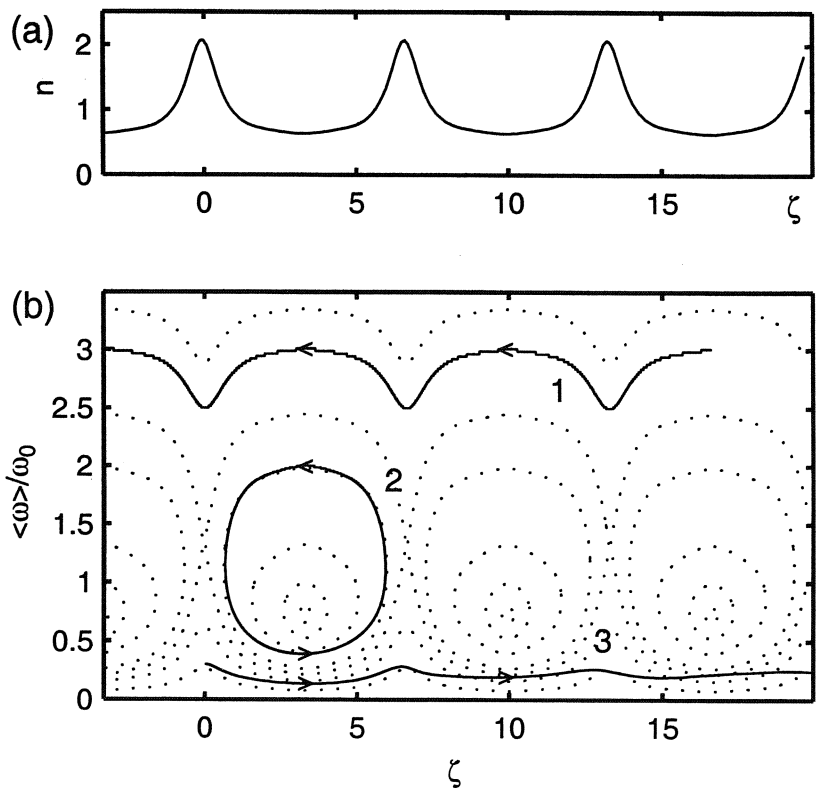

Figure 3.1: Photon acceleration in the 1D case in a stationary plasma wake: (a) electron density in the plasma wave (normalized to its background value), the plasma wave propagates in the $-\zeta$ direction; (b) averaged frequency of the probe pulse spectrum as a function of the pulse position in the plasma wave frame (solid line), and phase space trajectories, obtained as a solution to Eqs. (3.1) and (3.2) (dotted lines); $\zeta = k_p\xi = (\omega_{p0}/c)\xi$, $\tau = (\omega_{p0}^3/\omega_0^2)t$. The parameters of the simulations are given in the text. The indices 1, 2, and 3 correspond to pulses with initial wavelengths 0.133 μm, 0.2 μm, and 1.33 μm respectively.

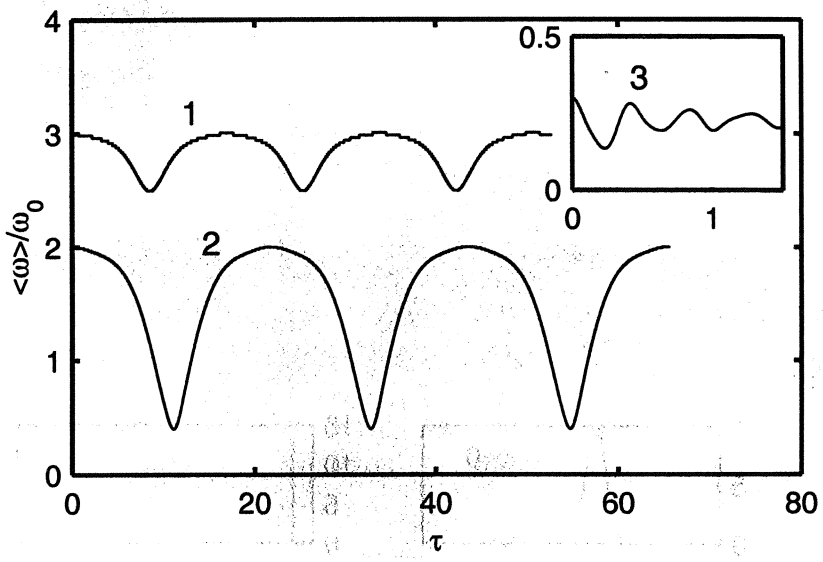

Figure 3.2: Averaged frequency of the probe pulse spectrum as a function of time in the simulations of Fig. 3.1.

Eqs. (3.1) and (3.2). This is essentially due to the contributions from the front and rear parts of the pulse. When the pulse passes the turning points and moves forward in the plasma wave frame it shortens again and the results of the simulation become close to the predicted ones. In the simulation the tunneling of the pulse through the density barriers is negligible though it can be important for pulses whose phase trajectories are close to the separatrix. The untrapped pulse moving forward in the plasma wave frame becomes somewhat shorter as it passes the maxima of the density. Nonetheless, due to the inharmonic shape of the wake, its width there is comparable with the density inhomogeneity scale. As a consequence, the average frequency of the spectrum here is a little greater than the one predicted by Eqs. (3.1) and (3.2).

3.1.3 Photon acceleration in the 1D case in a nonstationary plasma wake

The dynamics of the plasma wave source leads to a nonstationary plasma wake. We have investigated photon acceleration in such a nonstationary plasma wake for the case of a relativistically intense laser pulse plasma wave source.

The characteristic depletion time of the pulse producing the plasma wake (main

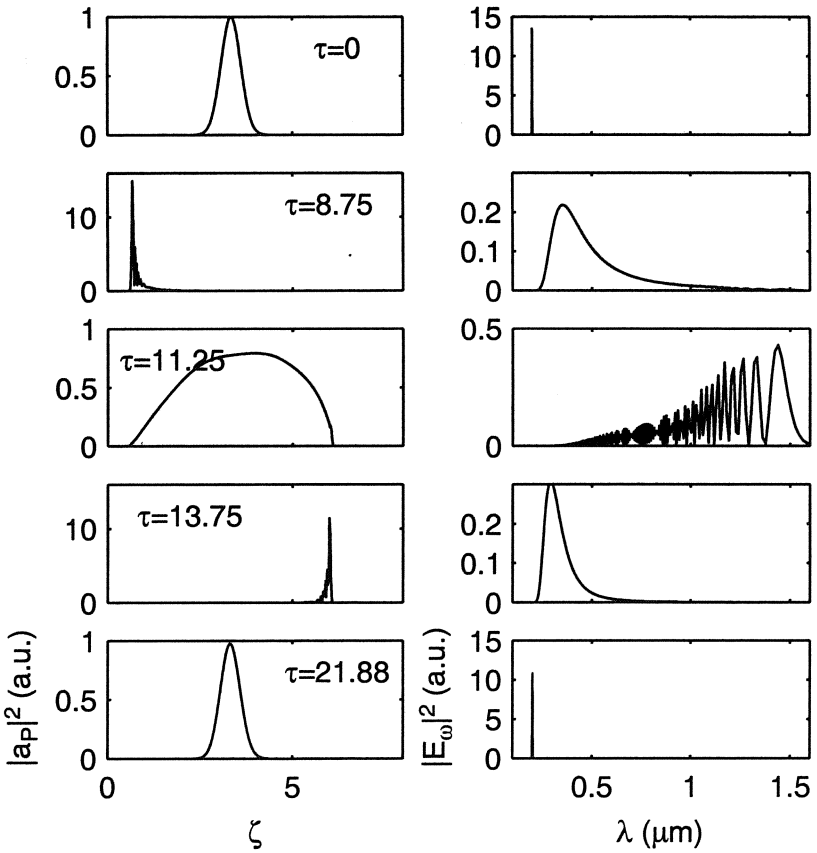

Figure 3.3: Trapped pulse vector potential (on the left) and spectral intensity (on the right) at different times during one oscillation in the simulation of Fig. 3.1.

pulse) due to energy transfer to the plasma wake in 1D is given by [48]:

$$t_{dep} = \frac{\omega_0^2}{\omega_{p0}^3}\frac{8}{3\pi}\frac{\lambda_p}{\int |a|^2 d\xi},$$

where $|a| = e|A|/mc^2$ is the amplitude of the main pulse vector potential and λ_p is the plasma wavelength. This equation was obtained for an ultra-intense laser pulse ($|a| \gg 1$) under the assumption that $(\omega_{p0}\tau)|a| < 1$, where τ is the pulse duration.

For a stationary plasma wake, the period of small oscillations of a photon near the "O-type" equilibrium state according to Eqs. (3.1) and (3.2) is

$$T_1 \geq 2^{3/2}\pi\frac{\omega_0^2}{\omega_{p0}^3}\sqrt{\frac{1-n_1}{n_1}},$$

where $n_1 = 1 - N_{\min}/N_0$ is the plasma wave amplitude at minimum density. This expression becomes an equality for a linear plasma wave ($n_1 \ll 1$). In the linear limit ($|a| \ll 1$) for a linearly polarized main pulse with a normalized intensity profile of the form $a^2 = a_0^2 \sin^2(\pi\xi/L)$ for $0 < \xi < L$ and $a^2 = 0$ for $\xi < 0$ and $\xi > L$, one can obtain, using the cold fluid equations, $n_1 = (a_0^2/4)\sin(\pi L/\lambda_p)/[1-(L/\lambda_p)^2]$ [10].

The time taken by a photon that is untrapped and moving forward in the plasma wave frame to cross (in this frame) one plasma wavelength can be roughly evaluated as $T_2 = 4\pi\omega_0^2/\omega_{p0}^3$ (here it is supposed that $\omega^2 \gg \omega_0^2$, where ω is the photon frequency) and the corresponding time for the photon moving backward in the plasma wave frame as $T_3 = 4\pi\omega^2/\omega_{p0}^3$ (when $\omega^2 \ll \omega_0^2$).

A comparison of these times in the parameter range where they are applicable shows that in the practical case of a relativistically intense main pulse ($|a| \geq 1$) with a duration of the order of a plasma period, only untrapped photons moving backward in the plasma wave frame will have full oscillations of their frequency before the depletion of the main pulse, as $T_1, T_2 \sim t_{dep}$ and $T_3 < t_{dep}$ ($T_3 \ll t_{dep}$ when $\omega^2 \ll \omega_0^2$). This prediction is verified by our numerical simulations.

In Figs. 3.4-3.6 we present the results of the simulation for an untrapped photon moving backward in the plasma wave frame. The parameters of the simulation are the following: the background plasma density is $N_0 = 1.74 \times 10^{17}$ cm^{-3}, the wake is produced by a 30 fs (FWHM), 0.2 μm main pulse of Gaussian shape with maximum vector potential amplitude $a_0 = 1.3$ at initial time, and a ratio $\omega_{p0}/\omega_0 = 0.0025$. The 30 fs (FWHM), 1 μm probe pulse was loaded in the minimum of the electron density.

The evolution of the envelopes of the main and probe pulse vector potentials, and of the plasma wave, is shown in Fig. 3.4. The main pulse first steepens and increases in amplitude at its rear part [48] [see $\tau = 1.6$, 3.2, where $\tau = (\omega_{p0}^3/\omega_0^2)t$ is

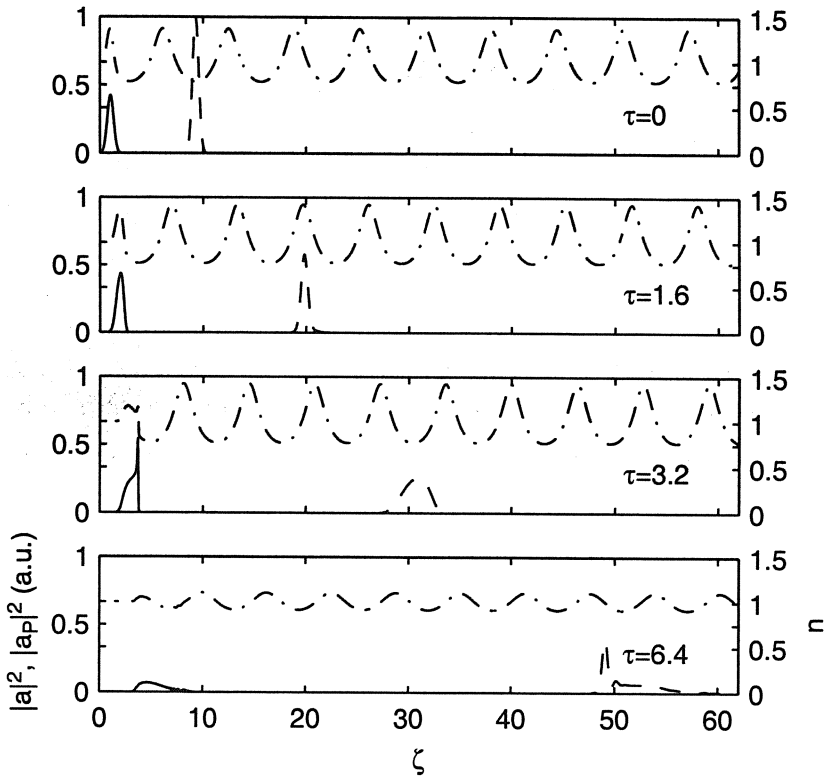

Figure 3.4: Photon acceleration in the 1D case in a nonstationary plasma wake: main pulse vector potential (solid line), probe pulse vector potential (dashed line), and electron density in the plasma wake (dash-dot line) at different normalized times. The parameters of the simulation are given in the text.

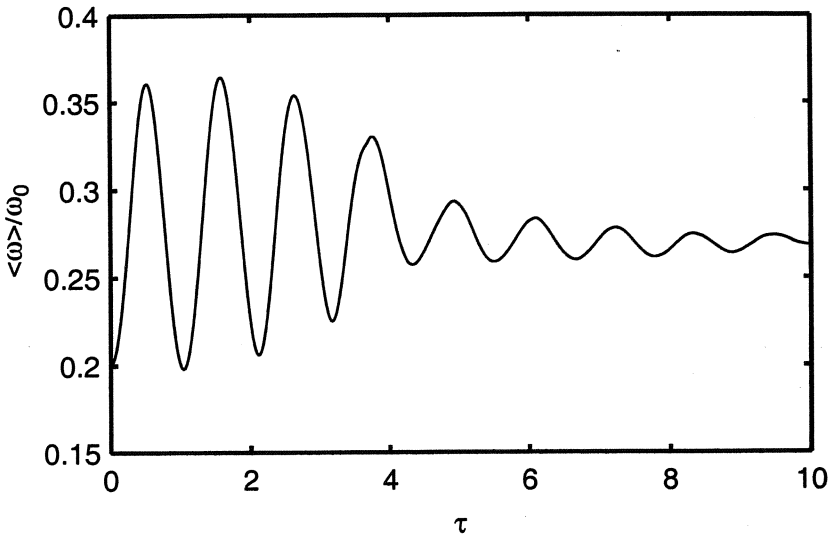

Figure 3.5: Averaged frequency of the probe pulse spectrum as a function of time in the simulation of Fig. 3.4.

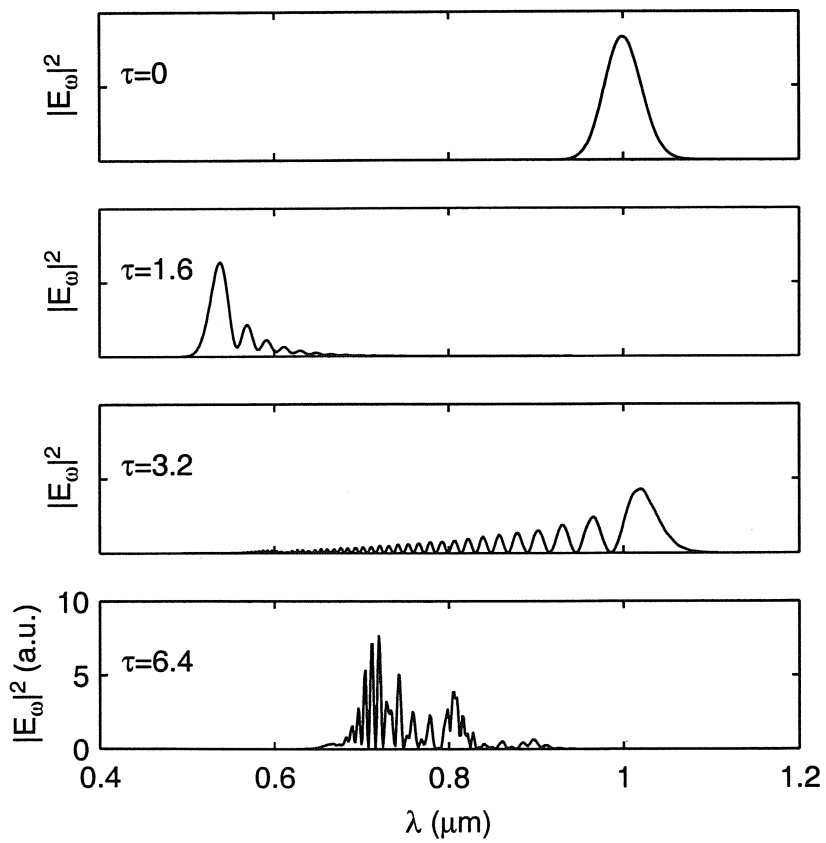

Figure 3.6: Probe pulse spectrum at different times in the simulation of Fig. 3.4.

the dimensionless time] and then becomes very weak loosing its energy ($\tau = 6.4$). Due to the strong steepening and increase in amplitude of the main pulse the plasma wave amplitude first becomes a little greater but then decreases due to the depletion of the main pulse. The probe pulse frequency (Figs. 3.5 and 3.6) oscillates first with an increasing and then with decreasing amplitude following the evolution of the plasma wave amplitude.

We have also made simulations (not shown) that correspond to trapped photons and untrapped photons moving forward in the plasma wave frame. For a relativistically intense main pulse with a duration close to the plasma period we observe only a fraction of one frequency oscillation before the main pulse is depleted. Nevertheless the maximum frequency shift was of the order of the initial frequency for both the trapped photons and the untrapped photons moving forward in the plasma wave frame (when the initial frequency of the last is not much larger than the main pulse frequency).

Summarizing the results of this section we conclude that the acceleration of photons with $\omega \geq \omega_0$ in the plasma wake, behind a relativistically intense laser pulse, is complicated by main pulse depletion. This depletion takes place on the same time scale as photon acceleration. The theory of photon acceleration in the plasma wake with constant amplitude is not sufficient in this case. The "acceleration" time is smaller than the depletion time of the main pulse only for untrapped photons with $\omega < \omega_0$. The theory of photon acceleration in the plasma wake with constant amplitude is sufficient for untrapped photons with $\omega^2 \ll \omega_0^2$.

3.1.4 Photon acceleration in the axially symmetrical 2D case

Strong plasma wakes can be excited if intense laser pulses are focused in plasma. Weak probe pulses can be used for their diagnostics. The information can be obtained measuring the frequency (phase) shift of the probe pulses propagating in the plasma wake. Usually for such measurements the focal plane of the laser beam is imaged with a lens on the spectrometer measuring the spectrum of the probe pulse after the propagation in plasma. Given the necessary magnification of the image it is possible to measure not only the averaged frequency shift in the probe pulse but also the frequency spectra at different r (transversal coordinate). It can give important information about the plasma condition in the focal region with longitudinal and transversal resolution.

3.1.4.1 Analytical estimation of the frequency and phase shift of the probe pulse in the case of small refraction

In this paragraph we will suppose that the wake excitation is correctly described by the 2D, nonrelativistic, fluid model developed in Ref. [9], and perturbations in the probe pulse caused by the plasma wake (due to refraction) are small. According to the analytical model of Ref. [9] the density perturbations $n(r,\xi,z) = n_0 + \delta n(r,\xi,z)$ in the wake driven by a transversally and longitudinally Gaussian (linearly polarized) laser pulse with the normalized vector potential

$$a^2(r,\xi,z) = a_m^2(z) e^{-[r/\sigma_r(z)]^2 - [\xi/\sigma_z]^2}$$

($\xi = ct - z$) are:

$$\frac{\delta n}{n_0}(r,\xi,z) \equiv n_1 =$$

$$-\frac{\sqrt{\pi}}{4} a_m^2 e^{-(r/\sigma_r)^2} \left[1 + \frac{4}{(k_p\sigma_r)^2}\left\{1 - \left(\frac{r}{\sigma_r}\right)^2\right\}\right]\left[k_p\sigma_z e^{-(k_p\sigma_z)^2/4}\right] \sin k_p\xi. \qquad (3.3)$$

The theory is strictly correct if $\delta n \ll n_0$. The evolution of the width and amplitude of the laser pulse along the laser axis z is

$$\sigma_r = \sigma_{r_0}\left(1 + \frac{z^2}{k_0^2\sigma_{r_0}^4}\right)^{1/2}, a_m^2 = a_0^2\frac{\sigma_{r_0}^2}{\sigma_r^2},$$

where σ_{r_0} and a_0 are the waist (in the field intensity) and amplitude in the focus. The pulse self-focusing and depletion due to the wake excitation are neglected here. Let us consider a radially and longitudinally Gaussian probe pulse propagating in the wake behind the main pulse. Evolution of the complex amplitude of its vector potential (a_p) is described here by the paraxial wave equation

$$2ik\frac{\partial a_p}{\partial z} = -\Delta_\perp a_p + k_p^2 a_p n_1.$$

In the absence of density perturbation ($n_1 = 0$) the solution to this equation is:

$$a_p^{(0)}(r,\xi,z) = \frac{a_{p0}}{1 + i\frac{z}{k\sigma_{r_{p0}}^2}} \exp\left\{-\frac{r^2}{2\sigma_{r_{p0}}^2\left(1 + i\frac{z}{k\sigma_{r_{p0}}^2}\right)} - \frac{(\xi - \xi_0)^2}{2\sigma_{z_p}^2}\right\}, \qquad (3.4)$$

where $\sigma_{r_{p0}}$ and a_{p0} are the waist (in the field intensity) and amplitude in the focus (the focus is in the same point for the main and probe pulses), σ_{z_p} is the half width at $1/e$ in intensity, the pulse is centered in $\xi = \xi_0$. The slippage between the probe

pulse and the plasma wake will be neglected in this subsection. This slippage can be neglected in the focal region of the main pulse (where there is a strong wake) if:

$$2k_0\sigma_{r_0}^2\frac{\left|v_{gr}^{(m)}-v_{gr}^{(pr)}\right|}{c}k_p \simeq \sigma_{r_0}^2 k_p^2\frac{\omega_{p_0}}{\omega}\left|\frac{\omega_0}{\omega}-\frac{\omega}{\omega_0}\right| \ll \frac{\pi}{2},$$

where ω_0 and ω are the frequencies and $v_{gr}^{(m)}$ and $v_{gr}^{(pr)}$ are the group velocities of the main and probe pulses, respectively. We will suppose that density perturbations change slightly this solution (the condition for this will be found later) and will find a small perturbation induced by the wake $a_p^{(1)}(r,\xi,z)$ which in this case satisfies the equation

$$2ik\frac{\partial a_p^{(1)}}{\partial z} = -\Delta_\perp a_p^{(1)} + k_p^2 a_p^{(0)} n_1.$$

Solving this equation first for the Fourier images

$$A_p^{(1)} = \frac{1}{(2\pi)^2}\iint a_p^{(1)} e^{-ik_x x - ik_y y}dxdy$$

($r^2 = x^2 + y^2$) and then returning back to the originals we obtain:

$$a_p^{(1)} = -\frac{1}{4\pi}\int_{-\infty}^{z}\frac{dz'}{z-z'}\iint dx'dy' \exp\left(i\frac{[(x-x')^2+(y-y')^2]k}{2(z-z')}\right)k_p^2 a_p^{(0)} n_1. \quad (3.5)$$

This formula can be simply understood: we first calculate the propagation of the new radiation (perturbation) generated in the layer dz' (at z') to the plane z using the formula for the propagation in undisturbed plasma [integral on (x',y')] and then sum up the contributions (integral on z'). The integration on (x',y') can be performed in terms of elementary functions [for $a_p^{(0)}$ and n_1 of the form (3.3) and (3.4)]. After this integration the integration on z' can be performed in terms of elementary functions only for $x = y = 0$.

In obtaining (3.5) we have assumed that background plasma is homogeneous and infinite. In realistic experiments plasma is created in a finite region and the integration in Eq. (3.5) must be performed over this region. Besides, the propagation of the probe beam must be analyzed inside the plasma and outside. Particularly, in the case when ionization is produced by the same main pulse which produces the wake, a transversal plasma boundary with the gas arises [86]. In this case the parts of the probe pulse propagating inside the plasma and outside experience different phase shifts. Evidently, in neglecting this effect our theory is not sufficient, if the probe beam waist is larger than the transversal size of the plasma and an essential part of the probe pulse propagates outside the plasma.

We will estimate the phase and frequency shift of the probe pulse which can be measured in the scheme of plasma diagnostics mentioned at the beginning of the

section, that is when the focal plane is imaged by a lens on the spectrometer. In the absence of plasma density perturbations in the region $z > 0$ [except a short region Δz of transition to vacuum (or gas) before the diagnostics line, that does not cause a strong diffraction] the probe pulse field distribution in the focal plane is reproduced with a magnification in the image plane of the lens (with an additional phase factor depending on r). The generation of perturbations due to the plasma wake in $z > 0$ can be taken into account in the following way. Calculating the propagation of new radiation back in z to $z = 0$ we obtain a field distribution similar to that produced in this plane by the perturbation sources in $z < 0$ [$a_p^{(1)}\big|_{z=0}$ given by (3.5)]: the imaginary part is the same and the real part is of the opposite sign. Thus we conclude that the field

$$(a_p^{(0)} + 2i\mathrm{Im}a_p^{(1)})\big|_{z=0} \simeq a_p^{(0)} \exp\left\{\frac{2i\mathrm{Im}a_p^{(1)}}{a_p^{(0)}}\right\}\Big|_{z=0} \equiv a_p^{(0)}\big|_{z=0}\, e^{i\Phi},$$

where $\Phi = 2\mathrm{Im}a_p^{(1)}/a_p^{(0)}\big|_{z=0}$ will be reproduced in the image plane of the lens.

Because the integration in Eq. (3.5) can be performed in terms of elementary functions only for $r = 0$ we limit ourselves to estimate the phase (and frequency) shift in the image plane at $r = 0$. Calculating $a_p^{(1)}\big|_{z=0,r=0}$ from (3.5) we obtain:

$$\mathrm{Re}a_p^{(1)}/a_p^{(0)}\big|_{z=0,r=0} = Q\left[P\ln\left(\frac{1+\sqrt{1+\delta}}{\sqrt{\delta}}\right) + \frac{1}{1+\delta}\right]\sin k_p\xi,$$

$$\mathrm{Im}a_p^{(1)}/a_p^{(0)}\big|_{z=0,r=0} = \frac{\pi}{2}QP\sin k_p\xi,$$

where

$$Q = \frac{\sqrt{\pi}}{4}\left[k_p\sigma_z e^{-(k_p\sigma_z)^2/4}\right]a_0^2,$$

$$P = \frac{k_p^2\sigma_{r_0}^2}{2\sqrt{1+\delta}} + \frac{\delta}{(1+\delta)^{3/2}},$$

$$\delta = k^2/k_0^2 + 2\sigma_{r_0}^2/\sigma_{r_{p_0}}^2.$$

Φ is the phase shift per unit length accumulated by the probe pulse. The longitudinally averaged phase shift is:

$$\varphi = \frac{\int \Phi(\xi)|a_p^{(0)}|^2 d\xi}{\int |a_p^{(0)}|^2 d\xi} = \pi QPe^{-(k_p\sigma_{z_p})^2/4}\sin k_p\xi_0$$

and the shift of the probe pulse spectrum is:

$$\Delta\omega = \frac{\int ck'|a_{p_k}(k')|^2 dk'}{\int |a_{p_k}(k')|^2 dk'} = -\omega_p\pi QPe^{-(k_p\sigma_{z_p})^2/4}\cos k_p\xi_0,$$

where

$$a_{p_k}(k') = \frac{1}{2\pi}\int a_p(\xi)e^{ik'\xi}d\xi.$$

Our perturbation theory is correct if $|a_p^{(1)}| \ll |a_p^{(0)}|$. The strongest refraction of the probe pulse is at the laser axis. Substituting the values of $a_p^{(0)}$ and $a_p^{(1)}$ in $r = z = 0$ in this inequality we get:

$$Q\frac{k_p^2\sigma_{r0}^2}{2\sqrt{1+\delta}}\max\left\{\frac{\pi}{2}, \ln\frac{1+\sqrt{1+\delta}}{\sqrt{\delta}}\right\}\sin k_p\xi \ll 1$$

for arbitrary ξ inside the laser pulse. Obtaining this condition we have taken into account that $Q \ll 1$. It follows from the condition

$$Q\left[1+\frac{4}{(k_p\sigma_{r0})^2}\right] \ll 1,$$

which must be satisfied in order for the theory of wake excitation by the main pulse to be correct ($\delta n \ll n_0$).

3.1.4.2 Simulation of photon acceleration

We have simulated a probe pulse dynamics in the wake behind an ultra-intense short laser pulse using the 2D (axially symmetric) particle code WAKE. The parameters of these simulations are now attainable, for instance at the LOA. The plasma was assumed to be produced by the same main pulse focused into the center of a helium gas jet of some Rayleigh lengths width. We have made simulations both with a rectangular shaped gas jet (of two Rayleigh lengths width) and with a realistic jet of a smooth shape. The main pulse enters the jet with a maximum intensity that is much greater than the ionization threshold. Ionization then takes place at the front slope of the pulse, a long time before the peak. It is only this small front part of the pulse (whose energy is negligible compared with the total energy of the pulse) that is subject to ionization-induced refraction, while the main part propagates as in a preformed plasma.

The probe pulse was also focused at the center of the gas jet. We have varied the delay between the main and probe pulses in order to obtain photon acceleration in different phases of the plasma wave.

In order to obtain the maximum frequency shift, one needs to exclude the possible longitudinal drift of the probe pulse with respect to the plasma wake due to both a difference of the probe and main pulse group velocities and a change in plasma wavelength caused by nonlinear effects and variation of the jet density. To do this, it is better to use a gas jet with a nearly homogeneous density profile in the focal region. It is possible to compensate for a slight nonlinear increase in plasma wavelength with an increase in amplitude near the focal point increasing the jet density there. The difference between the plasma wave phase velocity (equal to the main pulse group

velocity) and the probe pulse group velocity can be compensated for by an additional ramping of the jet density profile in the longitudinal direction [78].

In the simulation, the interaction with the plasma wave was followed by a probe pulse optical collecting line with a 20 cm focal length lens of infinite aperture. Such optical collecting lines with sufficiently large aperture are currently used in experiments. We have calculated the pulse spectrum on the laser axis in the image plane of the lens.

In Figs. 3.7-3.13 the results of two simulations are presented for the case of a rectangularly shaped gas jet of two Rayleigh lengths in width. The wake is produced by a 30 fs (FWHM), 0.8 μm laser pulse of Gaussian shape. The frequency shifting of a 30 fs (FWHM), 0.4 μm probe laser pulse of Gaussian shape is investigated. The other parameters of the two simulations are shown in Table 3.1. The total energy of the main laser pulse is in both cases 0.5 J. We have also made a simulation with the parameters corresponding to Figs. 3.7-3.9 but with a realistic smoothly shaped gas jet $N = N_0 \exp[-(|z|/2)^{2.663}]$, where the longitudinal coordinate z is in mm. Although the last jet is rather inhomogeneous in the focal region the results of simulation were approximately the same as in Figs. 3.7-3.9. The plasma wave profile at the time when the main pulse passes its vacuum focus in the simulation with a smaller density is shown in Fig. 3.7 (the corresponding plasma wave profile in the simulation with a higher density is qualitatively the same and is not shown). In Figs. 3.8 and 3.10 the final spectrum of the probe pulse at the output of the collecting line, and in Figs. 3.9 and 3.11 the averaged wavelength, are shown for different delays between the main and probe pulses. As we see, the frequency shift in these simulations is a few percent. For the parameters of the simulation of Figs. 3.7-3.9 the analytical estimates of the previous subsection give the maximum frequency shift (when the probe pulse is on the longitudinal slope of electron density) $\Delta\omega \simeq 1.8\omega_p$, or in terms of wavelength $\Delta\lambda \simeq 0.9 \times 10^{-2}\mu$m. In the simulation the maximum shift $\Delta\lambda^{(num)} \simeq 0.53 \times 10^{-2}\mu$m. The agreement with the theory of the previous subsection can be considered as good, taking into account that the distance of interaction in our simulation is 2 Rayleigh lengths of the main pulse instead of infinite distance in the estimate. Also, we are near the limit of validity for the estimation: the amplitude of density oscillations in the focal plane is close to 1 and the perturbation in the focus becomes comparable with the zero-order solution.

For the parameters of the simulation with a higher density (the simulation of Figs. 3.10-3.13) our estimate is not acceptable, mainly because of the strong refraction of the probe pulse. We show the detailed picture of the probe pulse interaction with the plasma wake in this simulation in Figs. 3.12 and 3.13. We present the probe pulse

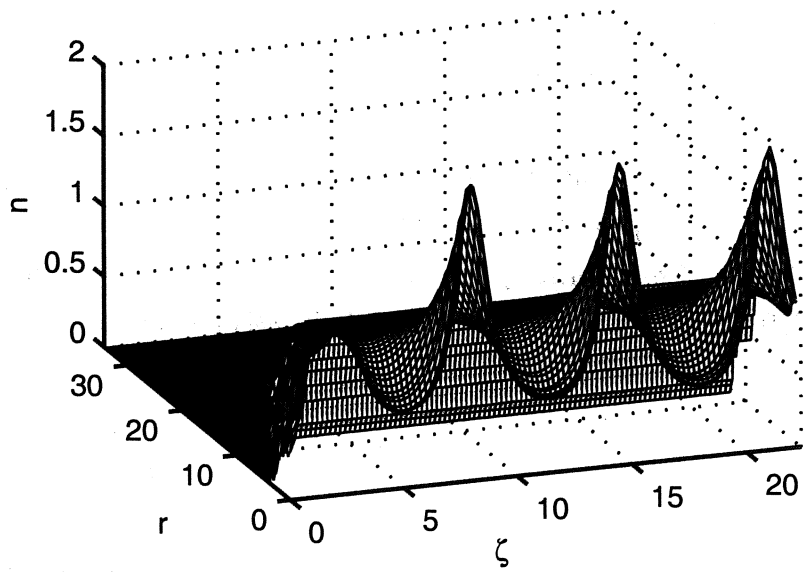

Figure 3.7: Electron density in the plasma wake at the time when the main pulse passes its vacuum focus for the simulation of Fig. 3.8. The transversal coordinate r is in units of k_p^{-1}.

Table 3.1: Parameters of the simulations of photon acceleration in the axially symmetrical 2D case. The other parameters are given in the text. N_0 is the unperturbed electron density, w_0 is the main pulse waist, $I_{\max}$ is the maximum vacuum main pulse intensity, and w_s is the probe pulse waist.

Figure	$N_0(\mathrm{cm}^{-3})$	ω_{p0}/ω_0	$w_0(\mu\mathrm{m})$	$I_{\max}(\mathrm{W/cm}^2)$	$w_s(\mu\mathrm{m})$
$3.7-3.9$	1.09×10^{18}	0.025	21.7	2.11×10^{18}	26.5
$3.10-3.13$	2.79×10^{18}	0.04	25.3	1.56×10^{18}	33.4

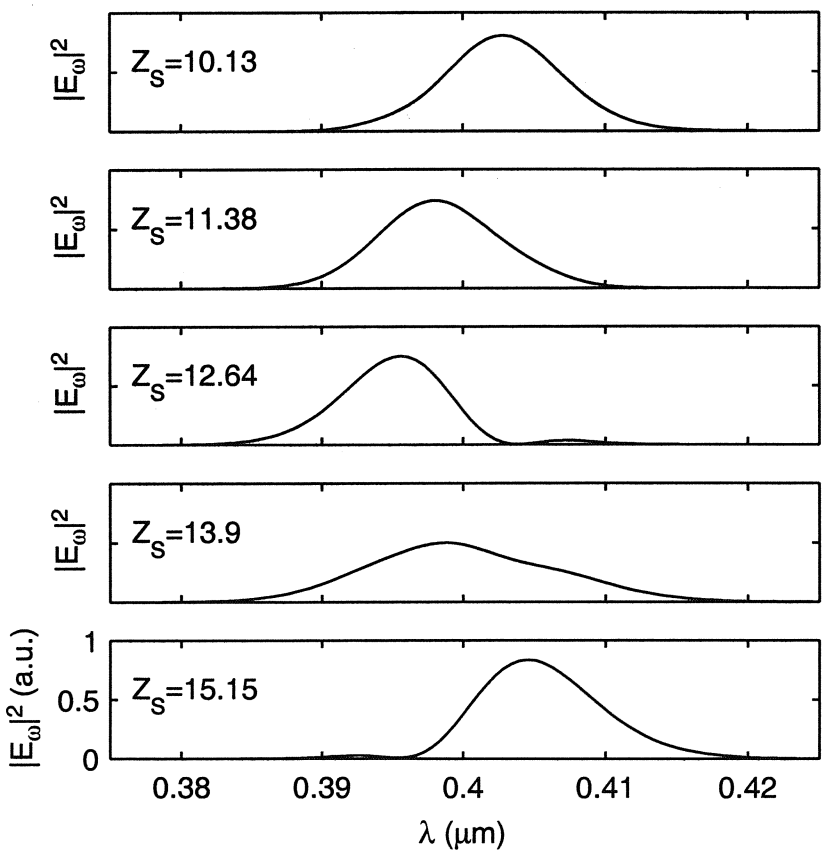

Figure 3.8: Photon acceleration in the axially symmetrical 2D case: probe pulse spectral intensity at the output of the optical collecting line for the different values of the initial position of the probe pulse in the plasma wave frame (in units of k_p^{-1}) Z_s. The parameters of the simulation are given in the text and in Table 3.1.

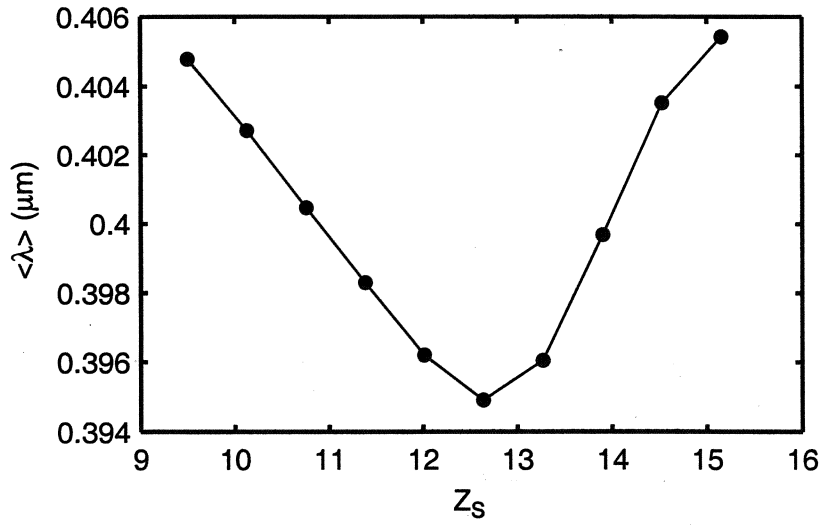

Figure 3.9: Averaged frequency of the probe pulse spectrum at the output of the optical collecting line as a function of Z_s in the simulation of Fig. 3.8.

intensity and plasma density distributions at different times (longitudinal positions z) in the simulations with the maximum up- (Fig. 3.12) and down- (Fig. 3.13) shifts in frequency. The plasma density profiles in the instantaneous shots have a so-called "horseshoe" shape [41, 89, 90, 91], because the plasma wavelength is greater on the axis due to the nonlinear relativistic wavelength increase with amplitude [16, 21, 35, 36, 46]. The plasma wave phase fronts in the periphery move uniformly with the velocity of the main pulse. On the other hand, the axial plasma wave phase fronts move backward (in the frame moving with the main pulse) as long as the on-axis intensity increases, and then they move forward after the focal plane. This effect as well as the difference between the main and probe pulse group velocities lead to the slippage between the probe pulse and the plasma wake. When the probe pulse approaches the focal plane it moves faster than the density humps. In the case of down-shifting in frequency (Fig. 3.13), the forward part of the pulse is subject to an additional defocusing as it approaches the density maximum in front of it. The defocused radiation stays a sufficient time in the region of density decrease where it is down-shifted in frequency. After the focal plane the density maximum in front of the pulse shifts forward, a part of defocused radiation returns back to the laser axis though a considerable part is diffracted. In the case of up-shifting in frequency (Fig. 3.12) the density maximum behind the probe pulse shifts backward when the pulse approaches the focal plane. The pulse up-shifting becomes smaller. At the focal plane the probe pulse finds itself attracted by the density minimum. The frequency

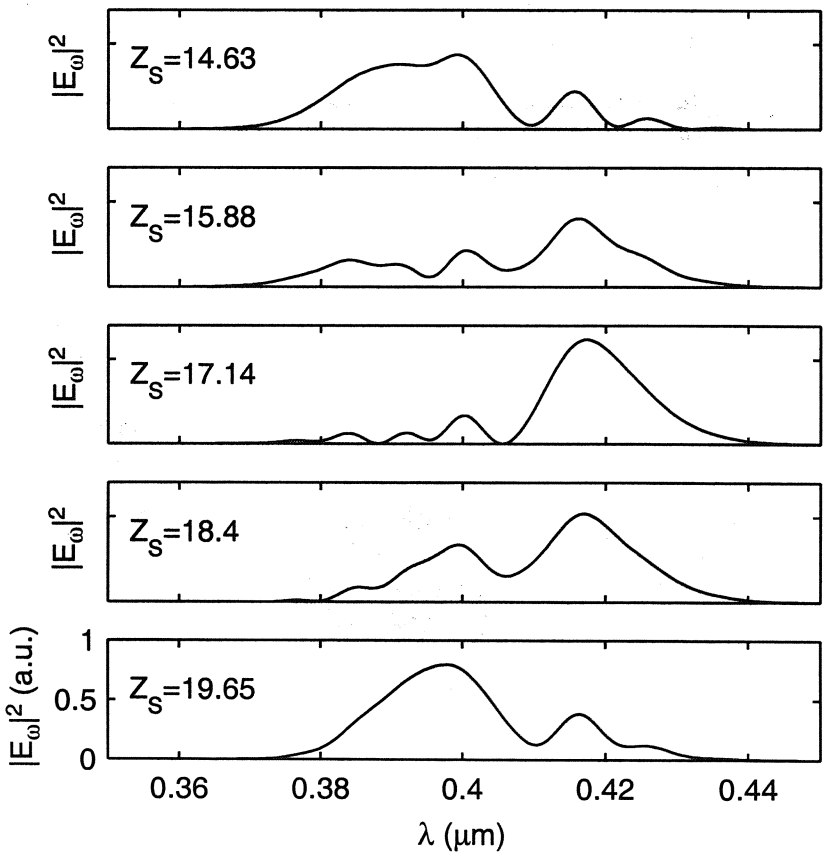

Figure 3.10: Photon acceleration in the axially symmetrical 2D case, probe pulse spectral intensity at the output of the optical collecting line for the different values of the initial position of the probe pulse in the plasma wave frame (in units of k_p^{-1}) Z_s. The parameters of the simulation are given in the text and in Table 3.1.

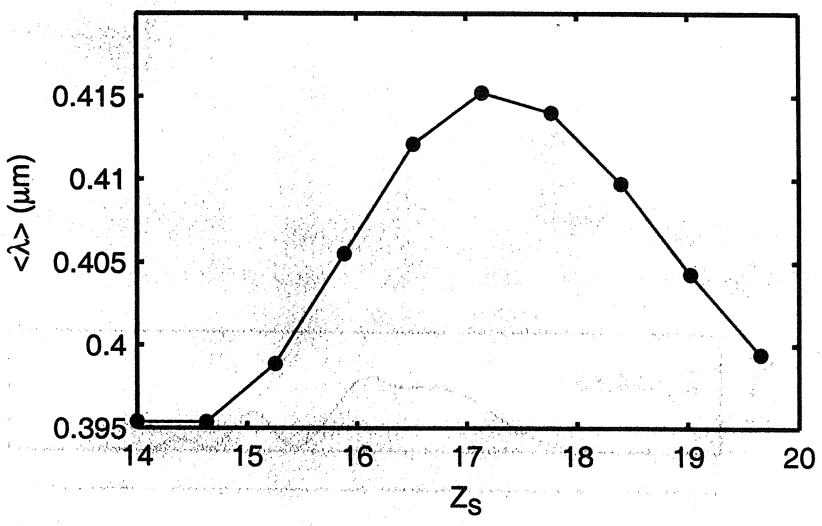

Figure 3.11: Averaged frequency of the probe pulse spectrum at the output of the optical collecting line as a function of Z_s in the simulation of Fig. 3.10.

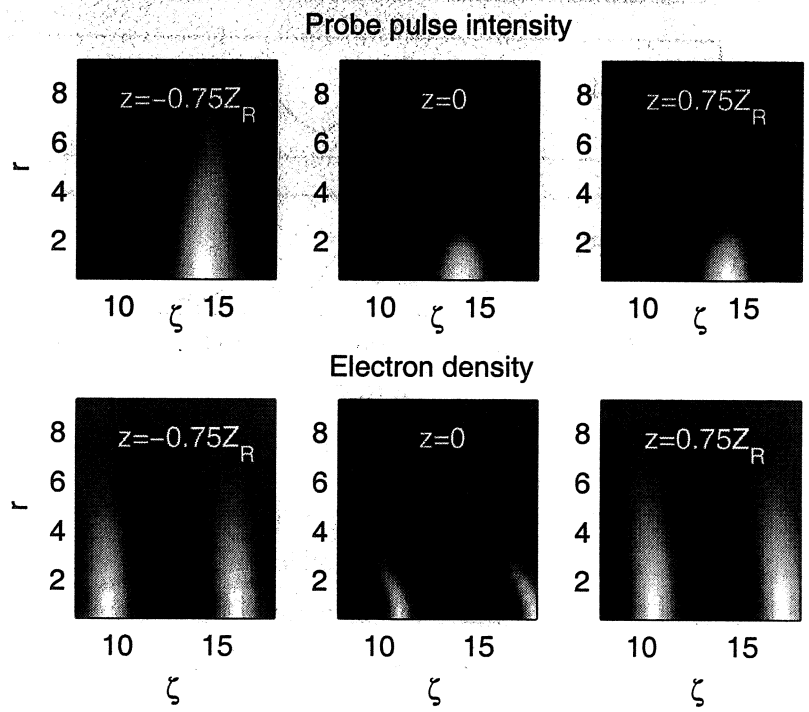

Figure 3.12: Probe pulse intensity distribution and electron density distribution in the vicinity of the probe pulse at different times (longitudinal positions z) for the simulation with the maximum frequency up-shifting ($Z_s = 14.4$) in Figs. 3.10 and 3.11.

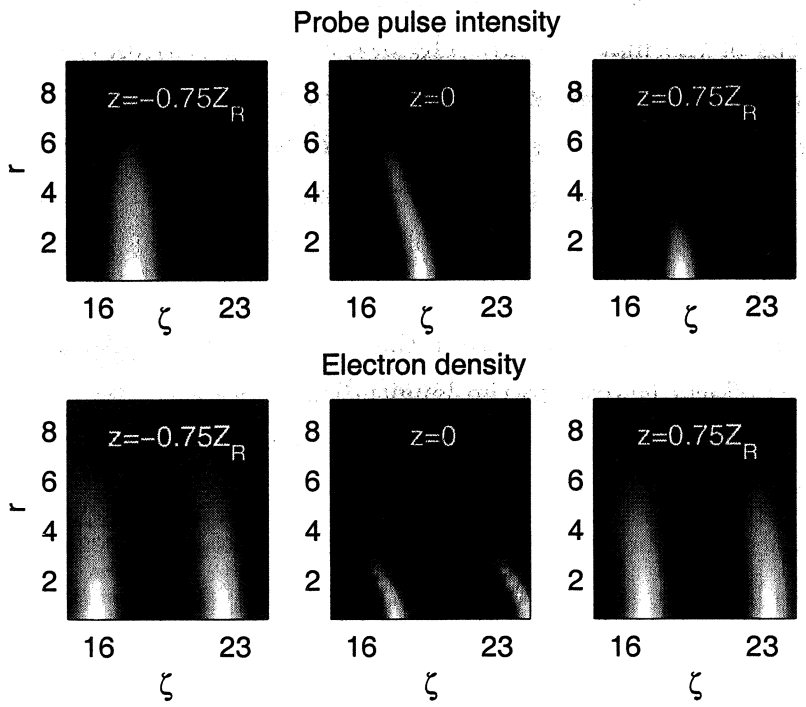

Figure 3.13: Probe pulse intensity distribution and electron density distribution in the vicinity of the probe pulse at different times (longitudinal positions z) for the simulation with the maximum frequency down-shifting ($Z_s = 17.3$) in Figs. 3.10 and 3.11.

shift in the density minimum is small and of opposite signs for the forward and backward parts of the pulse. After the focal plane the density maximum behind the pulse shifts forward, but because of the difference between the probe and the main pulse group velocities the probe pulse generally outruns the wake and only a small backward part of it is frequency shifted. Our simulation shows that, as a result, down-shifting in frequency is more efficient than up-shifting.

In the simulation with a smaller density (Figs. 3.7-3.9) the probe pulse refraction is weak, the difference between the main and probe pulse group velocities is smaller, as well as the longitudinal size of the region of interaction (which is equal to two Rayleigh lengths of the main pulse). The frequency up-shifting and down-shifting of the probe pulse in this case are nearly as efficient. However there is a slippage between the probe pulse and the "horseshoe" shaped plasma wake: the curvature and position of the plasma wave phase fronts change with z in the laser pulse frame. This slippage somewhat reduces the amplitude of the frequency oscillations which we see in Fig. 3.9.

The effects caused by the difference in the probe and main pulse group velocities, as well as other effects leading to the longitudinal motion of the probe pulse with respect to the plasma wake can be partially eliminated by choosing special shape for the gas jet.

Refraction of the probe pulse leads to a focusing effect in the regions of minimum density of the plasma wave, and to a defocusing effect in the regions of maximum density. This means that we can not make effective use of the regions of density gradient of a highly nonlinear plasma wake that are close to the density maxima. On the other hand, by focusing the probe pulse near the density minima one can increase the length of collimated propagation and accelerate the probe pulse through a greater interaction length.

3.1.5 Discussions

In this paragraph we have undertaken an investigation of photon acceleration in a plasma wake using particle simulations. Our 1D simulations confirm the existence of photon trajectories that are similar to the trajectories of charged particles in a plasma wave. These trajectories correspond to laser pulses that are trapped and untrapped by the plasma wave. The frequency of these laser pulses oscillates with an amplitude that is dependent upon the relation between the plasma wave phase velocity and the laser pulse group velocity. This amplitude is greater when the velocities are close to each other.

The plasma wave develops simultaneously with the evolution of the plasma wave source. The source evolution is caused by the transfer of energy to the plasma wake and by additional self-modulation. When a plasma wake is produced by a relativistically intense laser pulse with a duration of the order of a plasma period, only the untrapped back-drifting probe pulse still has some full frequency oscillations before the main pulse depletes.

Investigating photon acceleration in a 2D axially symmetrical case we have made analytical estimates of photon acceleration (as well as phase shift in the probe pulse) in the wake behind an ultra-intense short laser pulse. We have estimated the phase and frequency shift in the probe pulse which can be observed in the image plane of a lens imaging the focal plane. This estimate is applicable if the plasma-induced phase shift and refraction of the probe pulse are small. We have also made 2D axially symmetrical particle simulations of photon acceleration. We have simulated a 30 fs, 0.4 μm probe pulse interacting with a plasma wake produced in a gas jet behind a relativistically intense 30 fs, 0.8 μm laser pulse. We then calculated the probe pulse propagation in a typical optical collecting line as used in laboratory experiments. The probe pulse refraction in the presence of a nonlinear plasma wave and slippage between the probe pulse and the plasma wake lead to a stronger frequency down-shifting than up-shifting. The results of our analytical estimate and numerical simulations in the 2D axially symmetrical case can be useful for plasma diagnostics.

3.2 Phase velocity of the plasma wave in the scheme of Self-Modulated Laser Wake-Field Accelerator and electron acceleration. Relativistic self-focusing and self-similar laser pulse structures.

3.2.1 Phase velocity of the plasma wave in the scheme of Self-Modulated Laser Wake-Field Accelerator

As it was mentioned in Introduction the scheme of Self-Modulated Laser Wake-Field Accelerator is one of the promising schemes of electron acceleration in plasma. In this scheme plasma wave is excited in result of resonant modulational instability of a laser pulse. This instability leads to a longitudinal modulation of the pulse width and amplitude with a characteristic wave number $k_p = \omega_p/c$. Simultaneously a plasma wave is excited with a wave vector close to the resonant k_p. The self-modulation instability can be of a pure 1D or three-dimensional (3D) nature depending on the intensity and space size of the laser pulse and the value of plasma density [14, 54, 58, 59, 92]. In spite of the difference of the mechanisms of 1D and 3D instabilities the presence of a feedback between the excited plasma wave and the intensity modulation is common for them. In 1D the intensity modulation corresponds to a redistribution of energy of the laser field in the longitudinal direction. In the 3D case the effect occurs due to a redistribution of the laser field energy in different transversal cross-sections of the pulse. The synchronization of the redistributions is caused by the plasma wave. Physically it corresponds to the situation when in some transversal cross-sections focusing of the laser radiation takes place and in the others defocusing, that leads to the laser field modulation.

Resonant modulational instability was first observed in numerical simulations of ultra-short laser pulses interaction with plasma [14, 51, 52, 53, 55]. Analytical investigation of the perturbations of electron density and laser field connected through the pump wave based on the corresponding dispersion relation was performed in Ref. [14]. Longitudinal modulation of the pulse in a pure 1D geometry was investigated in Refs. [59, 92]. The initial stage of self-modulation of a laser pulse was studied in aberrationless approximation first in Ref. [54]. In Ref. [58] a comparison of 1D and 3D mechanisms of the instability was performed on the basis of the dispersion relation and solution of the equations for perturbations of electron density and field

in 1D and 3D (2D axially symmetrical) cases in aberrationless approximation. It was found that for a laser pulse with a sharp forward edge 1D mechanism is not essential if the following condition is satisfied:

$$\frac{k_p^2 r_0^2 a_0^2}{16} < \frac{\gamma_g^2}{k_p L + a_0^{-2}}, \tag{3.6}$$

here $a_0 = eA_0/mc^2$ is the dimensionless laser pulse amplitude, r_0 and L are the width (waist) and length of the pulse, respectively, $\gamma_g = (1 - v_{gr}^2/c^2)^{-1/2} \simeq \omega_0/\omega_p$ is the relativistic factor, corresponding to the laser pulse group velocity.

In the first works on the resonant modulational instability of a laser pulse, performed before the middle of 90-th, the most attention was devoted to the study of instability rates and prediction of the excited plasma wave amplitude. For the estimation of possible electron acceleration by the plasma wave it was usually assumed that the plasma wave phase velocity is so close to the laser pulse group velocity that one can neglect the difference between γ_{ph} and γ_g. The phase of the plasma wave excited in result of the resonant modulational instability was investigated first in Refs. [58, 93, 94]. The phase velocity of the plasma wave was found in different regimes at the linear stage of instability. It was shown, that the relativistic factor of the plasma wave γ_{ph} can be essentially less than γ_g and this can be important for using the regime of laser pulse self-modulation for acceleration of particles. However, as it was mentioned this question requires an additional analysis as it is supposed to accelerate electrons at the nonlinear stage of instability.

If it is supposed that γ_{ph} is close to γ_g the use of a sufficiently underdense plasma is required for the electron acceleration to high energies. Really, if one assumes for an estimation that the amplitude of electric field of the plasma wave is of the order of non-relativistic wavebreaking field (1.3) and electron acceleration length is equal to the dephasing length (1.5) it is possible to obtain the following relation for the maximum energy of electrons accelerated:

$$\Delta W[\mathrm{MeV}] \sim 10^{-9}(2/\pi) E_0[\mathrm{V/cm}] l_d[\mathrm{cm}] \simeq 2\left(\frac{\omega_0}{\omega_p}\right)^2. \tag{3.7}$$

The coefficient $2/\pi$ here is due to the averaging of electric field over the accelerating period (assuming that the longitudinal dependence of electric field is approximately sinusoidal). Therefore, for a given frequency of the laser radiation the maximum electron energy is inversely proportional to the electron density. One must also remember, estimating the maximum electron energy in particular cases, that Eq. (3.7) can overestimate it and one needs to make corresponding corrections. First, the acceleration length may be 2 times less than l_d from Eq. (1.5) as electrons typically

experience both longitudinal accelerating and radial focusing force in the phase interval of the plasma wave $k_p|\Delta\xi| = \pi/4$, that is only on half a total acceleration interval $\pi/2$. Electron acceleration in the plasma wave with a horse-shoe shape is an exception. Such a form of the plasma wave develops in the result of dependence of the plasma frequency on the amplitude of the wave and electron density which depend in their turn on the transversal coordinate [41, 89, 90, 91]. In the last case the phase interval where electrons experience both longitudinal accelerating and radial focusing force increases up to $\pi/2$. Second, the plasma wave amplitude in experiments is usually somewhat less than E_0 given by Eq. (1.3) [62, 95, 96] that we have taken into account formally in the similar estimate (4.1), (5.1).

In the case of a sufficiently underdense plasma for moderate pulse lengths the resonant modulational instability in plasma has a 3D character according to Eq. (3.6). The values of the phase velocity and relativistic factor for 3D instability was found in the aberrationless approximation in Refs. [58, 93, 94]. One can separate two characteristic regimes of instability:

- $(P/P_c)k_pL \gg 1$ (large power and/or pulse duration), in particular, the condition $P \geq P_c$ can be satisfied, when relativistic channeling of the laser pulse is possible; relativistic factor of the plasma wave in this regime of instability is:

$$\frac{\gamma_{ph}}{\gamma_g} = \left[1 + F\left(\frac{P}{P_c}k_pL\right)^{1/2}\frac{\gamma_0^2}{k_pz_R}\right]^{-1/2}; \tag{3.8}$$

- $(P/P_c)k_pL \ll 1$ (small power and/or pulse duration), that supposes $P \ll P_c$ and diffractionless propagation in this regime is possible only in the presence of a plasma channel; in this instability regime

$$\frac{\gamma_{ph}}{\gamma_g} = \left(1 + \frac{4\gamma_g^2}{k_pz_R}\right)^{-1/2}. \tag{3.9}$$

In these formulas L is the pulse length, $z_R = k_0r_0^2/2$ is the Rayleigh length, F is a coefficient of the order of 1, this result is obtained for a wide laser pulse $r_0 > k_p^{-1}$. As it is seen from Eqs. (3.8) and (3.9), the relativistic factor of the plasma wave can be essentially less than γ_g at the linear stage of instability.

The reduction of the plasma wave phase velocity (3.8) and (3.9) can be explained in the following way. The modulations of the intensity and plasma density appearing due to the self-modulation instability are shifted in phase, so that the electron density maxima turn to be ahead (and the minima behind) the intensity maxima by a quarter of a plasma period. The forward slopes of the intensity modulations are defocused close to the electron density maxima due to refraction, at the same

time the backward slopes are additionally focused close to the density minima. In result, the intensity maxima in the modulations are shifted backward as well as all the intensity structure as a whole. The electron density modulations excited by intensity modulations are also shifted backward in their turn.

In Ref. [94] a numerical simulation of the self-modulation of a laser pulse was performed as well. The system of equations in the simulations included the paraxial wave equation for the complex amplitude of the laser pulse and the equation for the electron density perturbations in the frame of hydrodynamic theory of cold plasma. Both the amplitude of the high-frequency field and electron density perturbations are supposed to be small in this approach ($eA/mc^2, \delta n/n_0 \ll 1$). The ratio of the laser frequency to the plasma frequency in the numerical simulation was chosen $\omega_0/\omega_p = 22.5$. The laser pulse profile at initial moment of time was Gaussian in the transversal direction with a width of $28k_p^{-1}$ (waist) and homogeneous in the longitudinal direction with a width of $54k_p^{-1}$ and with a sufficiently sharp forward edge. The pulse power was less than the critical power for self-focusing, $P = 0.68P_c$. The parameters of the simulation correspond to the first of the two regimes of self-modulation instability discussed above. According to the results of this simulation the relativistic factor of the plasma wave is essentially less than γ_g only at the initial stage of instability, at the late stage of self-modulation they are close.

We studied the problem of phase velocity of the plasma wave excited in result of the laser pulse self-modulation numerically using the code Wake. As our code is fully relativistic, in numerical simulations we were not limited to the case of weak laser fields and plasma density perturbations, and powers less than critical for relativistic self-focusing. We also considered an important case of self-modulation of a laser pulse with $P < P_c$ in a preformed plasma channel. It was suggested earlier to use self-modulation in the plasma channel for electron acceleration [57, 97], but a possible difference of γ_{ph} and γ_g was not taken into account. As we will see below, this difference is essential for electron acceleration in this scheme.

In our investigation we turned a special attention to the case of sufficiently weak plasma when electron acceleration by the plasma wave up to energies in the range of hundreds of MeV – GeV is possible, if the plasma wave phase velocity is equal to the laser pulse group velocity. As our simulations show, it requires $\omega_0/\omega_p \geq 30$, if the characteristic amplitude of electron density perturbations in the plasma wave $\delta n \sim n_0$ (large but the plasma wave is not broken yet, at least, just behind the laser pulse) and the width of the pulse is of the order of k_p^{-1} (it is the characteristic transversal size of the laser pulse due to self-focusing). As the acceleration length (1.5) in such an underdense plasma is essentially larger than Rayleigh length, rela-

tivistic channeling of the pulse or using a preformed plasma channel is necessary to compensate diffraction and to increase the propagation length. The results of two simulations are shown in Figs. 3.14 and 3.15. In Fig. 3.14 the results of a simulation are shown for the case of self-modulation of a laser pulse with $P > P_c$ in homogeneous plasma, and in Fig. 3.15 for the case of self-modulation of a pulse with $P < P_c$ in a plasma channel. Laser radiation is linearly polarized, in both simulations the pulse is initially Gaussian in the longitudinal and transversal directions with a width of 20 μm (waist) and duration 300 fs (FWHM), the laser wavelength is 0.5 μm. In the simulation in Fig. 3.14 the amplitude of the pulse in maximum $a_0 = 0.93$, the intensity 5×10^{18} W/cm^2, power $P = 1.2P_c$, electron density is 2.8×10^{18} cm^{-3}, $\omega_0/\omega_p = 40$. In the simulations of Fig. 3.15 the maximum amplitude of the pulse $a_0 = 0.61$, intensity 2×10^{18} W/cm^2, power $P = 0.5P_c$, the electron density profile in the channel is $n_e = 2.8 \times 10^{18} + 0.353 \times 10^{15} r^2_{\mu\mathrm{m}}$ cm^{-3}, $\omega_0/\omega_p|_{r=0} = 40$. The specific choice of parameters was determined, in particular, by the present possibilities for the experiment at the laboratory LULI, one of advanced in this field. We show the evolution of the axial distributions of electron density and laser intensity in Figs. 3.14-3.15 (a) and (b), respectively. Straight lines $\gamma = \gamma_g k$ (k is some coefficient) are trajectories of imaginary points that move in the direction of the laser axis with constant velocities, γ is the relativistic factors corresponding to these velocities. The line parallel to the trajectories of the phase fronts (for instance, minima or maxima of electron density) gives the relativistic factor of the plasma wave.

In the simulation of Fig. 3.14 the relativistic factor of the plasma wave is essentially less than γ_g at small times. At the same time at large times, at the stage of saturation of self-modulation instability $\gamma_{ph} \approx \gamma_g$. Self-modulation in this simulation starts after the steepening of the longitudinal intensity profile of the pulse. The central part of the pulse with $P > P_c$ is self-focused, while forward and backward parts with $P < P_c$ are subject to diffraction. Self-modulation starts when the forward slope of the pulse becomes sufficiently sharp and produces an initial perturbation of electron density for self-modulation. The first intensity modulation arises in the place of the central part of the pulse. Some other weaker modulations are behind it. In this simulation the first modulation contributes mainly to the plasma wave excitation at times $ct > 10$ mm. We simulated also the propagation of longer pulses than in this experiment, keeping the other parameters the same. The beginning of self-modulation in those experiments also coincided with the steepening of the central part of the pulse. In the result of self-modulation a larger number of intensity modulations arose, though the result for the phase velocity at the saturation stage of self-modulation was the same: $\gamma_{ph} \approx \gamma_g$. Note that at the late stage of

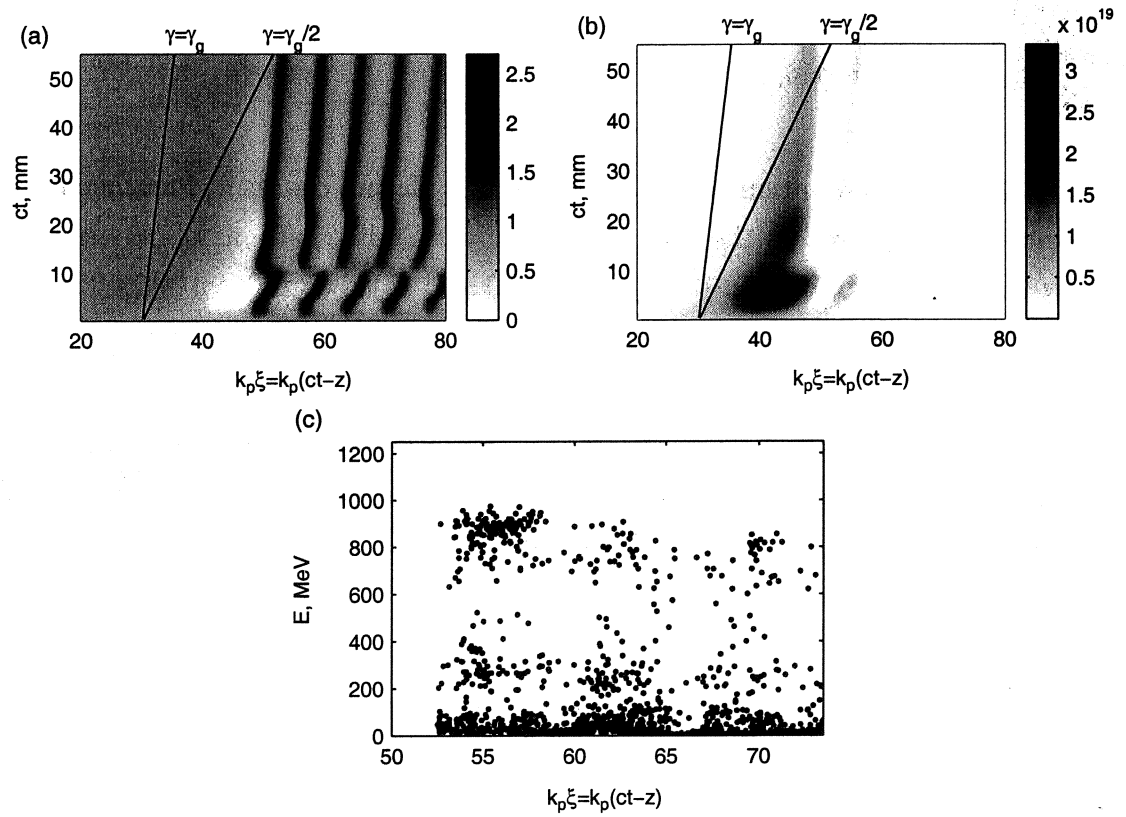

Figure 3.14: Self-modulation and relativistic self-channeling of a laser pulse in homogeneous plasma. The parameters of the simulation are given in the text. Evolution of the distributions of: (a) electron density (normalized to its non-perturbed value) and (b) radiation intensity (in the units of W/cm^2) with time (with longitudinal coordinate). (c) Dependence of the final energy of test electrons on the phase of injection in the plasma wave.

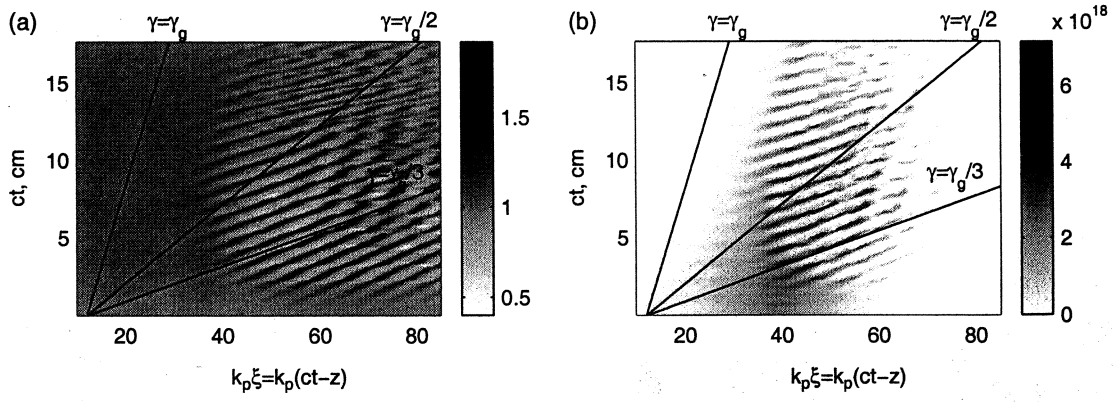

Figure 3.15: Self-modulation of a laser pulse in a plasma channel. Parameters of the simulation are given in the text. Evolution of the distributions of (a) electron density (normalized to its non-perturbed value) and (b) radiation intensity (in the units of W/cm^2) with time (with longitudinal coordinate).

self-modulation, in result of total diffraction of the radiation at the electron density maxima, a field structure forms at the axis that is a succession of short pulses with a period equal to the plasma period. These pulses resonantly excite the plasma wave, existing some time close to the laser axis before a total diffraction loose.

At the late stage of self-modulation instability of the laser pulse in the plasma channel on Fig. 3.15 the relativistic factor of the plasma wave is essentially less (3 times less) than the relativistic factor corresponding to the laser pulse group velocity γ_g. In this numerical simulation the laser pulse diffraction is compensated by refraction in the plasma channel. The main difference of this case from the case of self-modulation in a homogeneous plasma is that at the developed stage of self-modulation the forward parts of the modulations, defocused at the electron density maxima, are not lost due to diffraction. They return back to the axis after the refraction on the walls of the plasma channel. At this stage of self-modulation transverse intensity oscillations arise in the system moving with the pulse. The period of such transverse oscillations in the channel z_p is of the order of Rayleigh length associated with the characteristic width of the stationary transversal mode in the plasma channel in the absence of self-modulation. In particular, in the case of $P \ll P_c$ the period of small oscillations of the pulse width in the self-consistent plasma channel $n = n_0 + \Delta n_c(r^2/r_0^2)$ (where $\Delta n_c = 1/\pi r_e r_0^2$, $r_e = e^2/mc^2$ is the classical electron radius) in the absence of self-modulation is $z_p = \pi z_R = \pi k_0 r_0^2/2$ [57]. However, in the case of self-modulation, unlike in the case when it is absent, the phase of the transverse oscillations of intensity depends on the longitudinal

coordinate in the frame moving with the pulse. The region of the constant phase moves backward in this frame being shifted at one plasma wavelength λ_p in a time of z_p/c. Such a scenarios explains, in particular, the value of relativistic factor of the plasma wave obtained in linear theory for the case of $(P/P_c)k_pL \ll 1$ for a wide laser pulse (3.9).

We simulated test electrons acceleration in the plasma wake of the laser pulse. In the simulation of Fig. 3.14 we injected a beam of 2500 electrons with initial energies of 3 MeV in the plasma wake at the late stage of self-modulation at $z = 5$ mm. The transversal size of the injected electron beam was taken 5 μm and emittance 10 mrad (r. m. s.). In Fig. 3.14 (c) the electron energies after the interaction with the plasma wave are shown in dependence on the initial phase of electron injection, more precisely, on the initial coordinate in the pulse frame. As it is seen from this picture, the maximum electron energy in this numerical simulation is equal to 1 GeV. We also investigated electron acceleration in the simulation of Fig. 3.15, injecting test electrons at the developed stage of self-modulation. The real electron acceleration length, that is dephasing length, is around 4 mm in this simulation, due to the decrease of the plasma wave phase velocity. The maximum electron energy in this simulation is 140 MeV.

3.2.2 Relativistic channeling. Self-similar laser pulse structures.

Numerical simulation in Fig. 3.14 reveals one more very interesting characteristic of the laser pulse propagation. At the saturation stage of self-modulation a quasi-stationary field structure is produced, propagating in plasma more than 20 Rayleigh lengths without essential diffraction. Simultaneously a plasma wave of a large amplitude is excited. It can accelerate electrons effectively. The quasi-stationary structure consists of modulations of the laser pulse, produced in the result of instability. However, the first modulation plays the most important role. It is just this modulation that contributes mostly to the plasma wave excitation. The other weak modulations do not diffract due to the focusing properties of this plasma wave.

First of all, we remind that the difficulties of relativistic self-channeling of laser pulses with duration of the order or less than a plasma period and leading edges ($\delta L < \lambda_p$) of longer pulses were noted in Refs. [35, 36, 37]. The reason is that such pulses excite plasma waves. When the leading edge of the pulse excites the plasma wave, electron density increases in the pulse region. It produces a contribution to the refractive index of the opposite sign with respect to the contribution associated with

the relativistic mass increase of oscillating electrons. Therefore, refractive index does not increase in plasma just after the pulse coming but is set on a characteristic time of the order of the plasma wave excitation time, that is ω_p^{-1}. This effect makes self-focusing of short pulses and forward parts of long pulses more difficult. At the same time the investigation in Refs. [51, 52, 53, 98] shows that it is possible to increase the length of propagation using short laser pulses with a special profile. It is proposed to use laser pulses with a power equal to the critical power for self-focusing and width slowly decreasing with the longitudinal coordinate. As numerical simulation in Ref. [98] shows such pulses propagate in plasma without essential damping more than 10 Rayleigh lengths calculated with respect to the pulse width in its backward part (this width is of the order of k_p^{-1}). In Refs. [51, 52, 53, 98] the following interpretation of such a long pulse propagation was proposed. The forward part of the pulse is subject to diffraction, however as it has a large width the corresponding Rayleigh length is also large. Due to the smooth monotonic growth of the amplitude with the longitudinal coordinate the excitation of the plasma wave is practically absent in the region of the pulse. In the absence of the plasma wave the relativistic self-channeling of the intense backward part of the pulse is effective.

In Ref. [98] essential difficulties of producing such pulse structures with the width varying with the longitudinal coordinate in laboratories are noted. The construction of such structures from a series of partially overlapped ultra-short Gaussian pulses with different widths is proposed. In this case a phase synchronism between the pulses is very desirable (which is not simple to achieve at laboratories). Otherwise, as the numerical simulation in Ref. [98] shows, self-modulation can develop and the pulse can be broken in a number of shorter pulses.

As our simulation shows the pulse structures that are similar by their properties to that suggested in Refs. [51, 52, 53, 98] for relativistic self-channeling arise in result of natural evolution of available in laboratories Gaussian pulses. The structures with weak diffraction damping are produced at the late stage of self-modulation of such pulses with powers in the maximum larger than critical for relativistic self-focusing. They are produced from the first (forward) modulation of the pulse. In the plasma wake excited by this modulation other modulations propagate without an essential diffraction; these modulations are already essentially damped to this moment due to diffraction and energy loose for the plasma wave excitation at previous time. For obtaining such pulse structures it is sufficient and probably the most reasonable to use Gaussian laser pulses that are not too long, with a duration of the order of a few $(3-5)$ plasma periods, and with a power in the central transverse cross-section only a little exceeding the critical power for relativistic self-focusing. The parameters of

the simulation in Fig. 3.14 just correspond to such conditions. Quasi-stationary pulse structures excite regular plasma wakes of large amplitude, very convenient for electron acceleration to large energies.

In Ref. [99] an analytical formalism was developed describing quasi-stationary diffractionless pulse structures in underdense plasma for the pulse duration much less than a plasma period. We consider a generalization of this formalism to be very useful for the case of pulse duration comparable with the plasma period and exceeding it.

We will describe the evolution of the complex envelope of the vector potential of the quasi-monochromatic laser field $a = eA/mc^2$ (linear polarization is supposed for definiteness) and plasma wave scalar potential $\phi = e\Phi/mc^2$ using the following system of equations (see Ref. [54], for instance):

$$\left(2ik_0\frac{\partial}{\partial z} + \Delta_\perp\right)a = k_p^2\phi a, \tag{3.10}$$

$$\left(\frac{\partial^2}{\partial\tau^2} + \omega_p^2\right)\phi = -\omega_p^2\frac{|a|^2}{4}. \tag{3.11}$$

Here it is supposed that $|a| \ll 1$ and the width of the plasma-field structure is larger than k_p^{-1} (we neglect the transverse ponderomotive force that acts on plasma electrons), $\tau = t - z/v_{gr}$, $v_{gr} = c(1 - \omega_p^2/\omega_0^2)^{1/2}$, $\Delta_\perp = (1/r)(\partial/\partial r)(r\partial/\partial r)$ is the transverse Laplacian, $k_0 = \omega_0/c$ is the wave number. This system of equations has self-similar solutions

$$a = 2U(\zeta)f(\tau)\exp[i\gamma f^2(\tau)\omega_p k_p z/2\omega_0], \tag{3.12}$$

$$\phi = V(\zeta)f^2(\tau), \tag{3.13}$$

where $\zeta = k_p r f(\tau)$, $f(\tau) = \exp(\alpha\omega_p\tau)$, α and γ are positive constants. Self-similar functions $U(\zeta)$ and $V(\zeta)$ are the localized solutions of the system of equations

$$\Delta_\perp U - (\gamma + V)U = 0, \tag{3.14}$$

$$\zeta^2\frac{d^2V}{d\zeta^2} + 5\zeta\frac{dV}{d\zeta} + \left(4 + \frac{1}{\alpha^2}\right)V = -\frac{U^2}{\alpha^2} \tag{3.15}$$

(here the operator $\Delta_\perp$ has the expression shown above, in which r is changed by ζ and partial derivatives by full derivatives).

First of all we can mention that the value of the parameter γ determines only the position of the plasma-field structure along z axis as a whole: when we change the value of γ from γ to γ' the plasma-field structure shifts at $\Delta\tau = (1/2\alpha\omega_p)\ln(\gamma/\gamma')$. The only non-stationarity of the solution is in the phase of the high-frequency field

a. The non-stationarity of the phase is associated with an accumulation of the frequency shift along the propagation length (with increase of z). A frequency downshift of the wave field takes place, which is associated with the excitation of the plasma wave (as we will see below). It is possible to find the frequency shift in the pulse cross-section τ, differentiating the phase of the complex envelope a with respect to τ, it is $\Delta\omega = \alpha\gamma f^2(\tau)\omega_p^2 k_p z/\omega_0$.

The width of the pulse structure decreases exponentially with the increase of τ [as $f^{-1}(\tau)$] and the pulse amplitude on the longitudinal axis increases exponentially. At the same time the power in each transversal cross-section conserves $P = (m^2c^5/e^2)(\omega_0^2/\omega_p^2)\int_0^\infty U^2\zeta d\zeta$. The scalar potential ϕ on the longitudinal axis (it is negative) decreases exponentially with τ. It follows from Eq. (3.15) that

$$V(0) = -U^2(0)/(1+4\alpha^2), \tag{3.16}$$

and we obtain that the electron density increases on the axis $\Delta n/n_0|_{r=0} = (\phi + |a|^2/4)|_{r=0} = \exp(2\alpha\omega_p\tau)U^2(0)4\alpha^2/(1+4\alpha^2)$. We found the solutions of Eqs. (3.14) and (3.15) numerically supposing $\gamma = 1$ for different values of α. To find the solutions we used the following method. From the radial symmetry of the problem it follows that

$$\left.\frac{dU}{d\zeta}\right|_{\zeta=0} = 0, \quad \left.\frac{dV}{d\zeta}\right|_{\zeta=0} = 0.$$

For each α we found numerically the solutions of the Cauchy problem for Eqs. (3.14) and (3.15) with these initial conditions at $\zeta = 0$, different values of U at $\zeta = 0$, and condition (3.16). The solution corresponding to the physical problem statement is a localized solution (decreasing at large ζ) that is obtained as a result of the solution of Cauchy problem at some definite value of U at $\zeta = 0$. As we have found for each α only one such a solution of Eqs. (3.14) and (3.15) exists. On Figs. 3.16 (a, b, c, d) as examples the solutions for $\alpha = 0.1$, 0.3, 1, 3 are shown. As it leads from Eq. (3.15) $V = -U^2$ for $\alpha \to 0$ and the localized solution of Eq. (3.14) is the Townes mode [100]. For any α the solution is characterized by an exponential decrease of U at large ζ, $U \sim \exp(-\gamma\zeta)$. V oscillates at large ζ with a decreasing amplitude, $V \sim \zeta^{-2}\cos[\phi_0 + (1/\alpha)\ln\zeta]$. For the plasma wave potential we obtain $\phi \sim (k_p r)^{-2}\cos[\phi_0 + \omega_p\tau + (1/\alpha)\ln(k_p r)]$. The oscillations of ϕ with plasma frequency at large ζ are associated with a plasma wave excitation by the laser pulse. The amplitude and the phase of oscillations depend on the transversal coordinate r. Indeed, as it leads from Eq. (3.12), the time profiles of $|a|^2$ differ for different r only in the value of amplitude (by a coefficient inversely proportional to r^2) and by a shift to the region of larger τ when r increases. It gives that the plasma wave

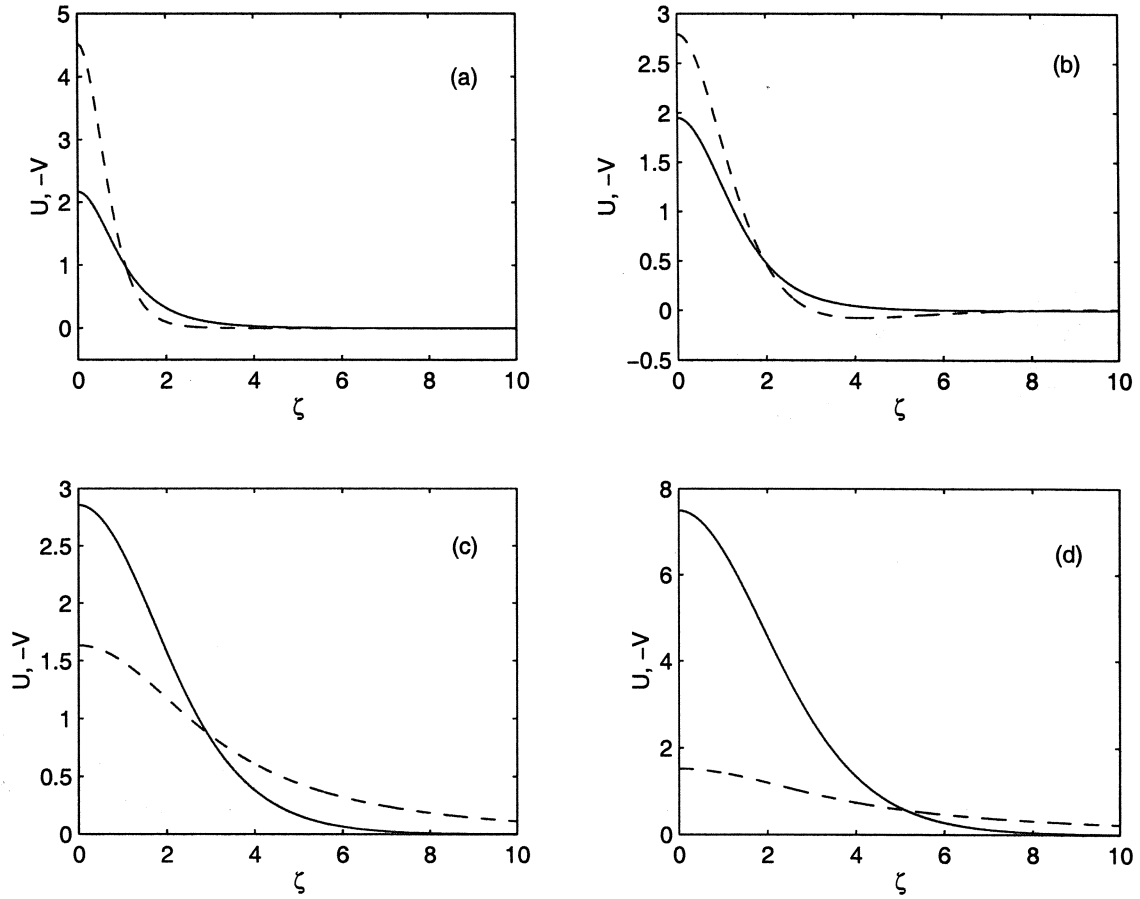

Figure 3.16: The solution of equations for self-similar functions U (solid line) and V (dashed line shows the dependence for $-V$) for $\gamma = 1$ and (a) $\alpha = 0.1$; (b) $\alpha = 0.3$; (c) $\alpha = 1$; (d) $\alpha = 3$.

amplitude is also inversely proportional to r^2 and the phase increases with r. We also show the dependence of P/P_c on α for the solutions found numerically in Fig. 3.17. At $\alpha \gg 1$ $P/P_c \simeq 6.8\alpha^2$ in agreement with the results of Ref. [99].

In Ref. [98] the laser pulse dynamics was investigated using the source-dependent expansion method (it is a sort of aberrationless approximation). In addition to our approximations the pulse in Ref. [98] was approximated by a Gaussian mode in radial direction:

$$A(\xi = ct - z, r, z) = A_0(\xi, z) \exp[-r^2/r_l^2(\xi, z) + \phi_0(\xi, z) + \phi_2(\xi, z) r^2]$$

with width, amplitude, and phase (including dependent on r and r^2 components) depending on ξ and z. In result an equation was obtained for the laser pulse width r_l. It is simple to check that the exponential dependence of r_l on ξ, $r_l \sim \exp(\alpha k_p \xi)$, when the dependence on z is absent, and while the power $P \sim A_0^2 r_l^2$ in each cross-

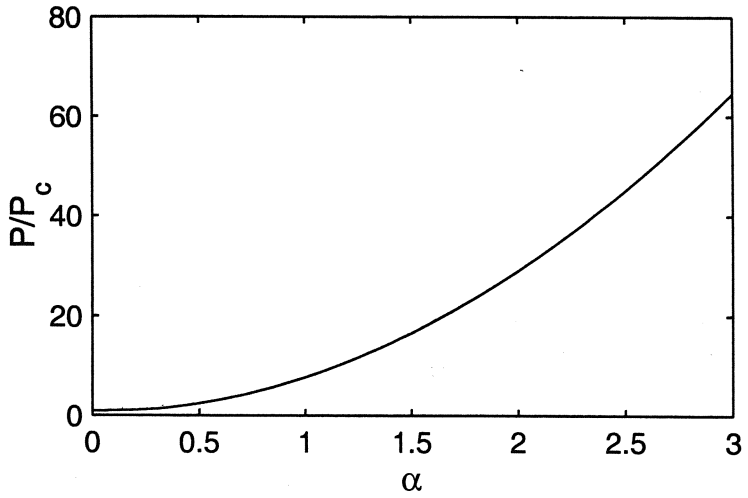

Figure 3.17: Dependence of P/P_c on α for the self-similar solutions found numerically.

section ξ is the same, satisfies this equation for the width. The dependence of P/P_c on α can be found analytically in this case (the expression will include special functions). Qualitatively it is similar to the dependence in Fig. 3.17.

The self-similar solution Eqs. (3.12-3.13) describes the structure of the wide part of the pulse capable to propagate in plasma without diffraction (its width is larger than k_p^{-1}). It must be matched with the solution at the leading edge of the pulse, which is not subject to nonlinear distortion due to the smooth switching-on of the potential ϕ. The local value of Rayleigh length at the leading edge is essentially larger than its value in the intense part of the pulse. The self-similar solution also does not describe the structure of the backward, narrow and most intense part of the pulse.

It is necessary to remind that the paraxial wave equation for the complex amplitude Eq. (3.10) is applicable only for a quasi-monochromatic high-frequency field. The assumption of monochromaticity is not fulfilled, in particular, after the frequency shift is accumulated along the propagation length.

The formalism suggested above indicates a possibility of long diffractionless propagation of the laser pulse with a specific profile in underdense plasma. At the same time it does not answer to the question if the solution, found, is stable with respect to small perturbations. The dynamics of the pulse requires an additional study in what it concerns the accumulation of the frequency shift and dynamics of the backward intense and narrow part of the pulse. The simulations in Refs. [51, 52, 53, 98] and our simulations [see Figs. 3.14 (a), (b)] give answers to these questions. The

results of simulations confirm the stability of such pulse structures with respect to small perturbations, at least for the case of powers a little larger than the critical power for relativistic self-focusing. At the same time the saturation of nonlinearity in the intense part of the pulse, frequency shift, and longitudinal energy transfer lead to the difference of the profile of the complex envelope from that corresponding to the quasi-stationary solution and to its dynamics, slow in a sufficiently underdense plasma on Rayleigh times.

As the results of our numerical simulations show [Fig. 3.14 (a), (b)] quasi-stationary structures are formed in result of a natural evolution of a laser pulse with a Gaussian longitudinal profile, with duration larger than a plasma period and with a maximum power larger than the critical power for relativistic self-focusing. In this case a limitation on the length of such structures is associated with the resonant self-modulation instability of the pulse – the length of its main intense part can not be larger than a plasma period. At the same time an achievement of rather large intensity values and pulse amplitudes $a_0 \sim 1$ becomes already possible on such lengths at small power excess over the critical power for self-focusing. Behind the laser pulse in this case a plasma wave is excited of a large amplitude. The plasma wave structure practically does not change during all the period of existence of the quasi-stationary pulse structure and the phase velocity of the plasma wave is close to the pulse group velocity. As our numerical simulations confirm, the plasma wave excited at long laser pulse propagation in the regime of relativistic self-channeling can be used for electron acceleration up to large energies, including energies in GeV range.

3.3 Ion dynamics in the plasma wake of a short laser pulse

When interaction of ultra-short terrawatt laser pulses with underdense plasmas is studied ion motion is often neglected. As the ion mass is essentially larger than the electron mass, $\delta = m/m_i \ll 1$, it is possible to neglect the oscillatory ion motion in the laser fields with amplitudes $eE/m\omega_0 c \sim 1$, when the oscillatory electron motion is already relativistic. However, strong quasi-stationary electromagnetic fields are excited when such pulses interact with plasma. If the time of the quasi-stationary electric fields existence in plasma and characteristic time of their variation is large enough, these fields pass an essential momentum to plasma ions. When the laser pulses with a power larger than critical for relativistic self-focusing are self-focused in plasma, radial Coulomb fields of charge separation are produced. These fields accelerate ions in the transverse direction and lead to the formation of a channel in plasma. Such plasma channels were observed in experiments, theoretical estimates describing the channel formation in plasma due to the ponderomotive action of the laser field were also obtained [33, 101, 102, 103].

In the present investigation we consider another aspect, important for understanding ion dynamics in plasma. Intense laser pulses propagating in underdense plasma excite fast plasma waves. While the energy of the laser pulse used for the plasma wave excitation is transformed into the energy of oscillatory electron motion and the energy of the plasma fields, the momentum passes to plasma ions. Besides, the ponderomotive force of the plasma wave displaces electrons in the radial direction. The electric field of the charge separation, that is produced, acts on plasma ions. As we will see, it leads also to the formation of an ion channel in plasma. In this part we consider, in fact, two problems that supplement each other. In Sec. 3.3.1 we study the longitudinal momentum transferred by a short laser pulse to ions. This investigation is performed in 1D geometry. The longitudinal ion acceleration takes place in this case simultaneously with the plasma wave excitation and the value of ion momentum is determined by the plasma wave amplitude. In Sec. 3.3.2 we investigate the transverse ion momentum in the plasma wake excited by the laser pulse. We investigate this problem in 2D geometry (with axial and plane symmetry), and the case is considered when the length of the plasma wake behind the pulse is much larger than the laser pulse length (later is of the order of a plasma period). In this case ion acceleration in the transverse direction (due to the effects, discussed above) in the wake region is more essential than in the pulse region. Ion

acceleration in the transverse direction leads to the formation of a plasma channel.

3.3.1 Longitudinal ion momentum in the plasma wake

3.3.1.1 Basic equations and quasistatic approximation

We will investigate the laser pulse momentum transfer to plasma in this Section in 1D geometry. According to the hydrodynamic theory of cold plasma the low-frequency plasma response is described on the basis of the set of equations (see, for example, Ref. [68]):

$$\frac{\partial n_e}{\partial t} + \frac{\partial}{\partial z}(n_e v_e) = 0, \tag{3.17}$$

$$\frac{\partial p_e}{\partial t} + v_e \frac{\partial p_e}{\partial z} = eE - \frac{mc^2}{4\gamma}\frac{\partial |a|^2}{\partial z}, \tag{3.18}$$

$$\frac{\partial n_i}{\partial t} + \frac{\partial}{\partial z}(n_i v_i) = 0, \tag{3.19}$$

$$\frac{\partial v_i}{\partial t} + v_i \frac{\partial v_i}{\partial z} = \frac{e_i}{m_i} E, \tag{3.20}$$

$$\frac{\partial E}{\partial z} = 4\pi(en_e + e_i n_i), \tag{3.21}$$

where E is the charge separation electric field, e, m, n_e, v_e and e_i, m_i, n_i, v_i are the charges, masses, densities and velocities of electrons and ions respectively, p_e is the momentum of the electron fluid per particle, related to the electron velocity by the formula $v_e = p_e/(m\gamma)$, where

$$\gamma = \left[1 + \left(\frac{p_e}{mc}\right)^2 + \frac{|a|^2}{2}\right]^{1/2}. \tag{3.22}$$

Here c is the speed of light, a is the slowly varying amplitude (envelope) of the dimensionless high-frequency electron momentum in the laser field. The ion motion is treated as nonrelativistic and their high-frequency motion is entirely ignored. From the set of Eqs. (3.17)-(3.21) the energy and momentum conservation laws follow:

$$\frac{\partial W}{\partial t} + \frac{\partial S}{\partial z} = \frac{mc^2 n_e}{4\gamma}\frac{\partial |a|^2}{\partial t}, \tag{3.23}$$

$$\frac{\partial P}{\partial t} + \frac{\partial T}{\partial z} = -\frac{mc^2 n_e}{4\gamma}\frac{\partial |a|^2}{\partial z}, \tag{3.24}$$

where W is the energy density

$$W = n_e mc^2\gamma + n_i \frac{m_i v_i^2}{2} + \frac{E^2}{8\pi}, \tag{3.25}$$

the energy density flow S is

$$S = n_e v_e mc^2 \gamma + n_i v_i \frac{m_i v_i^2}{2}, \tag{3.26}$$

the momentum density P is

$$P = n_e p_e + m_i n_i v_i, \tag{3.27}$$

the momentum density flow T is

$$T = n_e p_e v_e + m_i n_i v_i^2 - \frac{E^2}{8\pi}. \tag{3.28}$$

The right hand side terms in Eqs. (3.23) and (3.24) determine the energy and momentum which the laser pulse loses to generate the low-frequency plasma response.

If the energy and shape of a laser pulse vary insignificantly over the time of the order of the pulse duration, it is possible to consider all the values characterizing the plasma response as functions of the variable $\xi = v_g t - z$ only, where v_g is the group velocity of the laser pulse (the so called quasistatic approximation [35, 36]). Below we will suppose that $v_g \approx c$; as we have already mentioned in Introduction, it makes the plasma wave breaking impossible and corresponds really to limitations on the plasma wave amplitude [20, 21, 71].

In this approximation Eqs. (3.17)-(3.20) take the form

$$n_e \left(1 - \frac{v_e}{c}\right) = n_{e0}, \tag{3.29}$$

$$\gamma - \frac{p_e}{mc} = \psi, \tag{3.30}$$

$$n_i \left(1 - \frac{v_i}{c}\right) = n_{i0}, \tag{3.31}$$

$$\left(1 - \frac{v_i}{c}\right)^2 - 1 = -2\epsilon(\psi - 1), \tag{3.32}$$

where n_{e0} and n_{i0} are the electron and ion densities taken ahead of the pulse. They have to satisfy the plasma neutrality condition $n_{e0} = Z n_{i0}$, where Z is the ion charge number. The quantity $\epsilon = (Zm/m_i) \ll 1$ is a small parameter and ψ is the potential determined by the relation:

$$\frac{eE}{mc^2} = -\frac{d\psi}{d\xi} \tag{3.33}$$

and is equal to unity ahead of the pulse.

Using Eqs. (3.29)-(3.33) we reduce Eq. (3.21) to the form

$$\frac{d^2\psi}{d\eta^2} = \frac{1}{2}\left(1 + \frac{1 + |a|^2/2}{\psi^2}\right) - 1 - \epsilon(\psi - 1), \tag{3.34}$$

where $\eta = k_p\xi$, $k_p = \omega_p/c$, and $\omega_p = (4\pi e^2 n_{e0}/m)^{1/2}$ is the plasma frequency, we have also performed an expansion in the exact equation in power series of the small parameter $\epsilon = (Zm/m_i) \ll 1$ and have left only the terms linear with respect to ϵ. For the case of immobile ions ($\epsilon = 0$) Eq. (3.34) is well investigated (see, for example, Refs. [35, 36, 46, 104, 105, 106]).

Keeping in mind that the laser pulse is absent at $\eta \to -\infty$, we integrate Eq. (3.34) with the result

$$\left(\frac{d\psi}{d\eta}\right)^2 + \psi + \frac{1}{\psi} - 2 + \epsilon(\psi - 1)^2 = -\int_{-\infty}^{\eta} d\eta' \frac{|a(\eta')|^2}{2} \frac{d}{d\eta'}\left[\frac{1}{\psi(\eta')}\right]. \tag{3.35}$$

All the hydrodynamical quantities characterizing the plasma response to the laser pulse can be expressed via the potential ψ:

$$\gamma = \frac{1}{2\psi}\left(1 + \psi^2 + \frac{|a|^2}{2}\right), \tag{3.36}$$

$$\frac{n_e}{n_{e0}} = \frac{\gamma}{\psi} = \frac{1}{2\psi^2}\left(1 + \psi^2 + \frac{|a|^2}{2}\right), \tag{3.37}$$

$$\frac{p_e}{mc} = \gamma - \psi = \frac{1}{2\psi}\left(1 - \psi^2 + \frac{|a|^2}{2}\right), \tag{3.38}$$

$$\frac{v_e}{c} = 1 - \frac{\psi}{\gamma} = \frac{1 - \psi^2 + |a|^2/2}{1 + \psi^2 + |a|^2/2}, \tag{3.39}$$

$$\frac{n_i}{n_{i0}} = \frac{1}{\sqrt{1 - 2\epsilon(\psi - 1)}}, \tag{3.40}$$

$$\frac{v_i}{c} = 1 - \sqrt{1 - 2\epsilon(\psi - 1)}. \tag{3.41}$$

Also more complicated functions (3.25)-(3.28) can be expressed in terms of ψ (see Ref. [107], for the region behind the pulse we will write the corresponding expressions below). The ion contributions to these hydrodynamic expressions are negligibly small for $\epsilon \to 0$ except the expression for the ion momentum density, that is finite for $\epsilon = 0$:

$$P_i = m_i n_i v_i = n_{e0} mc(\psi - 1).$$

Thus, we can conclude that ion motion plays an essential role only for the momentum density of the plasma wave. Below we will neglect the small corrections proportional to ϵ for the other quantities, as well as in the equations for ψ.

3.3.1.2 The energy and momentum of the plasma wake

Let the trailing edge of the laser pulse be placed at $\eta = 0$. Then, in the region $\eta > 0$, the laser pulse is absent and only generated nonlinear plasma wave may exist there. Neglecting the ion motion where its influence is weak, we obtain from Eqs. (3.25)-(3.28) the following relatively simple expressions:

$$U = \frac{1-\psi^4}{4\psi^3} + I, \tag{3.42}$$

$$N = \frac{1-\psi^4}{4\psi^3}, \tag{3.43}$$

$$Q = Q_e + Q_i = \frac{1-\psi^4}{4\psi^3} + (\psi - 1), \tag{3.44}$$

$$G = \frac{1-\psi^4}{4\psi^3} + (\psi - 1) - I, \tag{3.45}$$

where the value I determines the result of the laser pulse action on a plasma,

$$I = -\frac{1}{4}\int_{-\infty}^{0} d\eta |a(\eta)|^2 \frac{d}{d\eta}\left[\frac{1}{\psi(\eta)}\right]. \tag{3.46}$$

This quantity may also be rewritten in another form:

$$I = \frac{1}{4}\int_{-\infty}^{0} d\eta \frac{1}{\psi(\eta)}\frac{d}{d\eta}|a(\eta)|^2. \tag{3.47}$$

It should be noted that the expressions for Q and G contain the same term $\psi - 1$, though in Eq. (3.44) it originates from the ion motion, while in Eq. (3.45) it is of the electron origin. The straightforward substitution of Eqs. (3.42)-(3.45) into Eqs. (3.23) and (3.24), taken in the quasistatic approximation, clearly demonstrates that the conservation laws are satisfied.

Behind the laser pulse the nonlinear plasma wave is a periodical function of η. This means that all the hydrodynamic variables characterizing this wave may be represented as a sum of two parts. One of them is purely oscillatory and another one is independent on η. The latter one we shall call the average or mean part of a variable. However, it can be shown that for such quantities, as the energy density flow (3.43), the electron part of the momentum density in Eq. (3.44), and the current density, the average parts are equal to zero. As an example, let us consider the energy density flow (3.43), presenting it in the form

$$N = \frac{1-\psi^2}{2\psi^2} \times \frac{1+\psi^2}{2\psi}.$$

Eqs. (3.34) and (3.35), written for $\epsilon = 0$, in the region $\eta > 0$, where $|a|^2 = 0$, give

$$\frac{1-\psi^2}{2\psi^2} = \frac{d^2\psi}{d\eta^2}, \quad \frac{1+\psi^2}{2\psi} = 1 - \frac{1}{2}\left(\frac{d\psi}{d\eta}\right)^2 + I. \tag{3.48}$$

Using these equations, we can rewrite N in the form:

$$N = \frac{d}{d\eta}\left[(1+I)\frac{d\psi}{d\eta} - \frac{1}{6}\left(\frac{d\psi}{d\eta}\right)^3\right]. \tag{3.49}$$

Due to the periodicity of ψ (and therefore, its derivatives) the mean part of N equals zero. In particular, it means, that the electron part of the momentum density is purely oscillatory.

Analogously, one can prove that the average part of the electric current density is zero. Really, according to Eqs. (3.37), (3.39)-(3.41), and (3.34), in the wake-field region ($\eta > 0$), the dimensionless current density is:

$$J = \frac{en_e v_e + e_i n_i v_i}{en_{e0}c} = \frac{1}{2\psi^2}(1+\psi^2) - \frac{1}{\sqrt{1-2\epsilon(\psi-1)}} = \frac{d^2\psi}{d\eta^2}. \tag{3.50}$$

According to Eq. (3.44), the ion part of the momentum density of a plasma wave is

$$Q_i = \psi - 1. \tag{3.51}$$

Let us consider the averaged Eq. (3.51) integrating this expression over the plasma wavelength and dividing the result of integration by the wavelength.

The dimensionless plasma wavelength η_0 may be found by means of Eq. (3.48) and has the form:

$$\eta_0 = 2\int_{\psi_-}^{\psi_+} \frac{d\psi}{(d\psi/d\eta)} = 2\int_{\psi_-}^{\psi_+} \frac{d\psi\sqrt{\psi}}{\sqrt{(\psi_+-\psi)(\psi-\psi_-)}}, \tag{3.52}$$

where ψ_+ and ψ_- are the maximum and minimum values of ψ which may be found from Eqs. (3.48) as:

$$\psi_\pm = 1 + I \pm \sqrt{(1+I)^2 - 1}. \tag{3.53}$$

Following the definition given above, the average ion momentum density is

$$\overline{Q_i} = \frac{2}{\eta_0}\int_{\psi_-}^{\psi_+} \frac{d\psi\cdot\psi\sqrt{\psi}}{\sqrt{(\psi_+-\psi)(\psi-\psi_-)}} - 1. \tag{3.54}$$

The integrals in Eqs. (3.52) and (3.54) may be reduced to the complete elliptic integrals of the first [$\mathtt{K}(k)$] and second [$\mathtt{E}(k)$] kind [108]. As a result, we have:

$$\overline{Q_i} = \frac{2}{3}(\psi_+ + \psi_-) - 1 - \frac{\psi_-}{3}\frac{\mathtt{K}(k)}{\mathtt{E}(k)}, \tag{3.55}$$

where $k^2 = (\psi_+ - \psi_-)/\psi_+ = 1 - \psi_-^2$.

An essential simplification of Eq. (3.55) is achieved in the limit of small magnitudes of I ($I \ll 1$), corresponding to the small amplitudes of plasma waves $[(\psi_+ - \psi_-)/\psi_+ = k^2 \ll 1]$ for which $\psi_\pm \simeq 1 \pm (2I)^{1/2}$. Using the expansion series for the complete elliptic integrals in the limit of small k^2 [108], we find after long routine calculations:

$$\overline{Q_i} \simeq \frac{3}{2} I. \tag{3.56}$$

Another way to simplify (3.55) is to assume a square form of the laser pulse. In this case, from Eq. (3.46), it follows without any restriction that

$$I = \frac{a_0^2}{4}\left[1 - \frac{1}{\psi(0)}\right], \tag{3.57}$$

where $a_0^2 \equiv |a|^2$ characterizes the dimensionless intensity of the laser radiation and $\psi(0)$ is the potential at the trailing edge of the pulse. The maximum possible value of $\psi(0)$ is

$$\psi(0) = \psi_+ = 1 + a_0^2/2 \tag{3.58}$$

and it is reached if the laser pulse length is equal to an odd number of the half plasma wavelengths [46]. For such pulses from Eqs. (3.57) and (3.58) it follows that

$$I = \frac{a_0^4}{8}\frac{1}{1 + a_0^2/2}. \tag{3.59}$$

Using Eqs. (3.59) and (3.53) we can rewrite Eq. (3.55) as

$$\overline{Q_i} = \frac{1}{3\,(1 + a_0^2/2)}\left[1 + \frac{a_0^2}{2} + \frac{a_0^4}{2} - \frac{\mathrm{K}(k_e)}{\mathrm{E}(k_e)}\right], \tag{3.60}$$

where $k_e^2 = 1 - (1 + a_0^2/2)^{-1}$. A further simplification of Eq. (3.60) is possible for small or large a_0^2. In the former case of a low-intensity laser pulse ($a_0^2 < 1$) we get:

$$\overline{Q_i} \simeq \frac{3}{16}\frac{a_0^4}{1 + a_0^2/2}, \tag{3.61}$$

which is in full agreement with the result (3.56) for $a_0^2 \ll 2$.

For a relativistically strong laser pulse with $a_0^2 > 1$, it follows from Eq. (3.60) that

$$\overline{Q_i} = \frac{a_0^2 - 1}{3} + \frac{2}{3a_0^2}\left[2 - \ln\left(\frac{8}{a_0^2}\right)\right]. \tag{3.62}$$

Fig. 3.18 shows the plots for $\overline{Q_i}$ as a function of a_0^2, corresponding to Eqs. (3.60)-(3.62). One can see from this picture that the formula (3.61) may serve as a sufficiently good approximation to Eq. (3.60) for $a_0^2 < 1$ as well as for $a_0^2 > 1$.

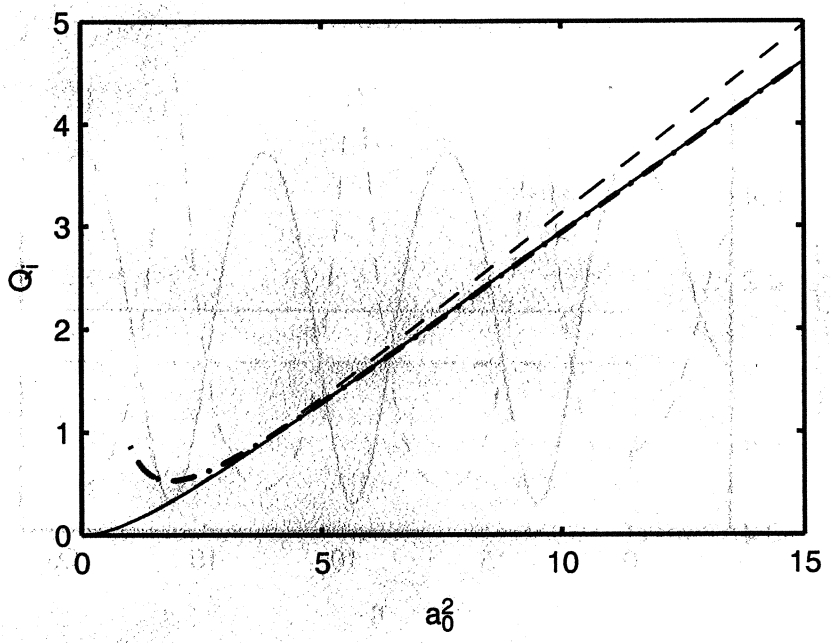

Figure 3.18: The average ion momentum density in the wake $\overline{Q_i}$ as a function of laser intensity a_0^2: solid line corresponds to Eq. (3.60), dashed curve to Eq. (3.61), and dash-dotted curve to Eq. (3.62).

3.3.1.3 Numerical simulations

In order to confirm the analytical results and to treat pulse profiles more general than the square shaped pulse profile we carried out some numerical simulations using the two-dimensional axially-symmetrical code Wake. We began with a square laser pulse profile in longitudinal direction just to have conditions in which the simple analytical results have been obtained. The radial pulse profile was Gaussian with the radial size R strongly exceeding plasma wavelength ($k_pR = 31.4$), to approximate the one-dimensional case. The parameter ϵ was taken equal to $1/1836$ (the hydrogen plasma).

Fig. 3.19 shows the dimensionless momentum density of ions and electrons for a short ($k_pL = 3.5$, where L is the pulse length) intense ($a_0^2 = 1$) laser pulse. This pulse length is approximately equal to half a plasma wavelength inside the pulse. In Fig. 3.19 the average magnitudes of ion and electron momenta are also shown. It can be seen that the magnitude of average electron momentum density is quite small (practically it is zero), while the average ion momentum density is 0.1244 in excellent agreement with estimation equal 0.125 obtained by means of Eq. (3.61).

The dimensionless current density is shown in Fig. 3.20 for the same parameters as in Fig. 3.19. The average current density on the pulse axis differs slightly from

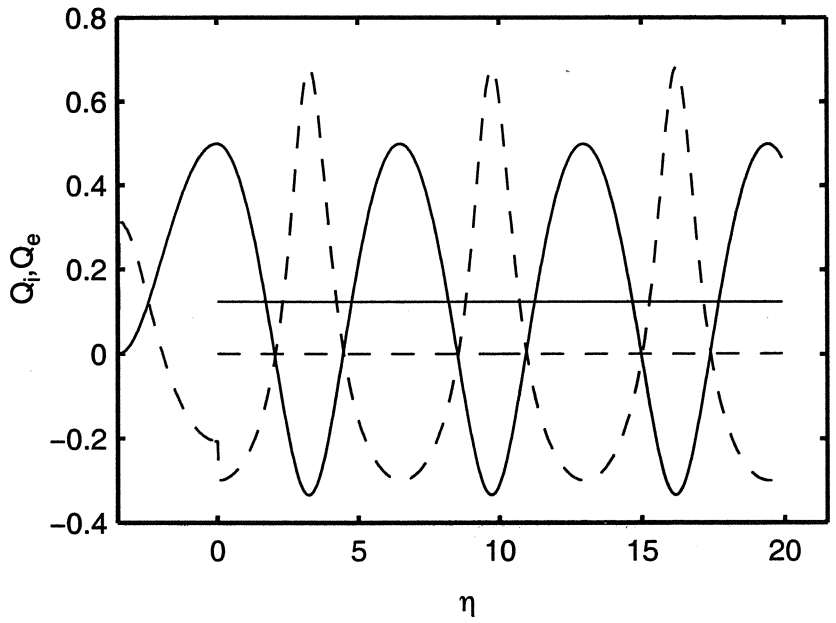

Figure 3.19: The dimensionless ion (solid line) and electron (dashed line) momentum densities as the functions of variable η for a short ($k_pL = 3.5$) intense ($a_0^2 = 1$) square profile laser pulse. The straight lines show the mean magnitudes of corresponding values in the wake region.

zero $\sim 10^{-3}$. This effect is due to two-dimensional geometry used in numerical simulations. We have verified that the average axial current increased as the laser pulse radius decreased.

In Fig. 3.21, the ion momentum density is shown for a laser pulse with Gaussian axial profile. The width of the pulse was $k_pR = 31.4$, as before, while the length of the pulse was taken equal to $k_pL = 3.14$ (FWHM in intensity). The maximum value of a_0^2 was 3. It is evident that non-zero mean ion momentum density also arises here, and its value is determined by the amplitude of the plasma wave.

3.3.1.4 Discussions

The process of the laser pulse momentum transfer to ions can be qualitatively explained as follows, for the simplicity, for the case of a rectangular laser pulse. The ponderomotive force, acting at the leading edge of a laser pulse, pushes the plasma electrons forward and leads to the increase of electron density. The charge separation electric field begins to accelerate ions in the direction of the laser pulse propagation. Thus, the initial momentum produced by the ponderomotive force at the pulse leading edge is conserved and transformed into the ion momentum. At

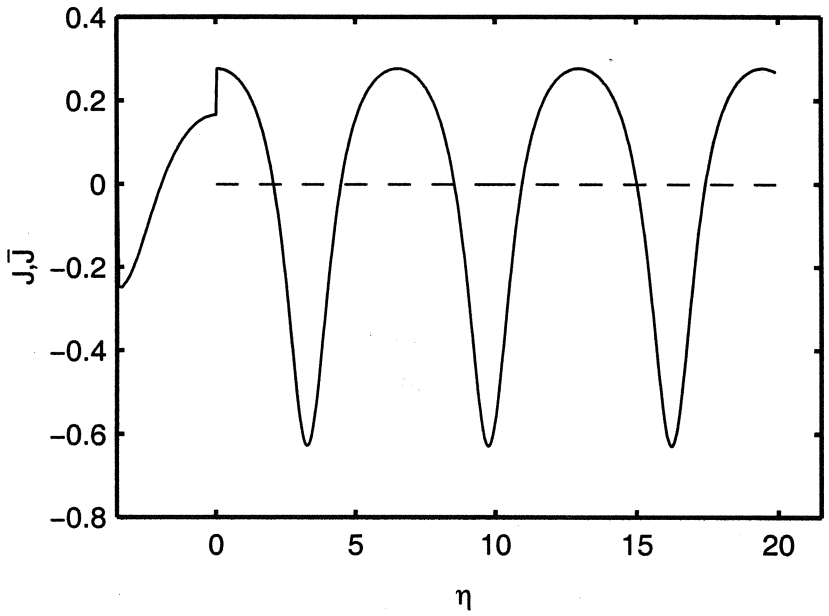

Figure 3.20: The dimensionless current density J versus η (solid line) for a square pulse with the same parameters as in Fig. 3.19. $\overline{J}$ (dashed line) is the mean value of the current.

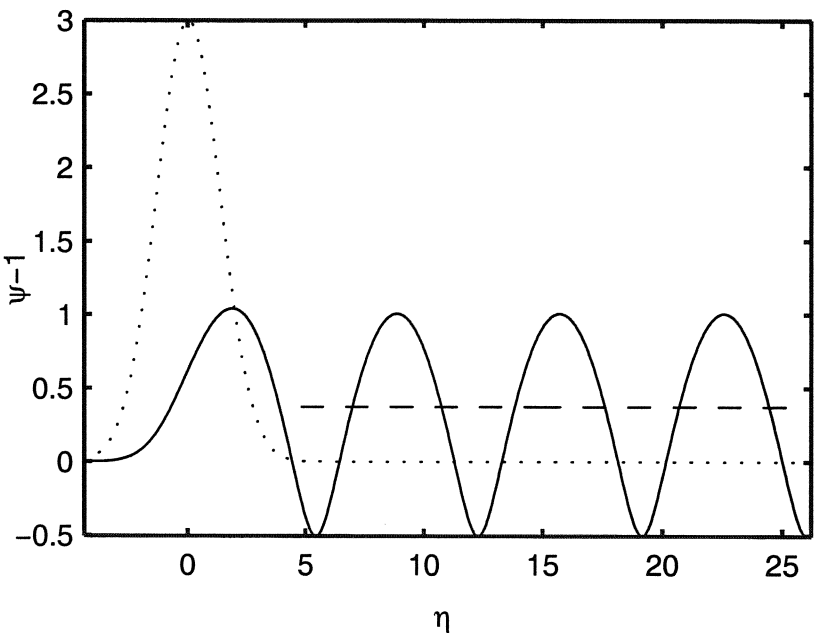

Figure 3.21: The ion momentum density (solid line) as a function of variable η for a Gaussian laser pulse, shown by dotted line [$a_0^2 = 3$, the pulse length $k_pL = 3.14$ (FWHM in intensity)]. The dashed line shows the averaged ion momentum density.

the trailing edge of the laser pulse the ponderomotive force pushes the electrons backward. The electrons obtain the momentum directed opposite to the initial momentum (see Fig. 3.19). However, the electron density at the trailing edge of the laser pulse is less than that at the leading edge. Hence, the momentum passed to electrons at the trailing edge is less than the momentum obtained by them at the leading edge of the pulse. As a result of such two-step action of ponderomotive forces, electrons as well as ions obtain momentum behind the pulse. In the limit of weak laser pulse, $a_0^2 < 1$, these momenta are $Q_e = -(a_0^2/2)[1 - (3/4)a_0^2]$ and $Q_i = a_0^2/2$ respectively. Thus, the momentum is conserved in the form of average currentless motion of the whole plasma including ions. Moreover, it turns out that ions are the real carriers of the momentum.

It is interesting to mention another particularity of the laser pulse momentum transfer to plasma. The transfer of the energy and momentum to the wake is determined by Eqs. (3.42)-(3.45). Averaging them over a plasma period, we obtain:

$$\overline{U} = I, \overline{N} = 0. \tag{3.63}$$

$$\overline{Q} - \overline{G} = I. \tag{3.64}$$

Because of absence of the average energy density flow in the cold plasma model, the average energy density of the wake $\overline{U}$ is equal to I, characterizing the amount of work produced by the laser pulse in plasma. Unlike the average energy density flow, the average momentum density flow is not equal to zero [see, also, Eq. (3.45)]. According to Eq. (3.64) only the difference between the average momentum density $\overline{Q} \approx \overline{Q_i}$ and average momentum density flow $\overline{G}$ equals the momentum lost by the laser pulse. In general case the expressions for $\overline{Q}$ and $\overline{G}$ are quite complicated [see, for example, Eq. (3.54)], but for nearly linear wake ($I < 1$) $\overline{Q} \approx (3/2)I$ [see, Eq. (3.56)], and consequently $\overline{G} = (1/2)I$. Note that opposite to the average momentum of the wake, which is carried mostly by ions, the average momentum density flow is determined by electrons.

To estimate the ion velocity v_i and energy $w_i = m_i v_i^2/2$, we use Eq. (3.61). In accordance with the determination of Q_i we find for hydrogen ions that $v_i = 1.8 \cdot 10^6$ cm/s, $w_i \simeq 2$ eV for $a_0^2 = 1$. For $a_0^2 = 10$ the corresponding values are $4.5 \cdot 10^7$ cm/s and 1.3 KeV. Note, that for modern experiments, where the relativistic intensities are reached in extremely small focal spots, the radial effects are evidently more essential than the axial one considered above.

3.3.2 Transverse ion momentum in the plasma wake

In this section we consider transverse ion momentum in the plasma wake excited by a short ultra-intense laser pulse. It is well known that ions can be accelerated in the direction perpendicular to the laser axis by the electric field of charge separation, that is produced after electron displacement by the ponderomotive force of the laser pulse [33, 101, 102, 103]. At the same time short laser pulses excite plasma waves of large amplitudes. Till now influence of these plasma waves on ion acceleration was not taken into account. In our investigation we will consider only the case of laser pulses with duration of the order of half a plasma period, which are supposed to be used in the standard scheme of electron acceleration in plasma. Due to their small duration ion acceleration in the pulse region is rather weak. At the same time such pulses excite large amplitude plasma wakes. As we will see, ponderomotive force of the plasma waves exists as well and it is sufficient to displace electrons transversally. The transversal electric field of charge separation acts on ions and leads to formation of a channel in plasma.

3.3.2.1 Analytical description of ion channel formation

An analytical description of the initial stage of ion channel formation due to the ponderomotive force of the plasma wake is possible using the linear hydrodynamic theory of cold plasma. The low-frequency (as compared to the laser frequency) velocity of the electron fluid $\mathbf{v}$ is described by the equation [109]

$$\frac{\partial^2 \mathbf{v}}{\partial t^2} + \omega_{p0}^2 \left[1 + \nu(\mathbf{r}, t)\right] \mathbf{v} + c^2 \nabla \times \nabla \times \mathbf{v} = -\frac{c^2}{4} \frac{\partial}{\partial t} \nabla |a|^2, \tag{3.65}$$

where $\omega_{p0} = (4\pi n_{e0} e^2/m)^{1/2}$ is the unperturbed electron plasma frequency; m and $-e$ are the electron mass and charge, respectively; n_{e0} is the electron density of plasma ahead of the laser pulse where the plasma is supposed to be neutral and $n_{e0} = z n_{i0}$ (z and n_{i0} are the ion charge number and density, respectively). The right hand side of Eq. (3.65) determines the action of the ponderomotive force of the laser pulse, where a is the normalized amplitude of the vector potential ($a = eA/mc^2$). The quantity $\nu = \delta n_e(\mathbf{r}, t)/n_{e0} = \delta n_i/n_{i0}$ is the dimensionless quasisteady and quasineutral plasma density perturbation resulting from the ponderomotive force of the wakefield. Behind the laser pulse ν is governed by the equation

$$\frac{\partial^2 \nu}{\partial t^2} = \frac{\delta}{2} \Delta_\perp \langle v^2 \rangle, \tag{3.66}$$

where $\delta = (zm/m_i) \ll 1$ and m_i is the ion mass; $\Delta_\perp$ is the transversal part of Laplace operator; the brackets denote the averaging over plasma oscillations which

are supposed to be high-frequency as compared with the temporal variation of ν. The set of Eqs. (3.65) and (3.66) is valid for $|\mathbf{v}| \ll c$, $|a| < 1$, and $\nu \ll 1$. Besides, the axial scale length of ν variation is supposed to be essentially larger than the radial one.

For an axially-symmetric laser pulse moving along the z axis, the electron velocity has a radial component v_r and an axial component v_z. In the quasistatic approximation [35, 36] they depend on $\xi = ct - z$ and r, where the laser pulse group velocity is taken to be equal to the speed of light. Following [109], we introduce an auxiliary quantity $\phi = |a|^2/4 - v_z/c$. Then the radial velocity is expressed via ϕ as

$$\frac{v_r}{c} = -\frac{1}{k_p^2}\frac{\partial^2\phi}{\partial r \partial \xi}, \tag{3.67}$$

where $k_p^2 = k_{p0}^2[1 + \nu(r,\xi)]$ and $k_{p0} = \omega_{p0}/c$. In the general case the equation for ϕ is written in Ref. [109]. A more simple form can be obtained for a laser pulse with a focal spot size larger than k_{p0}^{-1}:

$$\frac{\partial^2\phi}{\partial\xi^2} + k_{p0}^2[1 + \nu(r,\xi)]\phi = k_p^2\frac{|a|^2}{4}. \tag{3.68}$$

In terms of ϕ, Eq. (3.66) is given by:

$$\frac{\partial^2\nu}{\partial\xi^2} = \frac{\delta}{2}\Delta_\perp\left(\langle\phi^2\rangle + \frac{1}{k_p^4}\left\langle\left(\frac{\partial^2\phi}{\partial r\partial\xi}\right)^2\right\rangle\right). \tag{3.69}$$

The first and second terms in the right hand side of Eq. (3.69) describe the effects arising from the axial and radial components of the wake electric field, respectively.

Here we are interested in the case of a short laser pulse with duration of the order of ω_{p0}^{-1}, exciting a long wakefield tail. In the frame of our approximation, when $|a| < 1$, the value of ϕ is of the order of $|a|^2/4$. Therefore, the ratio of the ion velocity due to the wakefield action to the ion velocity due to the laser pulse itself is roughly given by $N|a|^2/4$, where N is the number of plasma wavelengths in the wake tail. When $N > (|a|^2/4)^{-1}$ the effect due to the wakefield is more important than that due to the laser pulse itself.

To show the main features of the new physical effect discussed here, we neglect the influence of the ion density perturbations on the wake-field structure itself and limit ourselves by linear approximation. We consider a laser pulse with a Gaussian form $a = a_0\exp(-r^2/r_0^2 - \xi^2/\xi_0^2)$, where r_0 and ξ_0 are the width and length of the pulse respectively. Then, behind the pulse the solution of Eq. (3.68), vanishing ahead of the pulse, has the form [3, 10]

$$\phi = \sqrt{\frac{\pi}{2}}\frac{a_0^2}{4}\eta_0\exp\left[-\frac{2\rho^2}{\rho_0^2} - \frac{\eta_0^2}{8}\right]\sin\eta, \tag{3.70}$$

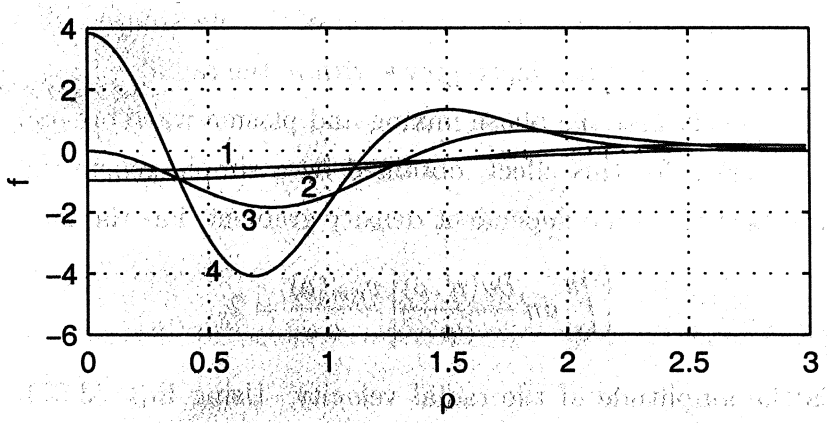

Figure 3.22: The radial form of channels produced by the laser pulses with different widths. The curves 1-4 correspond to $\rho_0 = 4.5$; 3.2; 2; 1.6, respectively.

where we introduced the dimensionless variables $\eta = k_{p0}\xi$ and $\rho = k_{p0}r$ and denoted by ρ_0 and η_0 the dimensionless width and length of the pulse, respectively.

Substituting (3.70) into (3.69), we find after simple calculations

$$\nu = \frac{\pi\delta a_0^4\eta_0^2}{256}\eta^2 e^{-\eta_0^2/4} f(\rho), \tag{3.71}$$

where the function $f(\rho)$, determining the radial profile of the plasma channel created by the ponderomotive action of the wakefield, is given by

$$f(\rho) = -\frac{16}{\rho_0^2} e^{-4\frac{\rho^2}{\rho_0^2}} \left[\left(1 - \frac{4}{\rho_0^2}\right) - 4\frac{\rho^2}{\rho_0^2}\left(1 - \frac{12}{\rho_0^2}\right) - 64\frac{\rho^4}{\rho_0^6} \right]. \tag{3.72}$$

In Fig. 3.22, we have plotted $f(\rho)$ for various values of ρ_0. It is seen that the plasma density has a minimum on the axis only for relatively wide laser pulses with $\rho_0 > 2\sqrt{2}$. For narrower pulses, the plasma density has an on-axis maximum which becomes higher when the pulse narrows. This effect is due to the radial structure of ponderomotive forces produced by the axial and radial components of the wakefield. The amplitude of the axial electric field has a maximum on the axis. So, the corresponding ponderomotive force expels the plasma electrons from the axis providing the density lowering there. On the other hand, the amplitude of radial electric field is zero on the axis and reaches a maximum at $\rho = \rho_0/2$. Hence, the corresponding ponderomotive force expels plasma electrons from a cylindrical surface at the radius $\rho_0/2$, compressing them near the axis and producing an annular channel.

It was shown earlier [20], that electron oscillations in a nonuniform plasma are subject to the phenomenon of fine-scale phase mixing. A multi-stream electron

motion arises in some time after the excitation of the electron oscillations. In our problem, as the plasma channel depth grows with η, the radial density gradient also increases with a result that the phase mixing and plasma wave breaking arise. The approximate criterion for this effect, obtained by a simple generalization of Refs. [20, 71] for the case of a time dependent density gradient, has the form

$$\left| \int_0^\eta d\eta' \frac{\partial \nu(\eta', \rho)}{\partial \rho} \right| \frac{v_{r,m}(\rho)}{c} = 2, \tag{3.73}$$

where $v_{r,m}$ is the amplitude of the radial velocity. Using Eqs. (3.67), (3.70), and (3.71), we obtain from (3.73) that the axial position of wave-breaking point is given by

$$\eta = \frac{8(3)^{1/3}(2)^{5/6}(\pi)^{-1/2}}{a_0^2 \sqrt[3]{\delta}} \frac{e^{\eta_0^2/8}}{\eta_0} [\mathcal{F}(\rho)]^{-1/3}, \tag{3.74}$$

where

$$\mathcal{F}(\rho) = \frac{4}{\rho_0^2} \left| \rho \frac{df(\rho)}{d\rho} e^{-2\rho^2/\rho_0^2} \right|. \tag{3.75}$$

Eq. (3.74) determines the position of the wakefield break point in the (η, ρ) plane. As we will see below from the results of our numerical simulations, the plasma wave is destroyed rather fast (during a few plasma periods) after the appearance of the multi-stream electron motion. Hence, the most interest presents the plasma wave break point, which is situated at the shortest distance from the laser pulse. To find this point $\eta_{\min} = \eta_*$ we have to know the maximum of the function (3.75). It is located at the point ρ_* where the derivative of (3.75) is zero. Substituting ρ_* in Eq. (3.74), we find η_*. This routine procedure, however, results in a quite complicated algebraic equation which we solved numerically and compared with the results of simulations.

3.3.2.2 Remarks about numerical simulations using the hydrodynamic code

Numerical simulations were performed with the axially symmetrical fluid code [110]. They show the plasma wave dynamics and plasma channel formation before the wavebreaking. We will discuss rather briefly the results of this numerical simulation, that was performed without direct participation of the author of the thesis. More complete information on the results of these simulations and their comparison with the theoretical estimates presented above can be found in Ref. [111]. The simulation was performed for the mass ratio $\delta = 1/2000$. This simulation shows the formation of the annular plasma channels for narrow laser pulses and channels with a plasma density minimum on the axis for sufficiently wide pulses. The results for

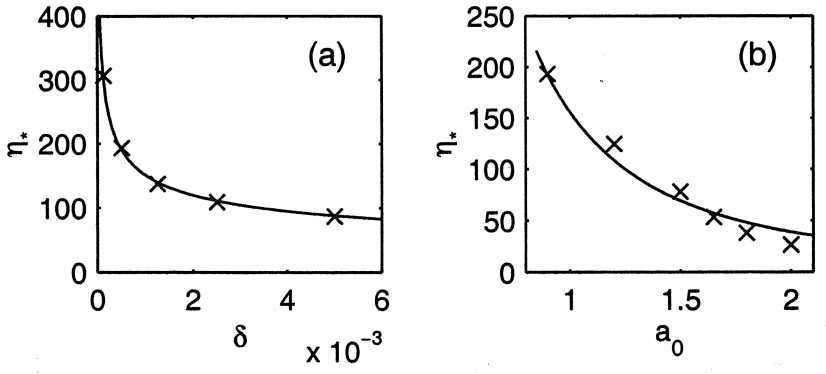

Figure 3.23: Dimensionless distance between the laser pulse and the first location of wavebreaking (η_*) vs mass ratio $\delta = zm/m_i$ (a) and laser pulse amplitude a_0 (b). The solid lines represent the analytical results, while the crosses correspond to results of numerical simulations.

the first plasma wave breaking point somewhat differ from the results of the simple theory. This difference is, first of all, due to the variation of the wakefield structure in the plasma channel that forms, which is not taken into account by the linear theory. According to Eq. (3.74) it is possible to obtain the following expression for the longitudinal coordinate of wavebreaking point:

$$\eta_* = \frac{C(\eta_0, \rho_0)}{a_0^2 \sqrt[3]{\delta}}, \tag{3.76}$$

where the factor $C(\eta_0, \rho_0)$ depends on the pulse form only. Fig. 3.23 shows the dependences of η_* on the mass ratio δ (a) and the pulse amplitude a_0 (b). The solid lines and crosses correspond to the results of Eq. (3.76) and simulations, respectively. To find the factor C in Eq. (3.76) we equalize it to the simulation result only in one (upper) point.

3.3.2.3 Numerical simulation of ion channel formation and plasma wave breaking with the code Wake

After plasma wave breaking the study of plasma dynamics requires a kinetic approach. We have performed simulations with the code Wake. In this case we were not limited by the hydrodynamic approximation. However, numerical difficulties did not permit us to perform simulations for the real ratio of ion and electron masses $\delta \geq 1836$ in axially symmetrical case. We have performed simulations for the case of $\delta = 200$ in plane geometry. In Figs. 3.24-3.27 the results of a simulation are shown

for a Gaussian laser pulse

$$a = a_0 \exp(-\chi^2/\chi_0^2 - \eta^2/\eta_0^2), \tag{3.77}$$

here $\chi = k_p x$ is the dimensionless transverse coordinate, the parameters of the pulse $\chi_0 = 3$, $\eta_0 = 2.67$. In Figs. 3.24 (a-d) the distributions of electron and ion densities are shown and in Figs. 3.24 (e-h) the distributions of the longitudinal and transverse components of electric field in plasma. Just after the laser pulse the plasma wave phase fronts are practically plane. However, as the ion channel forms the plasma wave phase fronts become curved. Simultaneously the amplitude of the electron density oscillations and the amplitude of the transversal electric field increase in the regions of strong transversal gradients of ion density in the channel. At the same time the amplitude of the longitudinal electric field decreases. Note, that such a dynamics of the components of electric field is typical for the plasma wave excitation in a plasma channel [109].

An ion density minimum arises at small distances behind the laser pulse, when the ion channel is formed by the ponderomotive force of the plasma wake. It means, that the component of the ponderomotive force, associated with the longitudinal electron motion in the plasma wake is more effective, than the component, associated with the transversal motion. Indeed, study of the ponderomotive force of the plasma wave for the case of plane geometry, similar to that performed above for the axially symmetrical case, shows, that if the influence of the ion density perturbations on the plasma wave structure is neglected, ion density minimum must arise on the axis for $\chi_0 > 2\sqrt{2}$ for the Gaussian laser pulse (3.77). At the same time at large distances behind the laser pulse an ion density maximum arises on the axis and the channel has an annular form in the simulation. It is associated with the growth of the transverse component of the electric field in the plasma channel, that is formed, and, consequently, with the growth of the transverse component of the plasma wave ponderomotive force.

At $\eta \approx 85$ the character of the plasma wave evolution changes. As Fig. 3.24 shows, during $2-3$ plasma periods its amplitude decreases essentially. As we will see it is associated with plasma wave breaking. It is the most convenient to study the plasma wave breaking and multi-stream electron motion, investigating the electron phase space. In Figs. 3.25 and 3.26 the distributions of plasma electrons in the planes (p_x, χ) and (p_z, χ) are shown for 16 values of the longitudinal coordinate η with an interval of $\delta\eta = \pi/2$. Note, that the total number of electrons in the simulation is much larger, than it is shown in these pictures. We have done an arbitrary sampling from the numerical particles to reduce the total number of points and to have a

possibility to observe the contrast of their density in the pictures. As we see from these figures, the approximation of one-fluid hydrodynamics for electrons is satisfied only for $\eta < 84$, when all electrons at each point (χ, η) have the same momentum. At $\eta > 84$ a multi-stream motion of electrons arises due to plasma wave breaking. Wavebreaking arises for the first time at $\eta \approx 84$ at some distance from the axis. When η increases the break point moves together with the plasma wave front to the longitudinal axis. It stops close to the ion density minimum in the annular plasma channel, that forms to this moment. Another wavebreaking point arises approximately in one plasma period after the first one. It appears again at some distance from the axis (approximately the same, as in the first case) and moves to the axis. New break points continue to appear with an interval of a plasma period. On Figs. 3.25 and 3.26 three plasma periods after the first wavebreaking are shown.

The criterion of plasma wave breaking in our simulation can be formulated as a generalization of the criterion for wavebreaking in 1D case, that is already known [20, 71, 112, 113]. In a 1D plasma wave, excited in a nonuniform plasma (with the inhomogeneouty gradient parallel to the plasma wave phase velocity) wavebreaking arises when the oscillatory electron velocity becomes equal to the plasma wave phase velocity. In our 2D case of a plasma wave in a nonuniform plasma wavebreaking takes place when the component of the electron oscillatory velocity perpendicular to the plasma wave phase front equals in some point in space to the plasma wave phase velocity. In this case a part of electrons outrun the other electrons in this point and a multi-stream electron motion arises. Our case corresponds to breaking of a plasma wave excited in a sufficiently rare plasma when the plasma wave phase velocity in the longitudinal direction is large (in the code the plasma wave phase velocity is supposed to be equal to the speed of light in vacuum in the equations for particles and low-frequency fields). It makes, in particular, the trapping of electrons in the longitudinal direction impossible and leads to the generation of bunches of fast electrons, moving at large angles with respect to the longitudinal axis (so called transverse plasma wave breaking [91]). The curvature of the plasma wave fronts increases with increase of η in the plasma channel. As electron oscillations take place in different phases at different distances from the axis, the finite transverse phase velocity arises for the plasma wave. The value of the transverse phase velocity at the ion channel walls decreases with η. The phase velocity in the direction perpendicular to the phase fronts is even less. The amplitude of the transverse component of electric field also increases with increase of η, at the same time the longitudinal component decreases. It leads to the increase of the transverse amplitude of the electron oscillations, while the longitudinal amplitude of the oscillations decreases.

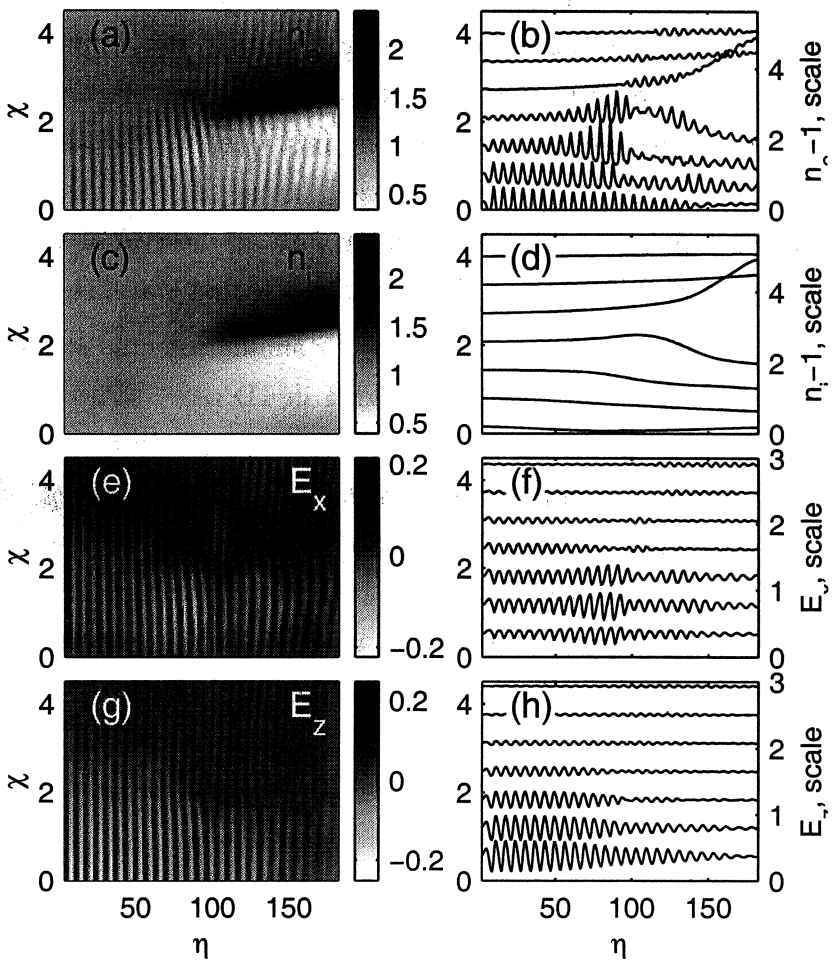

Figure 3.24: The distributions of electron density (a), (b) and ion density (c), (d), components of electric field, transverse (e), (f) and longitudinal (g), (h) in the plane (χ, η). Electron and ion densities are normalized to their unperturbed values. The components of electric field are in units of $m\omega_p c/e$. The longitudinal and transverse coordinates are in units of k_p^{-1}.

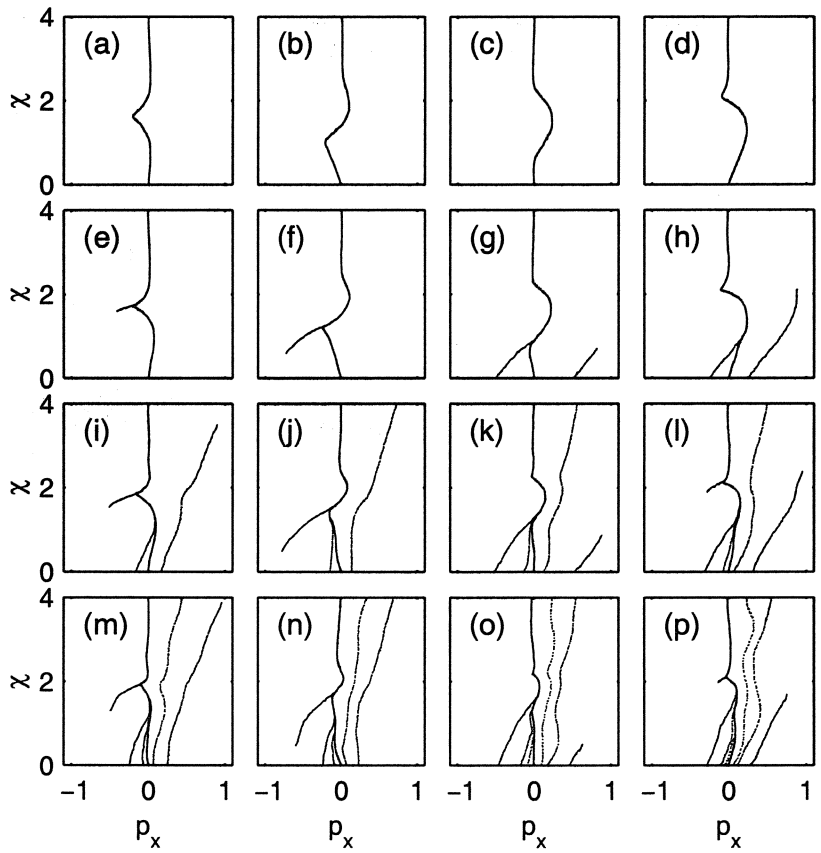

Figure 3.25: Plasma electrons in the space (p_x, χ) for 16 values of the longitudinal coordinate η, from $\eta = 78.44$ (a) to $\eta = 102$ (p), with an interval $\delta\eta = \pi/2$. The component of electron momentum is in units of mc.

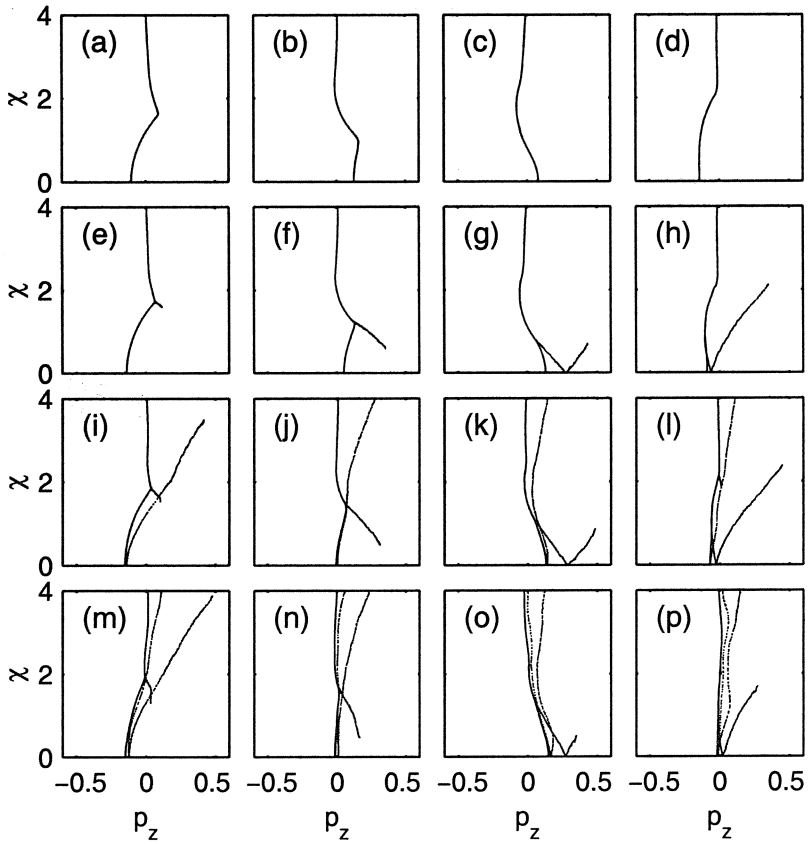

Figure 3.26: Plasma electrons in the space (p_z, χ) for 16 values of the longitudinal coordinate η, from $\eta = 78.44$ (a) to $\eta = 102$ (p), with an interval $\delta\eta = \pi/2$. The component of electron momentum is in units of mc.

At the moment of wave breaking the transverse amplitude of the oscillations of electron momentum is about two times larger than the longitudinal amplitude of oscillations [Figs. 3.25, 3.26 (a-d)]. When the transverse phase velocity of the plasma wave decreases sufficiently and the transverse amplitude of oscillations increases the criterion of wavebreaking, formulated above, is fulfilled and the plasma wave breaking arises. Our numerical simulation shows that wavebreaking arises on the curves in space (χ, η).

We denote, that plasma wave breaking in our simulation takes place by a somewhat different scenarios that it was suggested earlier in Ref. [91]. In Ref. [91] it is proposed (mainly on the basis of qualitative considerations) that the self-intersection of electron trajectories in the plasma wake with curved phase fronts takes place at the moment when the electron displacement from the equilibrium state is large (or maximum). At the same time in our case, as a detailed investigation of the electron phase space shows, the plasma wake breaks at the moment when the value of the oscillatory velocity is large, while the displacement from the position of equilibrium is small or absent at all. An additional investigation of conditions is needed, when plasma wave breaking takes place by the first or by the second scenarios, in general case.

As our simulation shows, bunches of fast electrons arise in plasma after the plasma wave breaking. The distribution function of fast electrons in the bunches is as narrow as the distribution function for electrons before the wavebreaking. Fast electrons are separated from the initial distribution function in the phase of the plasma wave when their transverse and longitudinal velocities are large (the electron displacement from the equilibrium is small at this moment, because the coordinate and velocity oscillate with the phase shift of $\pi/2$). These electrons outrun the plasma wave and continue to stay in its accelerating phase. As it follows from Figs. 3.25 and 3.26, they obtain in result a large transverse and longitudinal momentum. Fast electrons cross the longitudinal axis and fly out at large distances from the axis, moving from the other side of it.

The fast electrons take away the energy of the plasma wave with them. In Fig. 3.27 the energy balance in plasma is shown. We show the dependencies for the energies of electrons, ions, and low-frequency fields in a short plasma layer $\delta\eta$ on the longitudinal coordinate η in Figs. 3.27 (c), (d), and (e), respectively. In Fig. 3.27 (a) and (b) we show the dependence of the total energy in the layer $\delta\eta$ (that is the sum of the three first energies) on η, the instantaneous energy (a) and averaged over a plasma period (with the center in the point η) energy (b). All the quantities are normalized in these figures in such a way that the total energy just behind the

pulse, averaged over a plasma period, is equal to unity. Note, that small oscillations of the averaged total energy in Fig. 3.27 (b) are associated with the fact, that the oscillation period is different for different χ and η as the plasma channel forms. At the same time, we averaged over the plasma period just behind the laser pulse at $\chi = 0$. In Fig. 3.27 (f) we also show the energy of electrons that before the laser pulse coming were at $\chi < 4$, but in the process of interaction came to the region $\chi > 10$. It is clear, that these are fast electrons, produced after plasma wave breaking. We see, that in result of the plasma wave breaking the most part of its energy passes to fast electrons. The plasma wave is damped just after the wave breaking – during a few plasma periods. After the plasma wave breaking ion acceleration terminates, in result only about 12 % of the plasma wave energy is transferred into the energy of transverse ion motion. We have checked, that the longitudinal ion velocity after the interaction is much less than the transverse one.

In Figs. 3.27 (a) and (b) we observe an increase of the total energy in plasma in a short layer $\delta\eta$, when the wavebreaking takes place. This phenomenon is simple to understand, taking into account, that after wavebreaking the fast electrons transport the energy with them. Actually, the energy conservation law in plasma in the region behind the pulse is:

$$\frac{\partial W}{\partial t} + \mathrm{div}\mathbf{S} = 0, \tag{3.78}$$

where W is the energy density,

$$W = n_e mc^2(\gamma - 1) + n_i \frac{m_i v_i^2}{2} + \frac{E^2}{8\pi} + \frac{B^2}{8\pi},$$

and $\mathbf{S}$ is the energy density flow,

$$\mathbf{S} = n_e \mathbf{v}_e mc^2(\gamma - 1) + n_i \mathbf{v}_i \frac{m_i v_i^2}{2} + \frac{c}{4\pi}\mathbf{E} \times \mathbf{B}. \tag{3.79}$$

Integrating Eq. (3.78) with respect to the transverse coordinate and taking into account, that the energy density flow is absent at the boundaries of integration, we obtain the energy conservation law in the layer of a unity thickness, perpendicular to the axis:

$$\frac{\partial W^t}{\partial t} + \frac{\partial S^t}{\partial z} = 0, \tag{3.80}$$

where W^t is the energy in the layer,

$$W^t = \int_{-\infty}^{+\infty} W dx,$$

and S^t is the total longitudinal energy flow,

$$S^t = \int_{-\infty}^{+\infty} S_z dx.$$

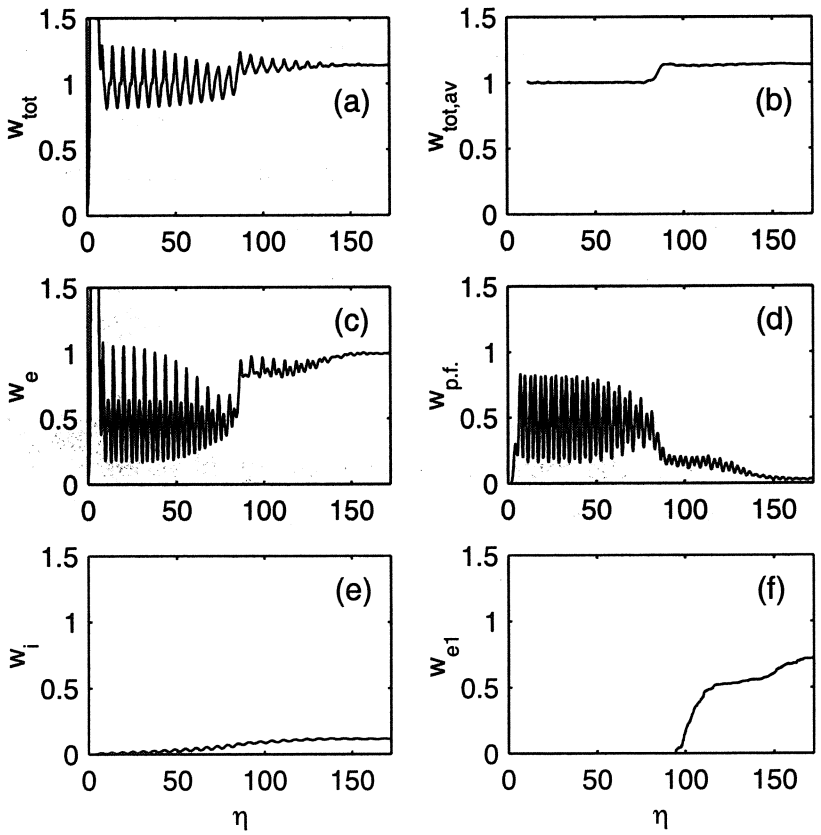

Figure 3.27: Energy balance in plasma. The total energy (a), total energy, averaged over a plasma period (b), electron energy (c), energy of the plasma wave fields (d), ion energy (e), fast electron energy (see the explanation in the text) (f) in a narrow transverse plasma layer $\delta\eta$ vs η. All the energies are normalized in such a way that the total averaged energy just behind the laser pulse is equal to unity.

In the quasistatic approximation the energy conservation law (3.80) has the form: $d/d\xi(cW^t - S^t) = 0$ or

$$cW^t - S^t = cW_0 = \text{const.} \tag{3.81}$$

We can rewrite Eq. (3.81) in dimensionless variables: $U^t - N^t = U_0$, where $U^t(U_0) = W^t(W_0)/n_{e0}mc^2$, $N^t = S^t/n_{e0}mc^3$. W_0 has a sense of the laser pulse energy used for the plasma wake generation. Actually, let us average Eq. (3.81) over a plasma period:

$$c\overline{W^t} - \overline{S^t} = cW_0. \tag{3.82}$$

Before the plasma wave breaks the averaged energy flow in a cold plasma is absent ($\overline{S^t} = 0$) and Eq. (3.82) signifies that the energy, used by the laser pulse for the excitation of electron oscillations in the layer, perpendicular to the axis, conserves, on the average over the period of oscillations. After the wavebreaking fast electrons have a longitudinal component of velocity (see Fig. 3.26) and contribute to the longitudinal energy flow, it is not equal to zero on the average over the plasma period, $\overline{S^t} \neq 0$. It follows from Eq. (3.82), that the energy in plasma increases in this case. It explains the jump of the total energy in plasma observed in Fig. 3.27 (b). We calculated in the code the longitudinal energy flow in plasma (3.79) and confirmed that the energy conservation law in the form (3.81) was fulfilled. Our simulation shows as well, that in spite the longitudinal electron energy flow is nonzero, the averaged over plasma oscillations and integrated on the transversal coordinate longitudinal electric current in plasma is absent, as it is required by the quasi-neutrality condition.

3.3.2.4 Discussions and conclusion

The results of our investigation show, that the ponderomotive force of the plasma wake, excited by an ultra-short ultra-intense laser pulse, leads to a formation of an ion channel in plasma. As the ion channel forms, the structure of the wake changes and the plasma wake breaks. Therefore, the plasma wake consists of a limited number of regular oscillations, that can be used for electron acceleration in the standard scheme of electron acceleration. We have performed a detailed study of the plasma wave breaking using numerical particle simulations. We have found the transformation of the electron distribution function and described the scenarios of wavebreaking. The plasma wave breaking leads to the generation of bunches of fast electrons, that dissipate the most part of the plasma wave energy.

We have investigated the dynamics of the plasma wave, excited by a short laser pulse in a uniform and infinite plasma. The ion acceleration in the transverse di-

rection terminates soon after the plasma wave breaking. Thus, only a small part of the plasma wave energy is transferred to the energy of transverse ion motion. The other part of the plasma wave energy passes mostly to fast electrons, that transport it to large distances from the axis. However, the situation can change, if the plasma wake is excited in a plasma of a finite width in the transverse direction. In this case, as our preliminary calculations and particle simulations show, the fast electrons, produced after the plasma wave breaking, do not fly out at large distances from the axis, but experience transverse oscillations through the plasma region under the influence of the returning force of the positive space charge, non-compensated. The cloud of fast electrons continues to accelerate ions in the transverse direction. Due to this an essentially larger part of the plasma wave energy can be transferred to ions. Such a situation takes place, in particular, when a short intense laser pulse propagates in gas. In this case the pulse ionizes the gas in the axial region, where its intensity is larger than the ionization threshold.

Chapter 4

Investigation of ultra-short ultra-intense laser pulse propagation in underdense plasma in application to laboratory experiments

4.1 Acceleration of injected electrons in a laser wakefield experiment

The standard scheme of electron acceleration in plasma is considered as rather simple in theoretical plan but at the same time as one of most attracting for application. In this scheme the relativistically fast plasma wave is excited by an intense laser pulse with a duration of the order of half a plasma period. To our opinion a particular simplicity and clearness characterize the mechanism of plasma wave excitation in this scheme, being compared with the other schemes of electron acceleration. The properties of the excited plasma wave are well predictable: its amplitude is a sufficiently simple function of the laser pulse amplitude and duration, while the phase velocity is close to the laser pulse group velocity. Such a simplicity of the mechanism of the plasma wave excitation is absent, in particular, in the other perspective scheme of electron acceleration, in the scheme of Self-Modulated Laser Wake Field Accelerator. In the latter scheme the plasma wave is excited in result of Raman instability of the laser pulse and the initial noise level determines the dynamics of this instability. It turns to be very difficult or even impossible to

control the phase of the plasma wave that is excited. In different regimes of the self-modulation instability the plasma wave phase velocity is less than the laser pulse group velocity that leads to a decrease of the maximum energy to which electrons can be accelerated. The plasma wave is also distorted in the result of its breaking that is practically inevitable in this scheme because of usually large increments of self-modulation instability.

In this paragraph we report the first sufficiently reliable experimental observation of electron acceleration using the standard scheme of electron acceleration in plasma. This experiment was performed at Laboratoire pour l'Utilisation des Lasers Intenses (LULI) at Ecole Polytechnique. The laser beam was focused in a gas-filled chamber (with helium) where a bunch of fast electrons was injected as well. In the experiment 400 fs (FWHM), 1.057 μm laser pulses were used with the energy up to $4 - 9$ J. After the compression about 20 % of the laser beam energy was focused in the focal spot with transversal dimensions 30×19 μm in horizontal and vertical planes. For the laser pulse energy of 1.5 J in the focal region the values of maximum power and intensity are $P_{\max} = 3.5$ TW, $I_{\max} = 4 \times 10^{17}$ W/cm^2. The intensity threshold for ionization of He^{2+} is roughly 10^{16} W/cm^2 [73, 114] and the interaction region in the experiment is completely ionized. As it is shown by additional diagnostics in this experiment, refraction in ionization region is not important for the gas pressures less than 4 mbar.

For an estimation of optimal conditions for the plasma wave excitation and electron acceleration one can use the linear theory of plasma wave excitation [9, 10]. If the time profile of the pulse intensity is described by $\exp[-(t/\tau_0)^2]$ the longitudinal (accelerating) component of the electric field of the excited plasma wave is proportional to $(\omega_p\tau_0)^2 \exp[-(\omega_p\tau_0)^2/4]$, for the fixed duration of the laser pulse. This function has a wide maximum at $\omega_p\tau_0 = 2$, that is for $\omega_p\tau = 4\sqrt{\ln 2}$, where τ is the pulse duration (FWHM). For $\tau = 400$ fs it corresponds to electron density of 2.2×10^{16} cm^{-3}, plasma wavelength $\lambda_p = 226$ μm, and the plasma wave relativistic factor $\gamma_p = 214$. It is just for this value of electron density (corresponding to the gas density of 0.45 mbar) the experiment on electron acceleration was performed. In the linear theory the amplitude of the longitudinal (accelerating) electric field of the plasma wave at resonance $E_z[\mathrm{GV/m}] = 1.35 \times 10^{-18} I_{\max}[\mathrm{W/cm^2}] \times (\lambda[\mu\mathrm{m}])^2/\tau[\mathrm{ps}]$. The relative longitudinal perturbation of electron density $\delta_{||} = E_z/E_0$, where $E_0 = mc\omega_p/e$. For the parameters in experiment $\delta_{||} = 10$ %. The ratio of transversal and longitudinal components of electric field at $r \approx w_0/\sqrt{2}$ in the linear theory $E_r/E_z = \sqrt{2}\lambda_p/\pi w_0$ here is equal to 4. The value of transverse electron density perturbation in the plasma wave [84] $\delta_\perp/\delta_{||} = (E_r/E_z)^2$ is equal to 16 for the experimental

parameters. It means that the plasma wave in the experiment is excited in transverse regime, that is transverse electric field is larger than longitudinal one.

An electron bunch with the energy of 3 MeV was injected in the interaction region in the direction of the laser axis. The bunch duration is 0.4 ms and the maximum current in the bunch is 3.15 ± 15 μA, corresponding roughly to 2000 electrons per 1 ps. The dispersion of electrons with respect to the transverse coordinate in the bunch focal spot for its propagation in vacuum is equal to 30 μm (r. m. s.) and angular emittence is 10 mrad (r. m. s.). After electrons interaction with the plasma wave their energy spectrum was measured by the deflection of trajectories in a constant magnetic field. Electron detector measured energies in the range of $3.3 - 5.9$ MeV. A typical electron spectrum in experiment is shown in Fig. 4.1. In this figure points show the number of electrons measured by different detectors. The part of the spectrum for small energies (from 3.3 till approximately 4.5 MeV) can be approximated by a decreasing exponent (dashed line on the figure). As it was found, the signal measured by electron detectors corresponding to the values of energy $E > 4.5$ MeV is a noise signal. Actually, as an additional verification shows [50], the most part of electrons detected by high energy detectors have an averaged energy of 2 MeV. These electrons were detected by those detectors because of essential deflection from the initial direction of motion (forward) in result of scattering in the transversal direction by the plasma wave. Because of the noise signal it is not possible to measure precisely the maximum electron energy in the experiment. For an approximate value of the maximum energy one can take the value, for which the approximating decreasing exponent is equal to 1 electron.

The maximum energy of electrons after the interaction can be estimated theoretically from the expression $\Delta W = ez_0E_z$, which for the length of propagation $z_0 \sim \pi z_R$ and Rayleigh length in experiment $z_R \approx 2.15$ mm gives the energy of 10 MeV. We note that this length of propagation is less than the dephasing length $l_d \approx 10$ mm that is necessary for the estimate to be valid. At the same time the maximum electron energy in experiment, determined as it is explained above, is less. As we will see below this difference can be due to the influence of the transversal component of the electric field, scattering the most of electrons a long time before the focal plane. Besides, as we have already mentioned, the presence of a noise does not permit to detect the small number of electrons accelerated to large energies.

Numerical simulations were performed for comprehension of the process of electron acceleration in the experiment. Different simulations of test electron acceleration were performed: for the plasma wave profile known from the linear theory of the plasma wave excitation by the laser pulse, as well as using the code Wake

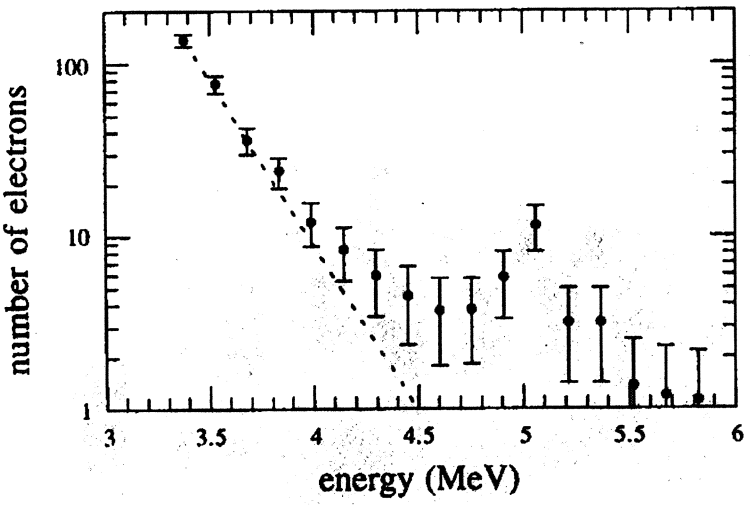

Figure 4.1: Typical electron spectrum in experiment. The part of spectrum for low energies is approximated by a decreasing exponent (dashed line).

that takes into account the self-consistent nonlinear dynamics of the laser pulse and plasma. We will report here only the simulations with the code Wake, performed by the author of the thesis. The propagation of a laser pulse in gas with the parameters of the experiment was simulated. The axially symmetrical version of the code was used and the radial size of the laser beam in the focal plane was taken to be equal to 25 μm (waist). The space distribution of the longitudinal and transversal components of the electric field of the plasma wave, excited by the laser pulse at the focus, is shown in Fig. 4.2. We see that the amplitude of oscillations of the transverse component of the electric field at some distances from the axis exceeds the amplitude of oscillations of the longitudinal electric field on the axis, more than in two times. Therefore, we confirm that the plasma wake is excited in the radial regime in the focal region. The dependence of the longitudinal electric field on the axis on the distance behind the pulse in the moment, when the laser pulse crosses the focal plane, is shown in Fig. 4.3. It leads from this picture that the characteristic time of plasma wave damping is 10 ps.

We simulated the propagation of a test electron beam in the plasma wave excited by the laser pulse. We used the parameters of experiment, except the duration: in the simulations the duration of the beam is 4 plasma periods, that is approximately 3 fs. The electron beam propagates in plasma just behind the laser pulse. The total electron number in the beam is 6000. The dynamics of 1000 electrons of the beam

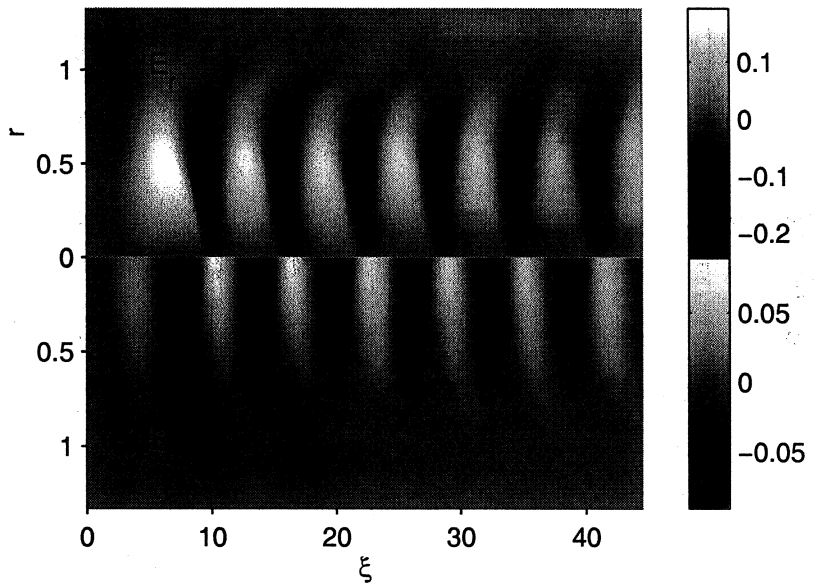

Figure 4.2: The distributions of radial (E_r) and longitudinal (E_z) components of the plasma wave electric field in space in the moment when the laser pulse crosses the focal plane. Electric field is in units of $m\omega_p c/e$, radial and longitudinal coordinates are in units of k_p^{-1}.

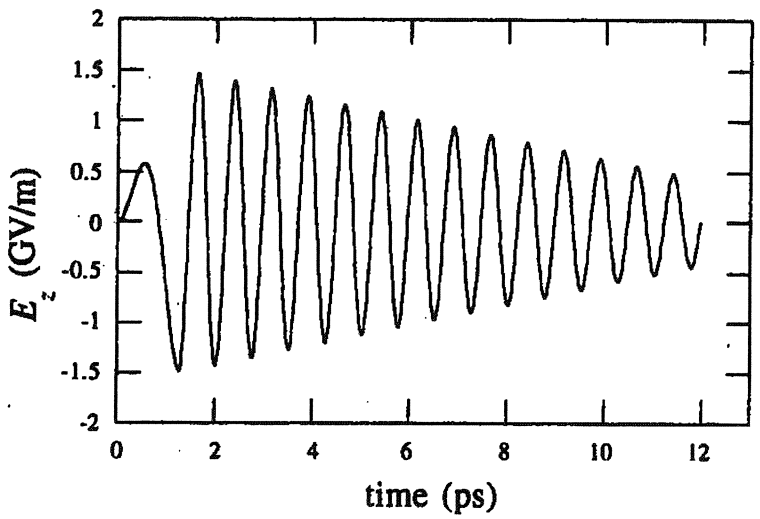

Figure 4.3: Plasma wave longitudinal electric field (E_z) calculated at the focal plane and on the laser axis, as a function of time.

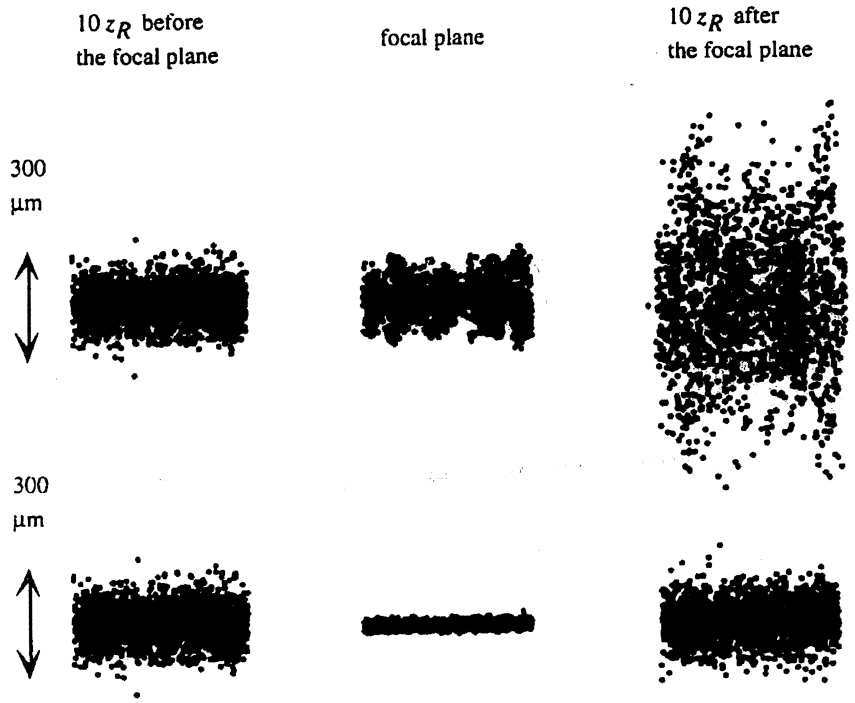

Figure 4.4: Evolution of an electron beam (3 ps duration) focused either under vacuum (bottom) or in the electron plasma wave (top): $10z_R$ before the focal plane, at the focal plane, and $10z_R$ after the focal plane.

(chosen randomly from their total number) and, for a comparison, their propagation in vacuum is shown in Fig. 4.4. In vacuum the electron beam is focused to the size of around 30 μm (r. m. s.) at the focal plane of the laser pulse. The beam radius increases again when it propagates from the other side of the focal plane. Its radius after 10 Rayleigh lengths behind the focal plane is the same as 10 Rayleigh lengths before it. In the presence of the plasma wave the beam is scattered in the transversal direction by a strong radial electric field of the plasma wake. So it can not be focused as good as in vacuum: its size in the focal plane is 5 times larger than in vacuum. 10 Rayleigh lengths after the focal plane the radial size of the beam becomes essentially larger than in vacuum.

On Fig. 4.5 the dependence of final electron energies on the phase of injection in the plasma wave (the longitudinal interval of one plasma period is taken into account that include 1500 test electrons) is shown for the simulated electron beam in the experiment and, for a comparison, for electrons moving on the axis, which are not subject to the transverse electric field of the plasma wave (speaking in another way, for an electron beam with a zero emittence). The dashed curve corresponds

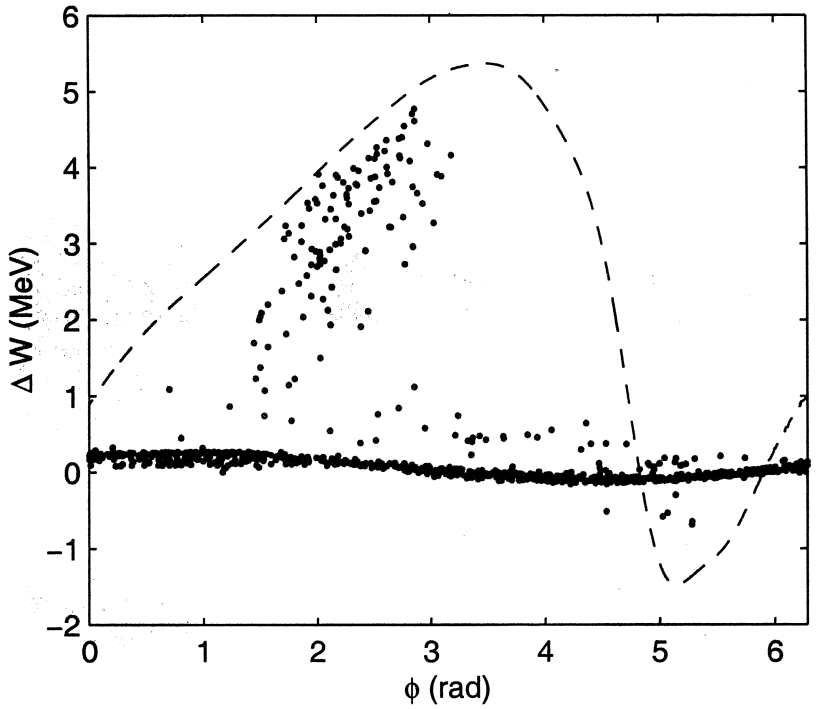

Figure 4.5: Energy gain of electrons in the simulation as a function of their injection phase in the plasma wave (dots). Energy gain of electrons propagating on the laser axis (dashed line). The longitudinal interval of one plasma period is shown.

to the electrons on the axis and points to electrons in experiment. The electrons of the beam are focused and defocused in different phases of the plasma wave due to the transverse electric field. The electrons in the defocusing phase are deflected from the axis and fly out from the accelerating region, so their energy gain is small. But even in the focusing phase of the plasma wave the energy gain of the most part of electrons is very small (or practically absent). Additional studies of the trajectories of particular electrons show that it is associated with scattering of the most of electrons under the influence of the strong radial electric field already a long distance before the focal region. Later is also seen from Fig. 4.4: the radius of the electron beam is essentially larger than the focal spot size of the laser pulse. However, a small part of electrons in the focusing phase are accelerated to the energies comparable with the energy of electrons on the axis. In this context, to reduce scattering we can suggest using of a gas jet for a limitation of the longitudinal size of the region, in which the plasma wave is excited, to a few Rayleigh lengths close to the focal plane, where an effective electron acceleration is possible.

The energy spectrum of the electron beam with realistic emittence after the interaction with the plasma wave is shown in Fig. 4.6. The width of the energy

channels of the detectors is the same as in the experiment. In the low energy region $3.3 < W < 4.5$ the spectra of Figs. 4.1 and 4.6 are similar, the spectrum in the simulation can be also approximated by a decreasing exponent with a damping coefficient close to the corresponding coefficient for the experimental dependence. In Fig. 4.6 we see that a part of electrons is accelerated to large energies. To approximate this part of the spectrum by some exponential dependence is not reasonable. We remind that the signal measured in the laboratory experiment by the high-energy detectors is of a noise level, and it is not possible to perform a comparison with the results of the numerical simulations (free of noise). One can also note a larger number of electrons accelerated in the simulations than the number of fast electrons in the experiment. We remember that the damping time of the plasma wave in the simulation is of the order of 10 ps. At the same time the duration of the electron beam in the simulation is 3 ps that is essentially less than the pulse duration in experiment. Therefore, the total number of accelerated electrons must be even more than it leads from Fig. 4.6. The reason of this difference is not clear finally. In Refs. [49, 50] it is proposed that the damping length of the plasma wave is of the order of 1 ps in the experiment. In this case for the same number of electrons accelerated on a unity of the plasma wave length it is possible to obtain close numbers of accelerated electrons in the experiment and in the simulations. To our opinion, this explanation is not absolutely satisfactory, as we do not see reasons for the damping length of the plasma wave essentially less than in our simulations.

In conclusion, we note that the numerical simulation performed with the code Wake is useful for understanding different aspects of the laboratory experiment: the laser pulse propagation, plasma wave excitation, and electron acceleration. The numerical simulation of the nonlinear dynamics of the laser pulse and plasma wave was necessary because the existing linear theory of the plasma wave excitation is not sufficient. This linear theory was used in the present investigation only for estimations. The investigation of the test electron dynamics explains the particularities of their acceleration, observed in the experiment. The results of this investigation can be used for the interpretation of the results of the other experiments on electron acceleration and for the comprehension of general characteristics of this process. The particularities of electron acceleration, which were observed, permitted us to propose possible improvements of the experimental setup for electron acceleration.

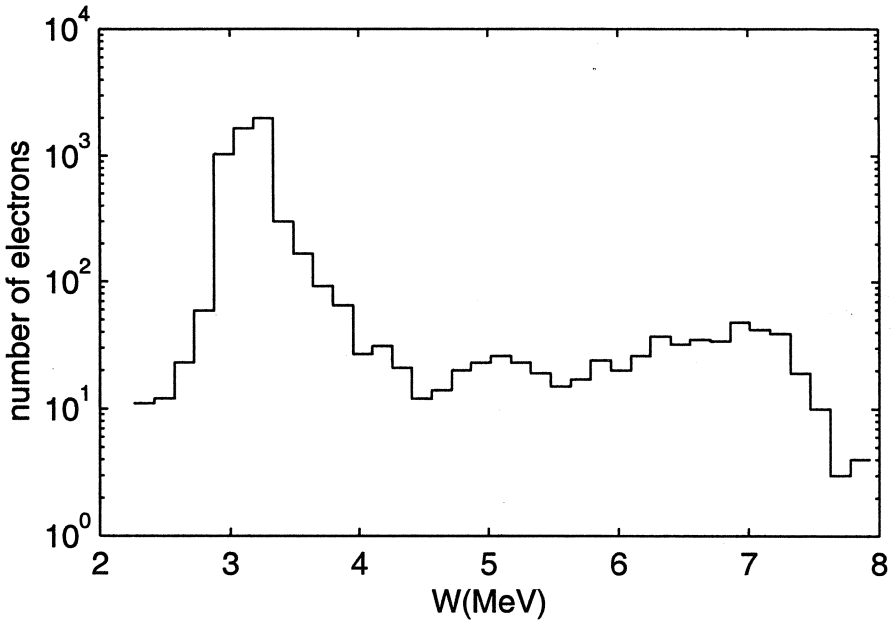

Figure 4.6: Electron energy spectrum in the simulation after their interaction with the plasma wave.

4.2 Propagation of a laser pulse in plasma in the self-modulated regime

As we discussed in the previous paragraph, the acceleration of electrons in the standard scheme of laser-driven electron acceleration in plasma is more predictable and more "fine" than in the Self-Modulated Laser Wake Field Accelerator. However, the last scheme has some apparent advantages as well. The intensity of the laser pulse increases due to the effect of relativistic and ponderomotive self-focusing. Besides, the plasma wave is resonantly excited by a number of short laser pulses – intensity modulations, produced in result of the instability. This permits to excite a plasma wave of a larger amplitude. When the plasma wave is broken (that is simply achieved in this scheme) fast electrons are produced, they can be trapped by the plasma wave and accelerated to large energies. So the use of an electron injector in this scheme can be unnecessary.

An experiment on the laser pulse propagation in the self-modulation regime was performed at laboratory LULI (Ecole Polytechnique). The laser pulses were used with the wavelength of 1.057 μm, duration from 370 fs to 4 ps, and energy up to 15 J. To avoid the refraction effects during the gas ionization and different effects associated with the plasma profile inhomogeneity in the longitudinal direction, the

laser pulse was focused on a sharp edge of a helium gas jet with a width of 4 mm and practically plane (close to rectangular) profile, shown in Fig. 4.7 (a). A narrower gas jet was used as well to reach higher densities. The focal spot radius was approximately 20 μm (waist). As the power up to 20 TW and intensities up to 4×10^{18} W/cm^2 were achieved, the radiation in the focus was ultra-intense. When the pulse parameters and plasma density were changed, the radiation power became more and less than the critical power for relativistic self-focusing.

The laser pulse in experiment was preceded by a prepulse of a few nanoseconds long and with intensity around 10^{14} W/cm^2. This prepulse was produced in result of amplified spontaneous emission of the radiation in the laser chain. The level of this emission depends, first of all, on the energy of the laser pulse. In the experiment the prepulse ionized completely the helium along the propagation length of the laser pulse. The hydrodynamic expansion of the heated plasma leaded to a formation of a channel in plasma to the moment of coming of the main part of the laser pulse, over all the width of the gas jet. Thus really the laser pulse propagated in a plasma channel and due to such a mechanism of its creation the perfect alignment of the channel and the laser axis was achieved.

For obtaining the information about the laser pulse propagation and the plasma profile different diagnostics were used. Interferometric measurements were performed in experiment and the images of the propagation region were obtained at different angles with respect to the direction of propagation, first of all, at the angle of 90 degrees and in the forward direction. The interaction region was also imaged in the forward direction on a spectrometer for obtaining the spectra of the transmitted radiation. An electron spectrometer was also used (set up in the forward direction) to measure the energy of fast electrons produced during the interaction.

A typical transversal profile of the plasma channel formed to the moment of coming of the main part of the laser pulse, obtained with interferometric measurements, is shown in Fig. 4.7 (b). The value of electron density on the axis $n_{e0} = 1 \times 10^{19}$ cm^{-3}, electron density is 4 times larger at the distance of 100 μm from the axis. The plasma density profile is approximately parabolic over the distance of $r < 75$ μm, where an approximation $n \approx n_{e0} + \Delta n_e (r/w_0)^2$ with a coefficient $\Delta n_e \approx 2.1 \times 10^{17}$ cm^{-3} (for $w_0 = 20$ μm) is possible. We remind that the condition of a diffractionless propagation of a Gaussian laser pulse with transversal size w_0 (waist) and power much less than critical for relativistic self-focusing in a parabolic channel $n = n_{e0} + \Delta n_e (r/w_0)^2$ is $\Delta n_e = 1/(\pi r_e w_0^2)$, where $r_e = e^2/mc^2$ is the electron classical radius. The condition of the diffractionless propagation of a laser pulse with $w_0 = 20$ μm is $\Delta n_e = 2.8 \times 10^{17}$ cm^{-3}. As the corresponding value in experiment

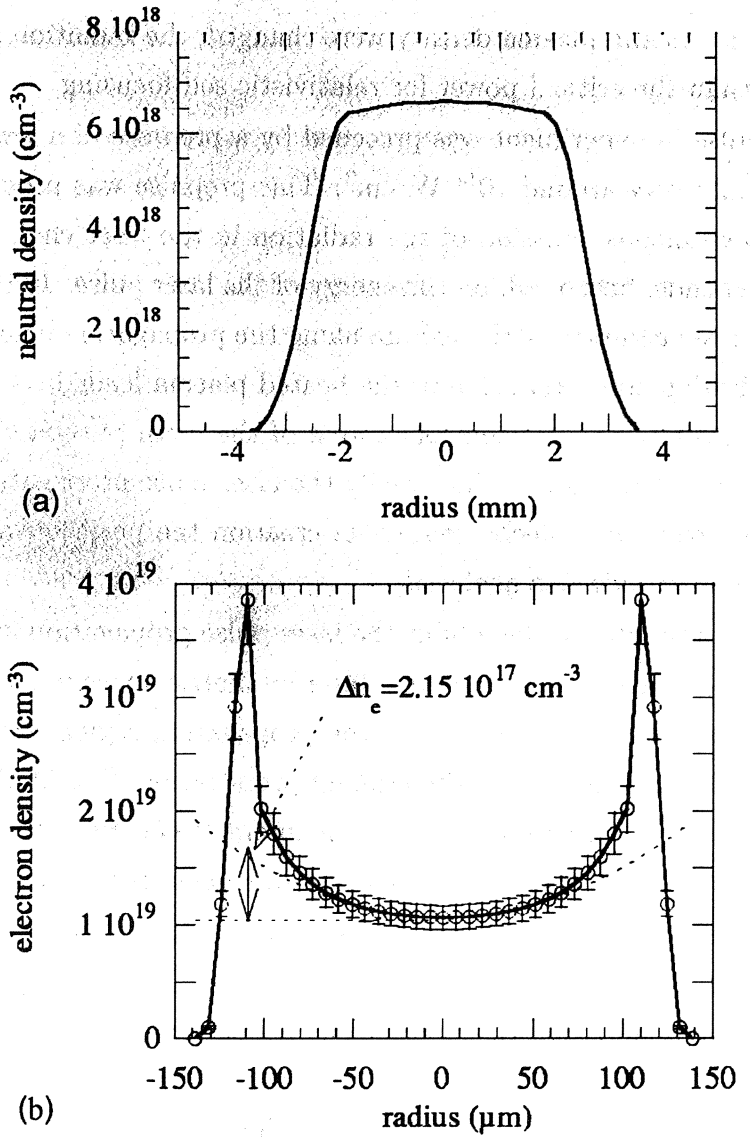

Figure 4.7: (a) Neutral density profile from the 4 mm gas jet in experiment. (b) Density profile retrieved from an interferogram (circles). Parabolic fit of the profile around the axis (dotted line).

is close to the theoretical one, the plasma channel can be used for a diffractionless propagation of a laser pulse in experiment, if its power is less than critical for self-focusing. The most of observations in the experiment were performed for laser pulses of the same energy, in particular, the repeatability of the channel formation was insured this way. At the same time different regimes of interaction were investigated changing the pulse duration and, therefore, the pulse power and intensity.

For the pulse duration around 7 ps the maximum intensity is $I_0 = 2\times10^{17}$ W/cm^2 and the maximum power $P < P_c$ ($P = 0.8P_c$). The interferometric measurements for this case show, that the laser pulse propagates along all the length of the gas jet, leaving a density depression behind – electrons and ions are expelled in the transverse direction by the ponderomotive force of the laser pulse. The radial size of the plasma depression region 20 ps after the laser pulse propagation is constant along the gas jet width. This result shows that the laser pulse propagates without a change of the transversal size, as otherwise the width of the plasma depression region must increase along the propagation length. The study of the spectra of the transmitted radiation [Fig. 4.8 (a)] shows an efficient generation of the second harmonic of the laser radiation, as well as distinct Raman satellites and Raman satellites of the second harmonic of the radiation.

The experiments at $P > P_c$ reveal a more complicated dynamics of the laser pulse and plasma. For the pulse duration of 370 fs the maximum power is $P = 15P_c$, the maximum intensity for the focusing in vacuum $I_0 = 4 \times 10^{18}$ W/cm^2. The interferometric measurements for this case, performed after the pulse propagation, show a long propagation of the radiation in plasma in the form of a narrow filament along the longitudinal axis. At the same time at the beginning of the gas jet (at the beginning of interaction) perturbations of plasma density at large distances from the axis are observed. These perturbations exist along the distance of the pulse propagation of the order of 1 mm, some of them have a form of filaments, that have a characteristic angle with respect to the laser axis of $5 - 10$ degrees. Self-focusing and radiation scattering at large angles with respect to the propagation axis can explain this phenomenon. We will discuss more this scattering below, when we will analyze the results of our numerical simulations. The main filament propagates in plasma along all the length of the gas jet. It is also seen from the plasma images at 90 degrees, where there is a narrow bright region along all the length of the gas jet. Its transversal size was not resolved in experiment, as the transversal resolution limit of the system was 100 μm.

As the experiments show, for $P > P_c$ the pulse is subject to different instabilities. The image in the transmitted light, obtained with a resolution of 5 μm, reveals small

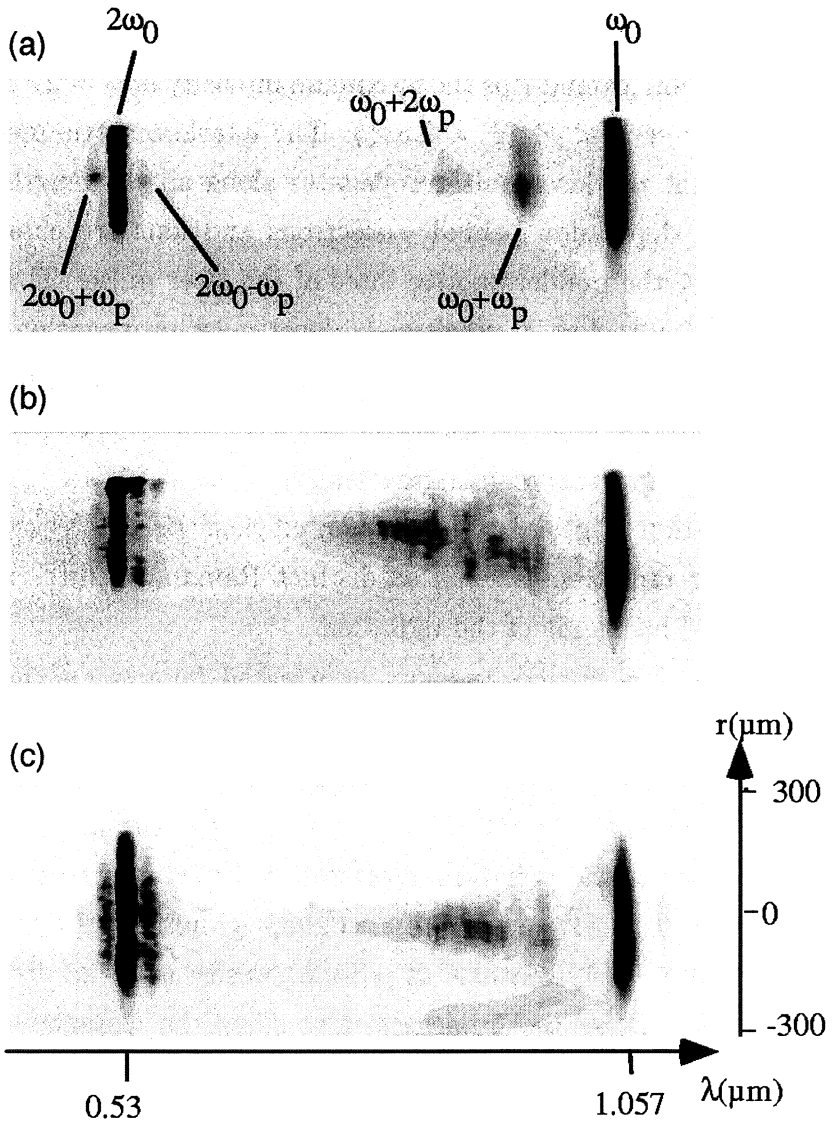

Figure 4.8: Transmitted spectra in experiment. The electron density is always 1×10^{19} cm^{-3}. (a) $P/P_c = 0.8$, $\tau = 7$ ps (pulse duration); (b) $P/P_c = 2.2$, $\tau = 3$ ps; (c) $P/P_c = 15$, $\tau = 370$ fs.

intensity structures with a characteristic size of the order of the resolution limit. The number of small structures increases with the power increase. Note that such small structures were absent in the experiments for $P < P_c$. The spectra of the transmitted light obtained in the experiments for $P > P_c$ [Figs. 4.8 (b) and (c)] show an efficient second harmonic generation, as it was for $P < P_c$. What concerns Raman satellites at the frequency of radiation, they become very broad for $P > P_c$ and overlap each other, they can not be separated, in fact. At the same time, Raman satellites at the second harmonic frequency are still narrow enough. We can also observe a very wide satellite at the distance of 300 μm from the axis on Fig. 4.8 (c). This observation correlates with the observation of filaments, obtained from the results of interferometric measurements.

It is important to mention, that in all the experiments discussed, performed using a gas jet with the diameter of 4 mm, shown in Fig. 4.7 (a), there were no fast electrons detected by the electron spectrometer. At the same time such electrons were observed for the propagation of a laser pulse with a duration of 370 fs in a narrower gas jet with a larger value of electron density of 2×10^{19} cm^{-3} and power $P = 28P_c$. In the similar experiments in Ref. [62] broadening of the Raman satellites with a simultaneous generation of a large number of fast electrons was identified as a plasma wave breaking, distortion of its regular structure. At the same time this interpretation is not fully applicable in the case of our experiment. We suppose that in our experiment with $P > P_c$, in which fast electrons were not detected, the plasma wave breaking still took place due to a strongly nonlinear character of interaction, observed in experiment and expected from theoretical implications. However, this plasma wave breaking was transversal (see Ref. [91] and paragraph 3.3 of the present thesis) and did not lead to the generation of a large number of trapped electrons.

For a comprehension of the physics of interaction of the laser pulse with plasma and interpretation of the experimental data we performed numerical simulations using the code Wake. Our code can be used only for simulations of a propagation of sufficiently short laser pulses in plasma, with a duration less than 1 ps. So we performed simulations only for the case of short laser pulses with the maximum power $P > P_c$. We present the results of a simulation, performed in plane symmetry, with parameters: laser wavelength $\lambda_0 = 1.057$ μm, laser beam waist $w_0 = 23.8$ μm ($z_R = 1.68$ mm), pulse duration (FWHM) $\tau = 300$ fs, power and intensity in the maximum $P/P_c = 6.3$, $I_0 = 1.2 \times 10^{18}$ W/cm^2. As the plasma transversal profile we took the density profile of the channel in experiment [Fig. 4.7 (b)]. We have also checked the possibility of using our code at such large powers by a comparison of our results with the results of simulations with a Particle-in-Cell code at the first 500

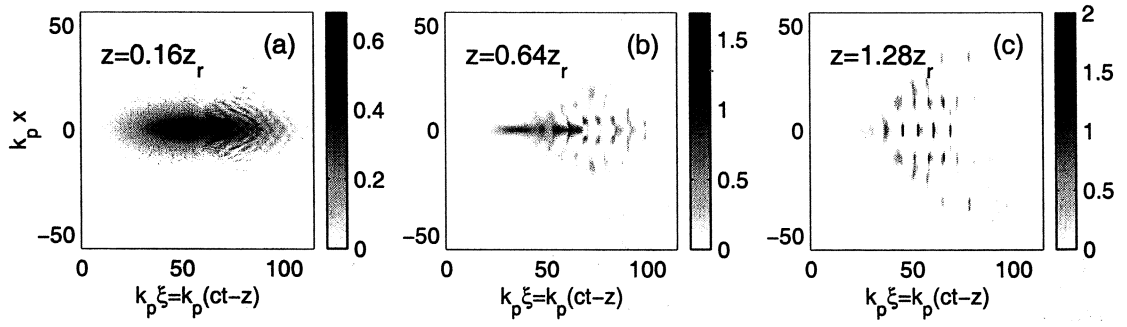

Figure 4.9: Numerical simulation of the laser pulse propagation. Intensity distributions for different z. Laser pulse parameters: $P/P_c = 6.3$, $\tau = 300$ fs, $w_0 = 23.8$ μm (Gaussian pulse).

μm of the propagation in plasma. After propagation the first 500 μm both codes predicted strong scattering at large angles with respect to the laser axis and there was a sufficiently good qualitative agreement between the two codes. The precise values were somewhat different, because the noise, initiating the instability, can have different causes in two codes.

Fig. 4.9 shows the results of our simulations. In Figs. 4.9 (a), (b), and (c) the intensity distributions in the frame moving with the pulse are shown for different values of z, coordinate along the propagation direction. At the beginning of interaction there is a strong scattering of radiation at large angles with respect to the propagation direction in the backward part of the pulse [Fig. 4.9 (a)]. Then the self-focusing of the forward and central parts of the pulse takes place and the self-modulation instability develops [Fig. 4.9 (b)]. The instability increases when the pulse propagates in plasma. An essential part of the pulse energy is scattered, only a part of the energy is trapped in the channel. At the same time well distinct intensity modulations propagate close to the axis [Fig. 4.9 (c)]. The investigation of the intensity distributions in a more sensitive to its small values logarithmic scale shows, that the plasma channel does not trap the radiation, produced in result of large angle scattering at the beginning of the interaction. At the same time, the radiation scattered later is trapped and propagates in the plasma channel. Also the forward part of the pulse with power less than P_c propagates practically without changing the form.

We simulated the propagation of a pulse with the same parameters, but in homogeneous plasma (in the absence of a plasma channel). The nature of interaction was very much the same, except very small details (in particular, a bit less maximum values of intensity). We can say that as a whole, the plasma channel plays a very small

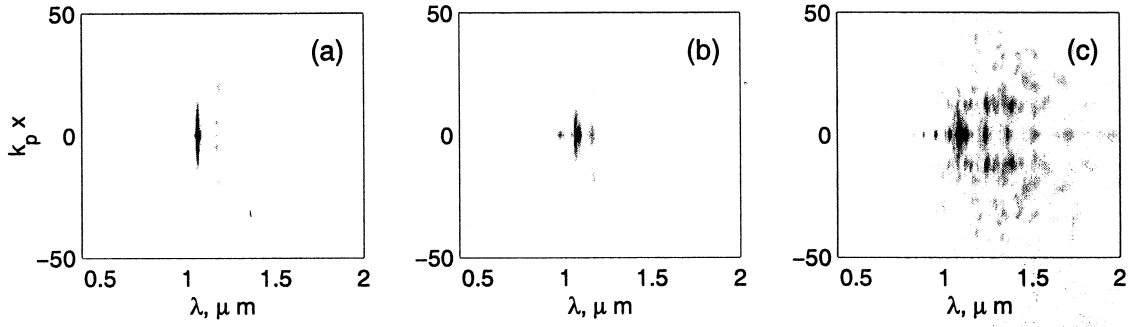

Figure 4.10: Simulated spectra of the radiation in plasma for the same values of z, that the intensity distributions in Fig. 4.9.

role for a propagation of a pulse with a power larger than critical for self-focusing on the distances of the order of 2 – 3 Rayleigh lengths, as in this simulation.

In Fig. 4.10 the spectra of the radiation in plasma are shown for the same values of z as the intensity distributions in Fig. 4.9. We remind that the code Wake does not describe harmonic generation (see, paragraph 2.1), so in the obtained spectra the radiation at the second harmonic of the laser frequency is absent. We observe a generation of Raman satellites, Stokes and anti-Stokes, the amplitude of the Stokes ones is larger. At large times the nonlinear dynamics of the laser pulse leads to dramatic changes of the spectrum. At large z the pulse spectrum essentially broadens, at the same time it shifts to small frequencies (large wavelengths) as a whole. The last is associated with the decrease of the radiation energy used for the plasma wave excitation, when the number of photons is conserved: it is possible only if the radiation frequency decreases. However, in the experiment only a part of the spectrum was measured, corresponding to the wavelengths $\lambda < 1.2$ μm. For larger wavelengths the sensitivity of the spectrometer was too weak. In Fig. 4.11 we show separately the part of the radiation spectrum after the interaction with plasma ($z = 2.38 z_R \approx 4$ mm) for $\lambda < 1.2$ μm. As in experiment, we do not observe distinct Raman (anti-Stokes) satellites in this picture.

The results of our numerical simulations can be interpreted as follows. For sufficiently small z the backward part of the pulse is scattered. This scattering is a consequence of Raman instability at large angles with respect to the propagation direction. As it follows from the investigation of Ref. [14], this Raman instability has the largest rate (together with backward Raman scattering, that is not taken into account in our model) and it arises first during the propagation of the pulse. Raman scattering at large angles with respect to the propagation direction is a 3-wave process and leads to the generation of a Stokes radiation only. Self-focusing

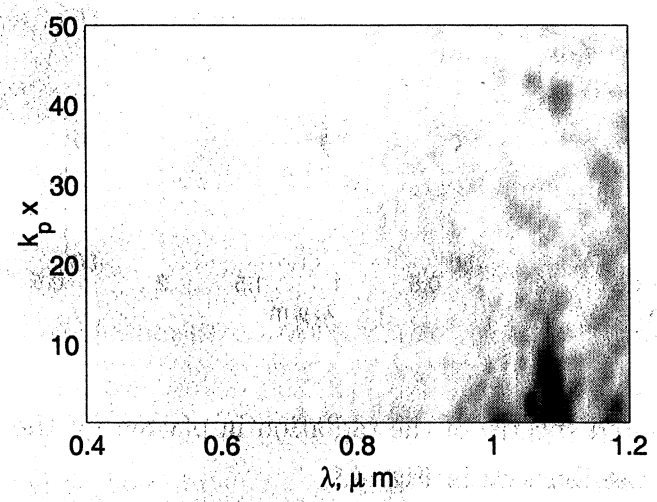

Figure 4.11: A part of the simulated spectrum for $\lambda < 1.2$ μm after the interaction with plasma ($z = 2.38 z_R$).

leads to essential focusing of the pulse at distances of $z \sim z_R/(P/P_c)$. Substituting in this expression the value of power in the pulse maximum, we obtain that the pulse central part is self-focused at $z \sim 0.16 z_R$. The part of the forward slope for which $P > P_c$ is also focused soon (at $z < z_R$). Self-focusing, that takes place at different times in different pulse transversal cross-sections, leads to a strong steepening of the longitudinal intensity profile of the laser field. This steepening, as well as the inhomogeneity of the profiles of intensity and plasma density due to Raman scattering at large angles with respect to the laser axis, act as initial perturbations for the self-modulation instability. The self-modulation develops first in the central part of the pulse and in the backward part, that was already essentially damped to this moment; it develops in the forward part after its self-focusing as well. Due to the large rates of the resonant modulation instability and strong initial perturbations the saturation of the instability takes place in fractions of a Rayleigh length.

It is necessary to mention that our numerical simulations can underestimate some effects in the experiment, such as self-focusing and ponderomotive electron expelling from the pulse region. First, these effects are underestimated in the plane geometry, and second, the power of radiation in numerical simulations is somewhat less than in experiment. As a whole, the results of simulations are in good agreement with the results of experiment and can be used for its interpretation. In the experiment with power $P > P_c$ a strong scattering of radiation at the beginning of interaction is observed. As it follows from our numerical simulation, it takes place due to Raman scattering at large angles with respect to the propagation direction. An essential

part of the energy is not trapped in the relativistic filament when self-focusing takes place because of the essential non-stationarity of the self-focusing process. Both in experiment and in our simulations distinct anti-Stokes Raman satellites are absent in the radiation spectrum after the interaction because of the large rates of the self-modulation instability.

4.3 Electron acceleration by the laser field and plasma wave in the experiment on laser-driven electron acceleration in plasma

Till recently in theoretical investigations of laser-driven electron acceleration in plasma the main attention was devoted to electron acceleration by the plasma wave excited by the laser pulse. At the same time a possible acceleration by the high-frequency laser field of the pulse was not considered. But recent three-dimensional Particle-in-Cell simulation [65] has shown that the high-frequency laser field can also accelerate electrons. When a laser pulse with a power larger than P_c propagates in plasma, it produces an electron plasma channel, self-focusing and expelling electrons from its region. In this plasma channel fast electrons, propagating in the forward direction, oscillate in the transversal direction (experience betatron oscillations) under the influence of the focusing electric field in the channel. Quasi-stationary magnetic field generated in plasma also leads to transversal oscillations of electrons in the plasma channel. Moving fast in the longitudinal direction the electrons observe a laser frequency in their own frame less than in the laboratory frame (due to the Doppler shift). At optimal longitudinal velocity this frequency becomes equal to the frequency of the electron betatron oscillations in the plasma channel. In this case favorable conditions for the electron acceleration by the laser field exist. The electron, oscillating in the plasma channel in the accelerating phase of the transversal component of the laser electric field, is effectively accelerated in the transversal direction. Lorentz force associated with the laser magnetic field, has a component in this process in the longitudinal direction, and turns the electron in the direction of the laser axis. Thus the energy of the transverse oscillatory electron motion is transformed into the energy of its progressive forward motion. As electron accelerates forward in such a way, it goes from the resonance with the high-frequency field, as the frequency of its betatron oscillations changes (because of relativistic mass increase) as well as the laser field frequency that it observes in its own frame does. After that the electron acceleration terminates. We will also find from our numerical simulation that the longitudinal laser field decelerates electrons in this process, decreasing the effectiveness of the laser field energy transfer to electrons. It is associated with the fact, that the electron accelerated by the transverse electric field is at the same time in the decelerating phase of the longitudinal electric field of the beam. Though the value of the longitudinal electric field is essentially less than the value of the transverse one, the electron energy decrease due to the longitudinal

field appears to be of the same order as its increase due to the acceleration by the transverse field (approximately two times less).

However, up to now a complete quantitative theory of this mechanism of electron acceleration by the laser pulse field is absent. In particular, reliable estimations of the maximum electron energy gain are absent, as well as a comparison of the effectiveness of the electron acceleration by the laser field and the plasma wave field is not performed.

Recently at Laboratoire d'Optique Appliquee (LOA) an experiment was performed on the interaction of an intense laser pulse with underdense plasma, where an effective generation of fast electrons was observed. The propagation of laser pulses with the wavelength of 0.82 μm, duration of 35 fs (FWHM) and energy up to 0.6 mJ was studied. To overcome refraction on the plasma inhomogeneouties arising due to gas ionization, the laser pulse was focused on a sharp edge of a helium gas jet with a profile close to rectangular one and the width of 2 mm. The focal spot size was 6 μm (waist), that corresponds to a typical power of 20 TW and intensity of 2×10^{19} W/cm^2. The plasma density was changed by changing the gas density in the jet. In experiment the value of electron density was in the range of $1.5 \times 10^{18} - 1.5 \times 10^{20}$ cm^{-3}. Changing the electron density in this range the pulse duration becomes larger and less than a plasma period: increasing the electron density we go from the classical regime of plasma wake excitation by a short laser pulse to the regime of self-modulation. Different diagnostics were used in experiment: the spectra of the radiation, transmitted and reflected at 180 degrees, were measured; Thomson scattering was studied and the images of plasma at 90 degrees with respect to the direction of the propagation were studied. The main attention was devoted to the study of the spectra of fast electrons, produced during the interaction, measured with an electron spectrometer.

Fast electron generation was observed in the experiment transferring from the classical regime of the plasma wave excitation to the self-modulation regime. The dependence of the maximum electron energy on the value of electron density in experiment is shown in Fig. 4.12 for the case of a laser pulse with a duration of 35 fs and energy of 0.6 J (roughly 50 % of this energy was focused in the focal spot). As we see, the maximum electron energy decreases with the electron density increase. The solid line denotes the theoretical dependence:

$$W_{\max} \approx 4\gamma_p^2 (E_z/E_0) mc^2. \tag{4.1}$$

This formula assumes, that the maximum electron energy equals the product of the force of the longitudinal electric field of the plasma wave and the dephasing length,

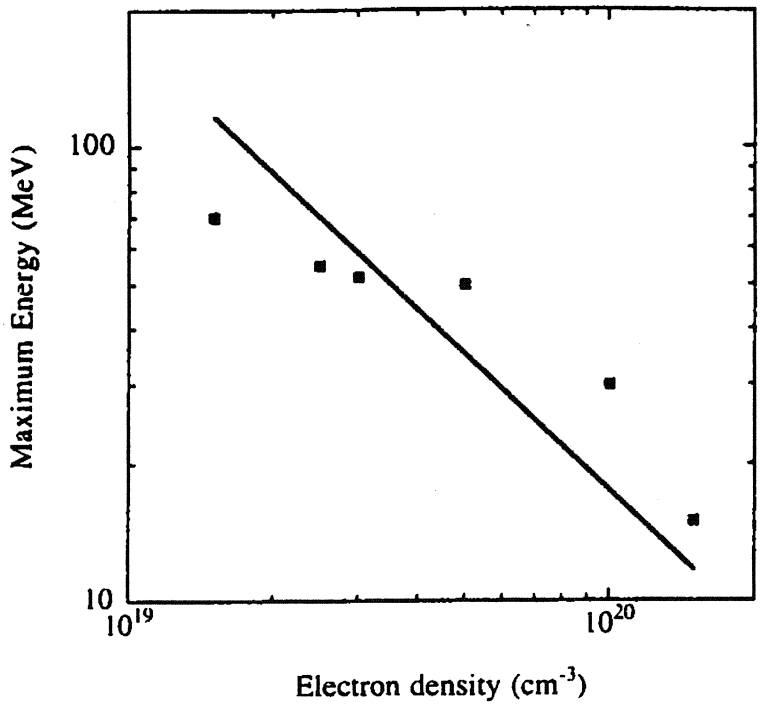

Figure 4.12: Maximum electron energy as a function of the electron density. Squares correspond to experimental values. Continues line corresponds to theoretical calculation Eq. (4.1) with a normalized electrostatic field $(E_z/E_0) = 0.5$. Laser pulse parameters: 0.6 J, 35 fs, 2×10^{19} W/cm^2.

Eq. (1.5). The amplitude of the plasma wave $(E_z/E_0) = 0.5$ for the dependence in Fig. 4.12. However, the dependence of Eq. (4.1) does not take into account the electron acceleration by the laser field. The measurement of electron spectra also shows a decrease of the fast electrons temperature with the plasma density increase in the jet. It is necessary to mention, that in the experiment of Ref. [67], performed recently, a different dependence for the maximum electron energy and temperature was obtained, which increased with the plasma density increase.

We have performed numerical simulations of the laser pulse propagation in plasma and electron acceleration in the experimental conditions, using the code Wake. Due to the approximations in our code we were limited to the case of pulse powers less than a few critical powers for relativistic self-focusing and pulse duration not much exceeding a plasma period. For the maximum laser energy of the present experiment it corresponds to electron densities up to 2×10^{19} cm^{-3}. We also made simulations with larger densities but with smaller powers. We investigated accelera-

tion of test electrons (non-interacting), injecting them in the fields region at the time of strong self-focusing for short pulses and at the developed stage of self-modulation for laser pulses longer than a plasma period. The results of our simulations confirm decreasing of the maximum electron energy with increasing the background electron density when the length over which self-focusing occurs is greater than the dephasing length.

In contrast to the other simulations where direct laser acceleration of electrons was investigated [65, 67], in our numerical simulation we were able to separate the contributions of the laser field and of the plasma wave field to electron acceleration. To compare these effects we calculated the following integrals along the test electron trajectories:

$$\Gamma_{p,l} = -\int_0^t \frac{e\mathbf{E}_{p,l} \cdot \mathbf{v}}{mc^2} dt'. \tag{4.2}$$

$\Gamma_{p,l}$ represent the electron energy change due to the interaction with the low-frequency plasma wave field and high-frequency laser field, respectively. The total electron energy is the sum of Γ_p and Γ_l. It is necessary to mention that our integrals Γ_p and Γ_l differ from the values Γ_z and $\Gamma_\perp$ in Ref. [67]. In Ref. [67] the integrals from the quantities of a type of $\mathbf{E} \cdot \mathbf{p}$ were calculated, instead of $\mathbf{E} \cdot \mathbf{v}$ in our approach. Therefore, in Ref. [67] the square of electron energy was calculated but not the energy, though they called their integrals as energies. Besides, in Ref. [67] the contributions of E_z and $\mathbf{E}_\perp$ to electron acceleration were calculated instead of $\mathbf{E}_p$ and $\mathbf{E}_l$ in our simulations to compare the effectiveness of the different mechanisms. In Fig. 4.13 we show test electron distributions in the space (Γ_p, Γ_l) at different moments of time in a typical simulation. This simulation corresponds to the present experiment, when the laser pulse with the energy of 0.6 J propagates in plasma with electron density of 2×10^{19} cm^{-3}. In this simulation the length of the laser pulse is close to one plasma period (FWHM). After the laser pulse self-focusing self-modulation leads to emerging of two modulations, though the backward modulation is rather weak. We injected a test electron beam, consisting of 3×10^4 particles after the laser pulse propagation over one Rayleigh length in plasma. We see that both mechanisms of electron acceleration are important. Because the acceleration length is larger than the dephasing length in this simulation, electrons accelerated by the plasma wave field at the beginning of interaction are decelerated by this field later. The energetic electrons propagate in the first period of the plasma wave, that is in the plasma period inside the laser pulse. Initially they are accelerated by the laser field and the plasma wave simultaneously, but after the propagation of a distance equal to the dephasing length these electrons come to the decelerating phase of

the plasma wave. At the same time, as our simulation shows, they continue to be accelerated by the laser field, in such a way electrons appear with $\Gamma_p < 0$ and $\Gamma_l > 0$. We mention, that in this simulation the electrons with maximum energy are accelerated mostly by the plasma wave field. We admit that at larger laser powers (much larger, than P_c), for the pulses, essentially longer than a plasma wavelength, the most energetic electrons will come from the acceleration by the laser field, as it is predicted in Ref. [65].

In Fig. 4.14 we show the electron distributions in space ($\Gamma_{l,||}$, $\Gamma_{l,\perp}$) at the same times as in Fig. 4.13, here

$$\Gamma_{l,||} = -\int_0^t \frac{e\mathbf{E}_{l,||}\cdot\mathbf{v}}{mc^2}dt', \Gamma_{l,\perp} = -\int_0^t \frac{e\mathbf{E}_{l,\perp}\cdot\mathbf{v}}{mc^2}dt' \tag{4.3}$$

represent the contributions of the longitudinal and transverse components of the laser field to electron acceleration. It is necessary to mention that the longitudinal electric field of the laser pulse decelerates electrons at the betatron resonance. It leads also from the consideration of the phase of the longitudinal laser field, in which electron propagates at the betatron resonance. Such an electron experiences two picks of acceleration by the transverse electric field of the laser pulse over the period of oscillation in the plasma channel (for laser field of a linear polarization). The transverse acceleration is maximal when the electron crosses the longitudinal axis, moving with the maximum velocity, and observes the maximum value of accelerating electric field. At the same time, the oscillations of the longitudinal and transverse laser fields are shifted in phase by $\pi/2$. When the electron is at its largest distance from the laser axis, it is in the maximum of the longitudinal electric field decelerating it. Though the amplitude of the longitudinal electric field is essentially less than the amplitude of the transversal one, $|E_z|/|E_\perp| \sim \omega_p/\omega_0$, the longitudinal electron velocity is essentially larger than the transversal one. The contribution to the acceleration is proportional to the product of the velocity and the electric field [see Eq. (4.3)]. Thus, the deceleration of electrons by the longitudinal field can be of the same order of magnitude as the acceleration by the transversal one. As our simulations show, the deceleration by the longitudinal electric field is approximately two times less than the acceleration by the transversal one; in result the laser field accelerates electrons. However, in Ref. [67] electron deceleration by the longitudinal laser field was attributed to the plasma wave field.

We must mention that the effect of "beam loading" [115] is not taken into account in our simulations. It consists in the excitation by fast electrons their own plasma wave, if their number is sufficiently large. As a rule, in result of superposition of the plasma waves, excited by the laser pulse and fast electrons, the amplitude of the

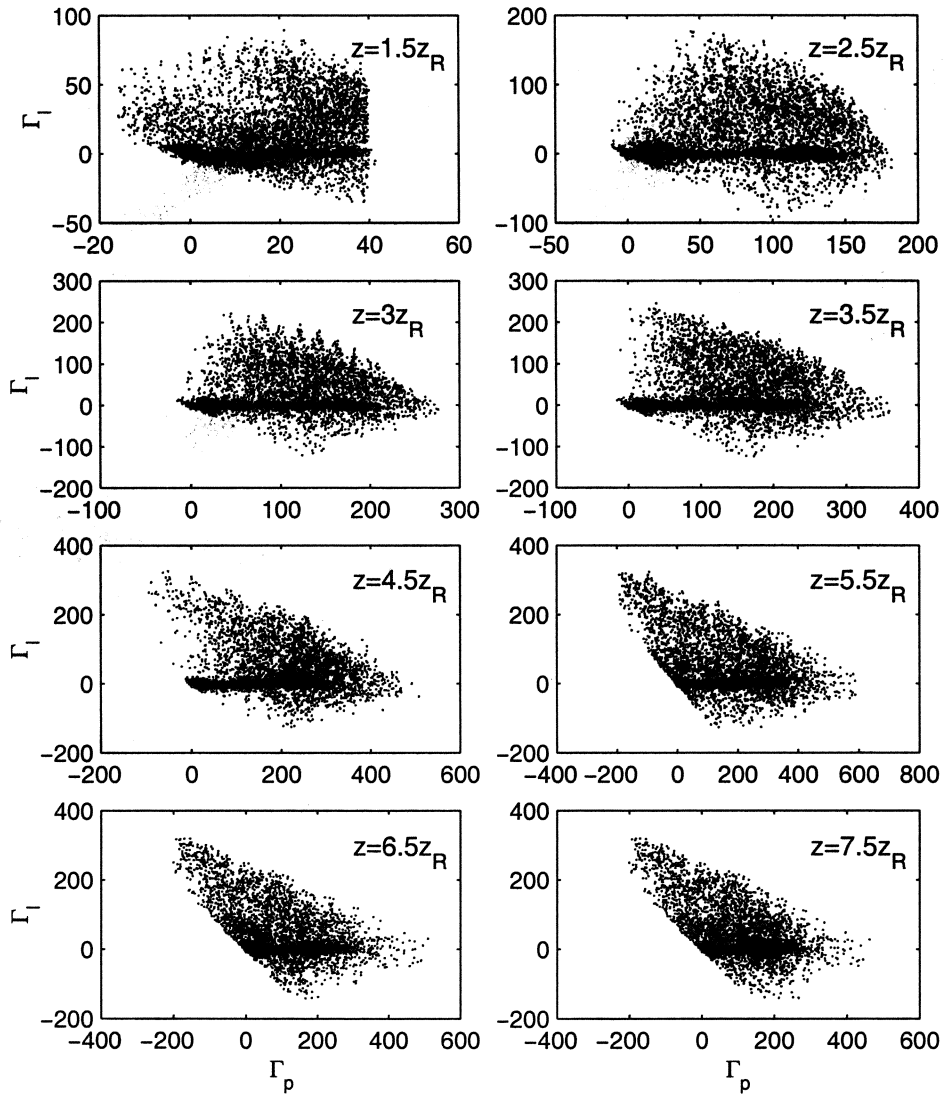

Figure 4.13: Electron distribution in space (Γ_p, Γ_l) at different moments of time in the simulation. The electrons are injected at $z = z_R$. The parameters of the laser pulse coincide with the parameters in experiment and the plasma electron density is 2×10^{19} cm^{-3}.

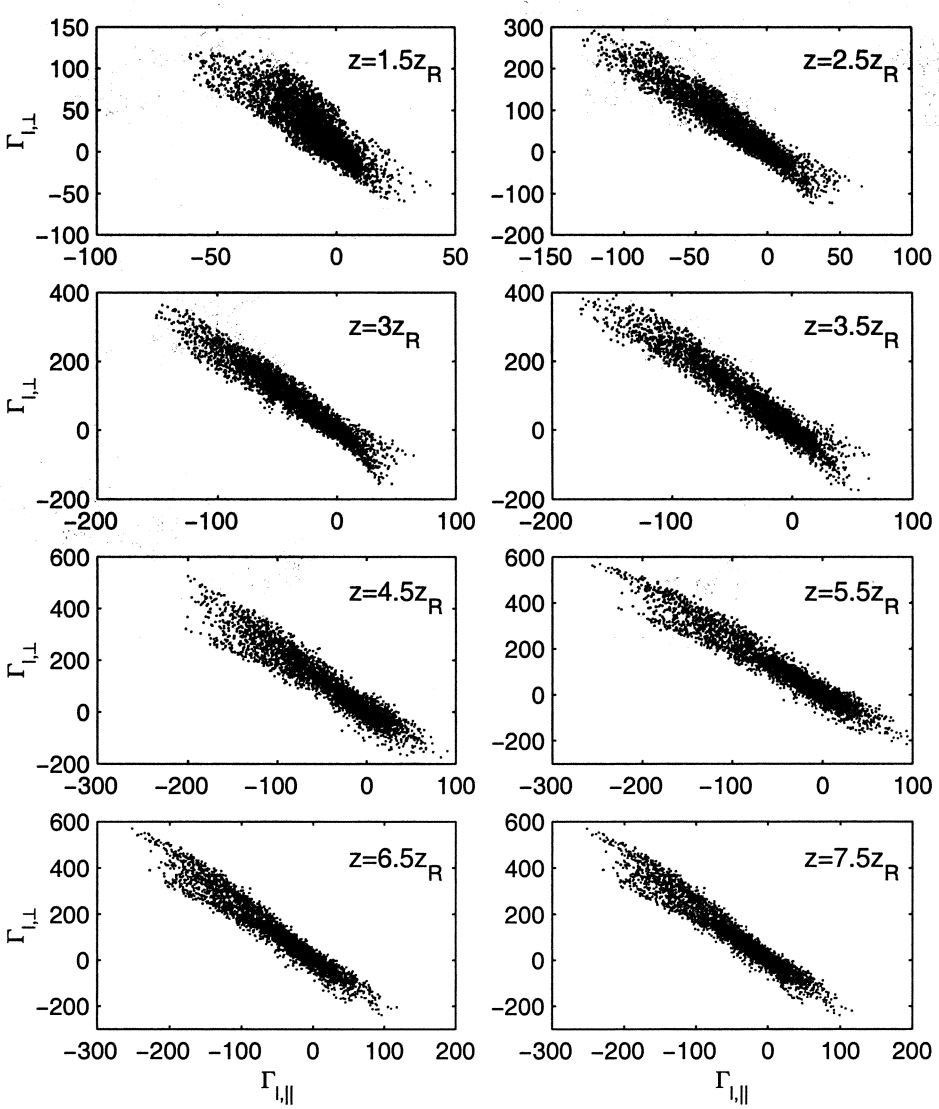

Figure 4.14: Electron distribution in space ($\Gamma_{l,||}$, $\Gamma_{l,\perp}$) at different moments of time in the simulation.

resulting plasma wave decreases.

In conclusion, our simulation of the laser pulse propagation and electron acceleration in this paragraph explains the particularities of fast electron generation in the conditions of the experiment at the LOA. In particular, we confirm the maximum electron energy decrease in experiment with the plasma density increase. As we have found, in the conditions of the experiment both mechanisms of electron acceleration are important: the acceleration by the longitudinal electric field of the plasma wave, excited by the laser pulse, and direct laser acceleration of electrons at the betatron resonance of electrons in a relativistic plasma channel. We state the necessity of a correct account of the work of the longitudinal laser field for the comparison of the effectiveness of these mechanisms of electron acceleration.

Chapter 5

Main results of the thesis

This thesis is the result of a theoretical investigation of the problem of ultra-short ultra-intense laser pulse interaction with underdense plasma. The work on the thesis included, first, an additional development of the code, used for numerical simulations of this interaction, and second, the investigations themselves.

For numerical simulations of the laser pulse interaction with plasma the fully-relativistic two-dimensional particle code Wake was used. It is described in Chapter 2 of the thesis. In the process of work on the thesis the author has performed a modification of the module, responsible for the simulation of plasma ion motion. This modification is necessary for the description of ion dynamics in the case of large perturbations of ion density. Additional diagnostics were included in the code, in particular, the diagnostics, permitting to investigate the electrons phase space during the interaction. However, the development of an additional module of the code describing the acceleration of a test electron beam is the main development, performed by the author. This module permits to investigate the motion of test (non-interacting) electrons in the high-frequency field of the laser pulse (linearly polarized) and low-frequency plasma fields, simulated with the code Wake. At the moment of injection the electron beam is assumed with a given finite emittence and with a Gaussian electron distribution with respect to the coordinate and angle in the beam focal plane. The electron energy is supposed to be the same for all the electrons at the moment of injection. The focal planes of the laser pulse and electron beam, the positions of the focal points in these planes and the symmetry axis of the radiation and electron beam can be, generally speaking, different. Different diagnostics can be used for the study of test electrons interaction with fields in plasma and controlling the changes of the global parameters of the beam. First of all, it is possible to control the change of the form of the beam in space and study the trajectories of particular electrons. The electron energy and angular spectra are

calculated at different moments of time during the interaction. For the comparison of the effectiveness of different mechanisms of electron acceleration the work of different components of electric field (high-frequency and quasi-stationary) is calculated. The simulation of test electron acceleration was used in the present investigation in paragraphs 3.2, 4.1, and 4.3 of the thesis.

The problems of the ultra-short ultra-intense laser pulses interaction with plasma are divided in two groups in this thesis, presented in Chapters 3 and 4. The first group includes the investigation of the problems, that have a general physical and applied interest and are not associated with particular laboratory experiments (Chapter 3). The second group includes the numerical simulation and analysis of particular experiments (Chapter 4). The first group includes: (i) investigation of photon acceleration by plasma waves, excited by laser pulses in plasma; (ii) study of the phase velocity of the plasma wave in the Self-Modulated Laser Wake Field Accelerator; study of the self-similar solutions, describing self-focusing of short ultra-intense laser pulses in plasma; (iii) investigation of ion dynamics during the excitation of the plasma wave by laser pulses. The second group includes numerical simulations and analysis of three experiments on the laser pulse propagation in plasma and electron acceleration at laboratories LULI and LOA.

In paragraph 3.1 we speak about photon acceleration by a relativistically-fast plasma wave. Our 1D simulations have confirmed the existence of photon trajectories that are similar to the trajectories of charged particles in a plasma wave. These trajectories correspond to laser pulses that are trapped and untrapped by the plasma wave. The frequency of these laser pulses oscillates with an amplitude that is dependent upon the relation between the plasma wave phase velocity and the laser pulse group velocity. This amplitude is greater when the velocities are close to each other.

The plasma wave develops simultaneously with the evolution of the plasma wave source. The source evolution is caused by the transfer of energy to the plasma wake and by additional self-modulation. When a plasma wake is produced by a relativistically intense laser pulse with duration of the order of a plasma period, only the untrapped back-drifting probe pulse still has some full frequency oscillations before the main pulse depletes.

Investigating photon acceleration in the two-dimensional axially symmetrical case we have made analytical estimates of photon acceleration (as well as phase shift in the probe pulse) in the wake behind an ultra-intense short laser pulse. We have estimated the phase and frequency shift in the probe pulse, which can be observed in the image plane of a lens imaging the focal plane. This estimate is

applicable if the plasma-induced phase shift and refraction of the probe pulse are small. We have also made 2D axially symmetrical particle simulations of photon acceleration. We have simulated a 30 fs, 0.4 μm probe pulse interaction with a plasma wake produced in a gas jet behind a relativistically intense 30 fs, 0.8 μm laser pulse. We then calculated the probe pulse propagation in a typical optical collecting line as used in laboratory experiments. The probe pulse refraction in the presence of a nonlinear plasma wave and slippage between the probe pulse and the plasma wave follow to a stronger frequency down-shift than up-shift. The results of our analytical estimate and numerical simulations in the two-dimensional axially symmetrical case can be useful for plasma diagnostics.

In paragraph 3.2 we studied the problem of phase velocity of the plasma wave, excited in result of self-modulation of a short laser pulse in plasma. As our numerical simulations show, at the late stage of the self-modulation of a laser pulse with a power larger than the critical power for relativistic self-focusing, in homogeneous plasma, the plasma wave phase velocity is so close to the laser pulse group velocity, that one can neglect the difference of the plasma wave relativistic factor and the relativistic factor, corresponding to the group velocity of the laser pulse. It means that the estimation of the maximum electron energy gain in the plasma wave, that is usually used, is applicable:

$$W_{\max} \approx 4\gamma_g^2 (E_z/E_0) mc^2, \tag{5.1}$$

where $\gamma_g \approx \omega_0/\omega_p$ is the relativistic factor, corresponding to the laser pulse group velocity, and E_z/E_0 is the amplitude of the accelerating longitudinal electric field of the plasma wave, normalized to $E_0 = cm\omega_p/e$. At the same time, our simulations show, that for the self-modulation of a laser pulse in a preformed plasma channel the relativistic factor of the plasma wave is essentially less than the relativistic factor, corresponding to the laser pulse group velocity, both at initial and late nonlinear stage of self-modulation. It is necessary to take into account this fact estimating the maximum energy of electrons, accelerated by the plasma wave; the estimation of Eq. (5.1) is not valid, the correct estimation is obtained by substituting the relativistic factor of the plasma wave in Eq. (5.1) instead of γ_g.

In this paragraph we also investigated self-similar structures for relativistic self-focusing of short laser pulses in plasma. We have generalized the formalism, developed earlier for ultra-intense laser pulses with duration much less than a plasma period, for the case of laser pulses with duration of the order of a plasma period and longer. The self-similar solutions are obtained in the weakly-relativistic limit. They describe the quasi-stationary pulses with an amplitude increasing with the

longitudinal coordinate exponentially and width, decreasing with the longitudinal coordinate, so that the power in each transversal cross-section is the same. This power is larger than critical for relativistic self-focusing and its excess over the critical power determines the value of the coefficient in the exponent rate. In the limit of power equal to the critical power for relativistic self-focusing the dependence on the transverse coordinate is given by the Townes mode. The refractive index on the longitudinal axis is also characterized by a growing exponential function. The oscillations of the refractive index at some distance from the axis describe a plasma wave, excited by the laser pulse. The self-similar solution describes the structure of the wide part of the pulse (being compared with k_p^{-1}), propagating in plasma without diffraction. It must be matched with the solution at the leading edge, that is not subject to nonlinear distortion and the local value of Rayleigh length at the leading edge exceeding essentially its value in the intense part of the pulse. The self-similar solution does not describe also the structure of the backward, narrow and the most intense part of the pulse.

As our simulations show, the similar quasi-stationary structures form in result of a natural evolution of a disposable in laboratories laser pulse with a Gaussian longitudinal profile. In this case the limitation on the length of the structure is associated with the self-modulation instability of the laser pulse – the width of its main intense part can not be much longer than a plasma period. At the same time even for powers a little exceeding the critical power for relativistic self-focusing reaching of rather large values of intensity and laser pulse amplitude $a_0 = eA_0/mc^2 \sim 1$ on such a duration is possible. In this case behind the laser pulse a plasma wave of large amplitude is excited. The structure of the plasma wave excited by the quasi-stationary laser pulse practically does not change and the phase velocity of the plasma wave is close to the laser pulse group velocity. As our simulation confirms, the plasma waves, excited at long propagation of the laser pulse in the regime of relativistic self-channeling, can be used for electron acceleration to large energies, in particular to the energies in GeV range.

In paragraph 3.3 the dynamics of ions in the plasma wake, excited by a laser pulse with duration of the order of a plasma period, is investigated. We investigated the longitudinal momentum in one-dimensional approximation and the transverse momentum in two-dimensional case with plane and axial symmetry.

Investigating the momentum conservation in plasma in one-dimensional case, we have obtained that behind the laser pulse in the wake region a plasma flow exists with an averaged momentum density, determined by ions. While the energy, used by the laser pulse for the wake excitation, is transformed to the energy of oscillatory

electron motion and plasma fields, the momentum passes to ions. The electron momentum density in the plasma wave is mainly oscillatory and its contribution to the averaged momentum density is negligibly small. In the frame of nonlinear two-fluid hydrodynamic model of cold plasma we have obtained, that the averaged ion momentum density in the plasma wave is determined by the plasma wave amplitude only. The average ion momentum is larger than the momentum lost by the laser pulse by a value of the averaged momentum flow in the plasma wave (associated with electron motion), divided by the speed of light. For the case of a rectangular laser pulse with duration equal to half a plasma period an expression is obtained for the averaged momentum density of ions through the complete elliptic integrals of the first and second kind. Asymptotic expressions are obtained for the averaged ion momentum for large and small values of the laser pulse amplitude, $a_0^2 \gg 1$ and $a_0^2 \ll 1$, as well as a simple expression, well approximating the exact value of the averaged momentum for arbitrary a_0^2.

Our investigation of ion dynamics in two-dimensional case shows, that similarly to the ponderomotive force of the laser pulse, the ponderomotive force of the plasma wake, excited by an ultra-short laser pulse, leads to the formation of an ion channel in plasma. The results of our approximate analytical description of the initial stage of the ion channel formation show that for a laser pulse with a width less than k_p^{-1} the ion channel has the form of a ring with an ion density maximum on the axis. For wider laser pulses a minimum of ion density on the axis is produced. The depth of the plasma channel increases with the distance behind the laser pulse. As the ion channel is produced the structure of the plasma wake changes. It results in plasma wave breaking, after that ions acceleration in the transverse direction terminates. It follows from our investigation, in particular, that the plasma wake behind the laser pulse consists of a limited number of regular oscillations that can be used for electron acceleration in the standard scheme of acceleration.

We have performed for the first time a detailed study of the plasma wave breaking using numerical particle simulations. We studied the electron phase space and have found the transformation of the distribution function in the process of wave breaking. The plasma wave breaking leads to generation of fast electron bunches and plasma wave energy dissipation. The wavebreaking takes place when the local phase velocity of the plasma wave equals the component of oscillatory electron velocity in the direction perpendicular to the phase front. In the case that we investigated, when the longitudinal plasma wave phase velocity is too large for trapping the fast electrons, electron bunches fly out from the axial region at large angles with respect to the longitudinal axis. The analysis of the energy balance in the process of the plasma

wave breaking shows, that the most part of the plasma wave energy is dissipated and the energy part that is transferred to the energy of transverse ion motion is rather small.

In Chapter 4 we speak about numerical simulation of three experiments at laboratories LULI and LOA performed in the frame of the thesis. In paragraph 4.1 we report on the experiment, performed at the laboratory LULI. In this experiment electron acceleration in the standard scheme of acceleration was studied, when the plasma wave is excited by a laser pulse with duration of the order of a plasma period. In this experiment the laser beam was focused in a gas-filled chamber (with helium), where an electron bunch was injected as well. In the experiment 400 fs (FWHM), 1.057 μm laser pulses were used with the energy of $4-9$ J, they were focused in the focal spot with a size of around 25 μm. The plasma electron density in experiment was 2.2×10^{16} cm^{-3}, that corresponds to the optimal conditions for the plasma wave excitation in the standard scheme of electron acceleration. A bunch of electrons with the energy of 3 MeV was injected in the region of interaction in the direction of the laser axis.

We have performed numerical simulation of the laser pulse propagation in plasma in the experimental conditions and simulated the acceleration of a test electron beam. Our simulation confirms that the plasma wave is excited in transversal regime in the experiment: the amplitude of the transverse component of the electric field more than in two times exceeds the amplitude of the accelerating longitudinal component at the focal plane. In these conditions, as our numerical simulation shows, the most part of electrons is scattered by the transverse electric field already a long distance before the focal plane of the pulse. This, first of all, explains the small number of accelerated electrons in the experiment. In this context, to reduce scattering we suggest using of a gas jet for a limitation of the longitudinal size of the region in which the plasma wave is excited. We have obtained the dependence of the energy of the accelerated electrons on the phase of injection in the plasma wave and the energy spectrum of electrons. The spectrum, obtained, is qualitatively similar to the electron spectrum in experiment, though predicts somewhat larger number of accelerated electrons and maximum energy.

In paragraph 4.2 we report on the numerical simulation of another experiment, performed at the LULI, where the laser pulse propagated in plasma in the self-modulation regime. Laser pulses with the wavelength of 1.057 μm were used, with duration from 370 fs to 4 ps and energy up to 15 J. The pulses were focused at the sharp edge of a helium gas jet with a width of 4 mm and rectangular profile. The radius of the focal spot was around 20 μm and the plasma electron density was

$1 \div 2 \times 10^{19}$ cm^{-3}. The laser pulse in experiment was preceded by a prepulse with duration of a few nanoseconds, that completely ionized helium along the propagation length of the pulse. The hydrodynamic expansion of the heated plasma leaded to a formation of a channel in plasma to the moment of the main part of the pulse coming. Thus, really the laser pulse propagated in a plasma channel. In most experiments laser pulses of the same energy were used but the duration was different. Therefore, different values of the pulse power and amplitude were reached and different regimes of interaction were investigated, when the pulse power is larger and less than the critical power for relativistic self-focusing. We have performed numerical simulations of the laser pulse propagation with duration of 300 fs in plasma with electron density of 1×10^{19} cm^{-3} for the case of the maximum power $P = 6.3P_c$. The results of our numerical simulations explain the main particularities in the experiment for the case of short laser pulses with the power exceeding the critical power for self-focusing. In our simulation the laser pulse propagates along all the width of the gas jet due to the effect of relativistic self-focusing. The comparison of the results of simulations in a homogeneous plasma and with a plasma channel (that is produced in experiment) shows that the channel plays a very minor role when the pulse with power larger than the critical power for self-focusing propagates on distances of a few ($2 - 3$ in the simulation) Rayleigh lengths. At the beginning of interaction a strong scattering of the backward part of the pulse is observed, which is the consequence of Raman scattering at large angles with respect to the laser pulse propagation direction. The self-focusing leads to an essential decrease of the transversal size of the pulse on the distances of $z \sim z_R/(P/P_c)$, after that the self-modulation instability starts. Due to the large rates of the self-modulation instability and essentially nonlinear nature of interaction a wide spectrum of the radiation is observed after the interaction, in which distinct anti-Stokes Raman satellites are absent.

In paragraph 4.3 we report the results of our simulation of the experiment at the LOA. In this experiment the propagation of laser pulses with the wavelength of 0.82 μm, duration from 35 fs, and energy up to 0.6 mJ was studies. The laser pulse was focused on a sharp edge of a helium gas jet with a profile close to rectangular and width of 2 mm. The focal spot size was 6 μm. The value of electron density in experiment was in the range of $1.5 \times 10^{18} - 1.5 \times 10^{20}$ cm^{-3}. When the plasma density is changed the pulse duration is larger and smaller than a plasma period: if the density is increased we pass from the classical regime of the plasma wave excitation by a short laser pulse to the self-modulation regime. If the pulse power in experiment was more than $3 - 5$ times larger than the critical power for relativistic self-focusing, generation of fast electrons was observed. The most attention in the

experiment was devoted to this fast electron generation. We have performed numerical simulations of the laser pulse propagation in plasma and electron acceleration in the experimental conditions, using the code Wake. Due to the approximations in our code we were limited to the case of pulse powers less than a few critical powers for relativistic self-focusing and pulse duration not much exceeding a plasma period. For the maximum laser energy of the present experiment it corresponds to electron densities up to 2×10^{19} cm^{-3}. We investigated acceleration of test electrons (non-interacting), injecting them in the region of the pulse and plasma wake. The results of our simulations confirm the decreasing of the maximum electron energy with the increasing of the background electron density when the length over which self-focusing occurs is greater than the dephasing length.

Analyzing electron acceleration we devoted a special attention to the comparison of the effectiveness of electron acceleration by the plasma wave and directly by the laser radiation at the betatron resonance of electrons in relativistic plasma channel. Unlike in the other numerical simulations (performed before us), in which direct laser acceleration of electrons was observed, we were able in our simulation to distinguish the contributions of the laser field and low-frequency plasma field to the electron acceleration. To compare these effects, we calculated the work of the high-frequency and plasma electric fields on electrons independently. Our numerical simulation shows, that for the plasma density in experiment in the range of $10^{19} - 10^{20}$ cm^{-3} and pulse power of the order of a few critical powers for relativistic self-focusing both mechanisms of electron acceleration are approximately equally effective. We admit that at larger laser powers (much larger, than P_c), for the pulses, essentially longer than a plasma wavelength, the most energetic electrons will come from the acceleration by the laser field, as it is predicted in Ref. [65]. We denote also the necessity of a correct account of the work of the longitudinal laser field for the comparison of the effectiveness of these mechanisms of electron acceleration.

Finally, we present the list of publications that were performed on the subject of the thesis:

- J. Faure, V. Malka, J.-R. Marques, F. Amiranoff, C. Courtois, Z. Najmudin, K. Krushelnick, M. Salvati, A. E. Dangor, A. Solodov, P. Mora, J.-C. Adam, and A. Heron. "Interaction of an ultra-intense laser pulse with a nonuniform preformed plasma," Phys. Plasmas **7**, 3009 (2000).

- L. M. Gorbunov, P. Mora, R. R. Ramazashvili, and A. A. Solodov. "Ion momentum driven by a short intense laser pulse in an underdense plasma," Phys. Plasmas **7**, 375 (2000).

- J. Faure, V. Malka, J.-R. Marques, F. Amiranoff, C. Courtois, Z. Najmudin, K. Krushelnick, M. Salvati, A. Dangor, A. Solodov, P. Mora, J.-C. Adam, and A. Heron. "Interaction of an ultra-intense laser pulse with a plasma channel," Scientific Report of LULI 1999 (Ecole Polytechnique, France, 2000, NTIS PB2000-105868), p. 30.

- A. A. Solodov, P. Chessa, and P. Mora. "Simulation of photon acceleration in a plasma wake," Phys. Plasmas **6**, 503 (1999).

- F. Dorchies, F. Amiranoff, V. Malka, J. R. Marques, A. Modena, D. Bernard, F. Jacquet, Ph. Mine, B. Cros, G. Matthieussent, P. Mora, A. Solodov, J. Morillo, and Z. Najmudin. "Acceleration of injected electrons in laser wakefield experiment," Phys. Plasmas **6**, 2903 (1999).

- F. Dorchies, F. Amiranoff, S. Baton, D. Bernard, B. Cros, D. Descamps, F. Jacquet, V. Malka, J. R. Marques, G. Matthieussent, Ph. Mine, A. Modena, P. Mora, J. Morillo, Z. Najmudin, and A. Solodov. "Electron acceleration in laser wakefield experiment at Ecole Polytechnique," Laser Part. Beams **17**, 299 (1999).

- A. Solodov and P. Mora. "Plasma wave phase velocity and electron acceleration in the scheme of self-modulated laser wakefield accelerator," Scientific Report of LULI 1998 (Ecole Polytechnique, France, 1999, NTIS PB99-130973), p. 6.

- J. Faure, V. Malka, F. Amiranoff, P. Mora, and A. Solodov. "Scaling laws for electron acceleration to GeV energies by self-modulated laser wakefields," Scientific Report of LULI 1998 (Ecole Polytechnique, France, 1999, NTIS PB99-130973), p. 9.

- F. Dorchies, F. Amiranoff, S. Baton, D. Bernard, B. Cros, D. Descamps, F. Jacquet, V. Malka, J. R. Marques, G. Matthieussent, Ph. Mine, A. Modena, P. Mora, J. Morillo, Z. Najmudin, and A. Solodov. "Observation of electron acceleration by a plasma wake excited by a laser pulse," Scientific Report of LULI 1997 (Ecole Polytechnique, France, 1998, NTIS PB98-152515), p. 8.

- L. M. Gorbunov, P. Mora, and A. A. Solodov. "Plasma ions dynamics in a wakefield of a short laser pulse," submitted to Phys. Rev. Lett.

- V. Malka, J. Faure, J. R. Marques, F. Amiranoff, J. P. Rousseau, S. Ranc, J. P. Chambaret, Z. Najmudin, B. Walton, P. Mora, and A. Solodov. "Analysis

of the maximum energy of electrons produced in the self-modulated laser wake field regime," submitted to Phys. Rev. E.

- J. Faure, J.-R. Marques, V. Malka, F. Amiranoff, Z. Najmudin, B. Walton, J.-P. Rousseau, S. Ranc, A. Solodov, and P. Mora. "Study of the dynamics of Raman instabilities using chirped laser pulses," submitted to Phys. Rev. Lett.

Bibliography

[1] G. Mourou and D. Umstadter, Phys. Fluids B **4**, 2315 (1992).

[2] T. Tajima and J. M. Dawson, Phys. Rev. Lett. **43**, 267 (1979).

[3] E. Esarey, P. Sprangle, J. Krall, and A. Ting, IEEE Trans. Plasma Sci. **24**, 252 (1996).

[4] M. Tabak, J. Hammer, M. E. Glinsky *et al.*, Phys. Plasmas **1**, 1626 (1994).

[5] N. H. Burnett and G. D. Enright, IEEE J. Quantum Electron. **26**, 1797 (1990).

[6] X. F. Li, A. L'Huillier, M. Ferray, L. A. Lompre, and G. Mainfray, Phys. Rev. Lett. **39**, 5751 (1989).

[7] K. W. D. Ledingham, I. Spencer, T. McCanny *et al.*, Phys. Rev. Lett. **84**, 899 (2000).

[8] T. E. Cowan, A. W. Hunt, T. W. Phillips *et al.*, Phys. Rev. Lett. **84**, 903 (2000).

[9] L. M. Gorbunov and V. I. Kirsanov, Zh. Eksp. Teor. Fiz. **93**, 509 (1987) [Sov. Phys. JETP **66**, 290 (1987)].

[10] E. Esarey, A. Ting, P. Sprangle, and G. Joyce, Comments Plasma Phys. Controlled Fusion **12**, 191 (1989).

[11] W. L. Kruer, The Physics of Laser Plasma Interactions. Reading, MA: Addison-Wesley, 1988.

[12] C. J. McKinstrie and R. Bingham, Phys. Fluids B **4**, 2626 (1992).

[13] T. M. Antonsen, Jr. and P. Mora, Phys. Rev. Lett. **69**, 2204 (1992).

[14] T. M. Antonsen, Jr. and P. Mora, Phys. Fluids B **5**, 1440 (1993).

[15] C. D. Decker, W. B. Mori, and T. Katsouleas, Phys. Rev. E **50**, R3338 (1994).

[16] C. D. Decker, W. B. Mori, K.-C. Tzeng, and T. Katsouleas, Phys. Plasmas **3**, 2047 (1996).

[17] K. C. Tzeng, W. B. Mori, and C. D. Decker, Phys. Rev. Lett. **5**, 1440 (1993).

[18] J. Faure, J.-R. Marques, V. Malka, F. Amiranoff, Z. Najmudin, B. Walton, J.-P. Rousseau, S. Ranc, A. Solodov, and P. Mora. "Study of the dynamics of Raman instabilities using chirped laser pulses," submitted to Phys. Rev. Lett.

[19] A. Ting, K. Krushelnick, H. R. Burris *et al.*, Optics Lett. **21**, 1096 (1996).

[20] J. M. Dawson, Phys. Rev. **133**, 383 (1956).

[21] A. I. Akhiezer and R. V. Polovin, Zh. Eksp. Teor. Fiz. **30**, 915 (1956) Sov. Phys. JETP **3**, 696 (1956).

[22] J. B. Rosenzweig, Phys. Rev. A **38**, 3634 (1988).

[23] T. Katsouleas and W. B. Mori, Phys. Rev. Lett. **61**, 90 (1988).

[24] A. G. Litvak, Zh. Eksp. Teor. Fiz. **57**, 629 (1969) [Sov. Phys. JETP **30**, 344 (1969)].

[25] C. Max, J. Arons, and A. B. Langdon, Phys. Rev. Lett. **33**, 209 (1974).

[26] G. Z. Sun, E. Ott, Y. C. Lee, and P. Guzdar, Phys. Fluids **30**, 526 (1987).

[27] A. B. Borisov, A. V. Borovskiy, O. B. Shiryaev *et al.*, Phys. Rev. A **45**, 5830 (1992).

[28] P. Gibbon, F. Jakober, P. Monet, and T. Auguste, IEEE Trans. Plasma Sci. **24**, 343 (1996).

[29] A. Chiron, G. Bonnaud, A. Dulieu *et al.*, Phys. Plasmas **3**, 1373 (1996).

[30] P. E. Young and P. R. Bolton, Phys. Rev. Lett. **77**, 4556 (1996).

[31] M. Borghesi, A. J. MacKinnon, L. Barringer, R. Gaillard, L. A. Gizzi, C. Meyer, O. Willi, A. Pukhov, and J. Meyer-ter-Vehn, Phys. Rev. Lett. **78**, 879 (1997).

[32] R. Wagner, S. Y. Chen, A. Maksimchuk, and D. Umstadter, Phys. Rev. Lett. **78**, 3125 (1997).

[33] A. Ting, C. I. Moore, K. Krushelnick *et al.*, Phys. Plasmas **5**, 1889 (1997).

[34] C. E. Clayton, D. Gordon, K. A. Marsh *et al.*, Phys. Rev. Lett. **81**, 100 (1998).

[35] P. Sprangle, E. Esarey, and A. Ting, Phys. Rev. A **41**, 4463 (1990).

[36] A. Ting, E. Esarey, and P. Sprangle, Phys. Fluids B **2**, 1390 (1990).

[37] P. Sprangle, E. Esarey, J. Krall, and G. Joyce, Phys. Rev. Lett. **69**, 2200 (1992).

[38] M. N. Rosenbluth and C. S. Liu, Phys. Rev. Lett. **29**, 701 (1972).

[39] C. M. Tang, P. Sprangle, and R. Sudan, Phys. Fluids **28**, 1974 (1985).

[40] C. Joshi and T. Katsouleas, Eds. New York: Amer. Inst. Phys., 63 (1985). T. Tajima, Laser Particle Beams **3**, 351 (1985).

[41] W. B. Mori, IEEE Trans. Plasma Sci. **PS-15**, 88 (1987).

[42] E. Esarey, A. Ting, and P. Sprangle, Appl. Phys. Lett. **53**, 1266 (1988).

[43] Y. Kitagawa, T. Matsumoto, T. Minamihata *et al.*, Phys. Rev. Lett. **68**, 48 (1992).

[44] C. E. Clayton, M. J. Everett, A. Lal *et al.*, Phys. Plasmas **1**, 1753 (1994).

[45] F. Moulin, F. Amiranoff, M. Laberge *et al.*, Phys. Plasmas **1**, 1318 (1994).

[46] S. V. Bulanov, V. I. Kirsanov, and A. S. Sakharov, Pis'ma Zh. Eksp. Teor. Fiz. **50**, 176 (1989) [Sov. Phys. JETP Lett. **50**, 198 (1989)].

[47] V. I. Berezhiani and I. G. Murusidze, Phys. Lett. A **148**, 338 (1990).

[48] S. V. Bulanov, I. N. Inovenko, V. I. Kirsanov, N. M. Naumova, and A. S. Sakharov, Phys. Fluids B **4**, 1935 (1992).

[49] F. Amiranoff, S. Baton, D. Bernard, B. Cros, D. Descamps, F. Dorchies, F. Jacquet, V. Malka, J. R. Marques, G. Matthieussent, P. Mine, A. Modena, P. Mora, J. Morillo, and Z. Najmudin, Phys. Rev. Lett. **81**, 995 (1998).

[50] F. Dorchies, F. Amiranoff, V. Malka, J. R. Marques, A. Modena, D. Bernard, F. Jacquet, Ph. Mine, B. Cros, G. Matthieussent, P. Mora, A. Solodov, J. Morillo, and Z. Najmudin, Phys. Plasmas **6**, 2903 (1999).

[51] P. Sprangle, E. Esarey, J. Krall, and G. Joyce, Phys. Rev. Lett. **69**, 2200 (1992).

[52] E. Esarey, P. Sprangle, J. Krall, A. Ting, and G. Joyce, Phys. Fluids B **5**, 2690 (1993).

[53] J. Krall, A. Ting, E. Esarey, P. Sprangle, and G. Joyce, Phys. Rev. E **48**, 2157 (1993).

[54] E. Esarey, J. Krall, and P. Sprangle, Phys. Rev. Lett. **72**, 2887 (1994).

[55] N. E. Andreev, L. M. Gorbunov, V. I. Kirsanov, A. A. Pogosova, and R. R. Ramazashvili, Pis'ma Zh. Eksp. Teor. Fiz. **55**, 551 (1992) [JETP Lett. **55**, 571 (1992)].

[56] N. E. Andreev, L. M. Gorbunov, V. I. Kirsanov, A. A. Pogosova, and R. R. Ramazashvili, Physica Scripta **49**, 101 (1994).

[57] N. E. Andreev, V. I. Kirsanov, and L. M. Gorbunov, Phys. Plasmas **2**, 2573 (1995).

[58] N. E. Andreev, L. M. Gorbunov, V. I. Kirsanov, A. A. Pogosova, and A. S. Sakharov, Fizika Plasmy **22**, 419 (1996) [Plasma Phys. Rep. **22**, 379 (1996)].

[59] C. D. Decker, W. B. Mori, T. Katsouleas, and D. E. Hinkel, Phys. Plasmas **3**, 1360 (1996).

[60] K. Nakajima, D. Fisher, T. Kawakubo *et al.*, Phys. Rev. Lett. **74**, 4428 (1995).

[61] C. Coverdale, C. B. Darrow, C. D. Decker *et al.*, Phys. Rev. Lett. **74**, 4659 (1995).

[62] A. Modena, Z. Najmudin, A. E. Dangor *et al.*, Nature **337**, 606 (1995).

[63] C. I. Moore, A. Ting, K. Krushelnick *et al.*, Phys. Rev. Lett. **79**, 3909 (1997).

[64] V. Malka, J. Faure, J. R. Marques, F. Amiranoff, J. P. Rousseau, S. Rank, J. P. Chambaret, Z. Najmudin, B. Walton, P. Mora, A. Solodov. "Analysis of the maximum energy of electrons produced in the self-modulated laser wake field regime", submitted to Phys. Rev. Lett.

[65] A. Pukhov, Z.-M. Sheng, and J. Meyer-ter-Vehn, Phys. Plasmas **6**, 2847 (1999).

[66] G. D. Tsakiris, C. Gahn, and V. K. Tripathi, Phys. Plasmas **7**, 3017 (2000).

[67] C. Gahn, G. D. Tsakiris, A. Pukhov *et al.*, Phys. Rev. Lett. **83**, 4772 (1999).

[68] P. Mora and T. M. Antonsen, Jr., Phys. Plasmas **4**, 217 (1997).

[69] P. Mora and T. M. Antonsen, Jr., Phys. Rev. E **53**, R2068 (1996).

[70] P. Chessa, P. Mora, and T. M. Antonsen, Jr., Phys. Plasmas **5**, 3451 (1998).

[71] R. C. Davidson. Methods in Nonlinear Plasma Physics (Academic, New York, 1972).

[72] A. M. Perelomov, V. S. Popov, and M. V. Terent'ev, Sov. Phys. JETP **23**, 924 (1965).

[73] M. V. Ammosov, N. B. Delone, and V. P. Krainov, Sov. Phys. JETP **64**, 1191 (1986).

[74] L. Oliveira e Silva and J. T. Mendonça, IEEE Trans. Plasma Sci. **24**, 316 (1996).

[75] W. M. Wood, C. W. Siders, and M. C. Downer, Phys. Rev. Lett. **67**, 3523 (1991).

[76] W. M. Wood, C. W. Siders, and M. C. Downer, IEEE Trans. Plasma Sci. **21**, 20 (1993).

[77] J. M. Dias, C. Stenz, N. Lopes, *et al.*, Phys. Rev. Lett. **78**, 4773 (1997).

[78] S. C. Wilks, J. M. Dawson, W. B. Mori, T. Katsouleas, and M. E. Jones, Phys. Rev. Lett. **62**, 2600 (1989).

[79] E. Esarey, A. Ting, and P. Sprangle, Phys. Rev. A **42** 3526 (1990).

[80] S. V. Bulanov, V. I. Kirsanov, F. Pegoraro, and A. S. Sakharov, Laser Phys. **3**, 1078 (1993).

[81] J. T. Mendonça and L. Oliveira e Silva, Phys. Rev. E **49**, 3520 (1994).

[82] V. A. Mironov, A. M. Sergeev, E. V. Vanin, and G. Brodin, Phys. Rev. A **42**, 4862 (1990).

[83] R. Bingham, J. T. Mendonça, and J. M. Dawson, Phys. Rev. Lett **78**, 247 (1997).

[84] J. R. Marquès, J. P. Geindre, F. Amiranoff *et al.*, Phys. Rev. Lett. **76**, 3566 (1996).

[85] J. R. Marquès, F. Dorchies, P. Audebert, *et al.*, Phys. Rev. Lett. **78**, 3463 (1997).

[86] J. R. Marquès, F. Dorchies, F. Amiranoff, *et al.*, Phys. Plasmas **5**, 1162 (1998).

[87] C. W. Siders, S. P. Le Blanc, D. Fisher, *et al.*, Phys. Rev. Lett. **76**, 3570 (1996).

[88] C. W. Siders, S. P. Le Blanc, A. Babine *et al.*, IEEE Trans. Plasma Sci. **24**, 301 (1996).

[89] C. Joshi, W. B. Mori, T. Katsouleas *et al.*, Nature **311**, 525 (1984).

[90] S. V. Bulanov, F. Pegoraro, and A. M. Pukhov, Phys. Rev. Lett. **74**, 710 (1995).

[91] S. V. Bulanov, F. Pegoraro, A. M. Pukhov, and A. S. Sakharov, Phys. Rev. Lett. **78**, 4205 (1997).

[92] A. S. Sakharov, V. I. Kirsanov, Phys. Rev. E **49**, 3274 (1994).

[93] N. E. Andreev, V. I. Kirsanov, L. M. Gorbunov, and A. S. Sakharov, IEEE Trans. Plasma Sci. **24**, 363 (1996).

[94] N. E. Andreev, V. I. Kirsanov, A. S. Sakharov, P. W. Van Amersfoort, and V. V. Goloviznin, Phys. Plasmas **3**, 3121 (1996).

[95] A. Ting, K. Krushelnick, C. I. Moore *et al.*, Phys. Rev. Lett. **77**, 5377 (1996).

[96] S. P. Le Blanc, M. C. Downer, R. Wagner *et al.*, Phys. Rev. Lett. **77**, 5381.

[97] N. E. Andreev, V. I. Kirsanov, A. A. Pogosova, and L. M. Gorbunov, Pis'ma Zh. Eksp. Teor. Fiz. **60**, 694 (1994) [JETP Lett. **60**, 713 (1994)].

[98] J. Krall, E. Esarey, P. Sprangle, and G. Joyce, Phys. Plasmas **1**, 1738 (1994).

[99] L. A. Abramyan, A. G. Litvak, V. A. Mironov, and A. M. Sergeev, Zh. Eksp. Teor. Fiz. **102**, 1816 (1992) [JETP **75**, 978 (1992)].

[100] R. Y. Chiao, E. Garmire, and C. H. Townes, Phys. Rev. Lett. **13**, 479 (1964).

[101] K. Krushelnick, A. Ting, C. I. Moore *et al.*, Phys. Rev. Lett. **78**, 4047 (1997).

[102] R. Annou, V. K. Tripathi, and M. P. Srivastava, Phys. Pasmas **3**, 1356 (1996).

[103] G. S. Sarkisov, V. Yu. Bychenkov, V. T. Tikhonchuk *et al.*, Pis'ma Zh. Eksp. Teor. Fiz. **66**, 787 (1997).

[104] U. de Angelis, Phys. Scr. **30**, 210 (1990).

[105] K. Nakajima, Phys. Rev. A **45**, 1149 (1992).

[106] S. Dalla and M. Lontano, Phys. Lett. A **173**, 456 (1993).

[107] L. M. Gorbunov, P. Mora, R. R. Ramazashvili, A. A. Solodov, Phys. Plasmas **7**, 375 (2000).

[108] I. S. Gradshteyn and I. M. Ryzhik, Tables of Integrals, Series and Products (Academic, New York, 1980), pp. 232, 905.

[109] N. E. Andreev, L. M. Gorbunov, V. I. Kirsanov, K. Nakajima, and A. Ogata, Phys. Plasmas **4**, 1145 (1997).

[110] N. E. Andreev, E. V. Chizhonkov, and L. M. Gorbunov, Russian Journal of Numer. Analysis and Mathem. Modeling **13**, 1 (1998).

[111] L. M. Gorbunov, P. Mora, and A. A. Solodov. "Plasma ions dynamics in the wake of a short laser pulse", submitted to Phys. Rev. Lett.

[112] J. Albritton and P. Koch, Phys. Fluids **18**, 1136 (1975).

[113] S. V. Bulanov, L. M. Kovrizhnih, and A. S. Sakharov, Zh. Eksp. Teor. Fiz. **72**, 1809 (1977).

[114] S. Augst, D. Strickland, D. D. Meyerhofer, S. L. Chin, and J. H. Eberly, Phys. Rev. Lett. **63**, 2212 (1989).

[115] T. Katsouleas and J. M. Dawson, Phys. Rev. Lett. **51**, 392 (1983).

Abstract

Interaction of ultra-short ultra-intense laser pulses with underdense plasmas

Different aspects of interaction of ultra-short ultra-intense laser pulses with underdense plasmas are studied analytically and numerically. These studies can be interesting for laser-driven electron acceleration in plasma, X-ray lasers, high-order harmonic generation, initial confinement fusion with fast ignition. For numerical simulations a fully-relativistic particle code WAKE was used, developed earlier at Ecole Polytechnique. It was modified during the work on the thesis in the part of simulation of ion motion, test electron motion, diagnostics for the field and plasma.

The studies in the thesis cover the problems of photon acceleration in the plasma wake of a short intense laser pulse, phase velocity of the plasma wave in the Self-Modulated Laser Wake-Field Accelerator (SM LWFA), relativistic channeling of laser pulses with duration of the order of a plasma period, ion dynamics in the wake of a short intense laser pulse, plasma wave breaking. Simulation of three experiments on the laser pulse propagation in plasma and electron acceleration were performed.

Among the main results of the thesis, it was found that reduction of the plasma wave phase velocity in the SM LWFA is crucial for electron acceleration, only if a plasma channel is used for the laser pulse guiding. Self-similar structures describing relativistic guiding of short laser pulses in plasmas were found and relativistic channeling of initially Gaussian laser pulses of a few plasma periods in duration was demonstrated. It was shown that ponderomotive force of a plasma wake excited by a short laser pulse forms a channel in plasma and plasma wave breaking in the channel was analyzed in detail. Effectiveness of electron acceleration by the laser field and plasma wave was compared and frequency shift of probe laser pulses by the plasma waves was found in conditions relevant to the current experiments.

Key words: ultra-short laser pulses, ultra-intense laser pulses, laser-plasma interaction.

Résumé

Interaction d'impulsions laser ultra-courtes et ultra-intenses avec des plasmas sous denses

Différents aspects de l'interaction d'une impulsion ultra-courte et ultra-intense avec un plasma sous-dense ont été étudiés analytiquement et numériquement. Ces études présentent un intérêt pour l'accélération laser de particules dans les plasmas, les lasers à rayons X, la génération d'harmoniques d'ordre élevé, le concept d'allumeur rapide pour la fusion par confinement inertiel. On a utilisé le code particulaire relativiste WAKE développé précédemment à l'Ecole Polytechnique. Ce code a été modifié au cours de la thèse pour traiter le mouvement des ions, pour calculer des trajectoires d'électrons tests, et pour inclure des diagnostics divers sur les champs et les particules.

Les sujets traités dans cette thèse sont les suivants: l'accélération de photons dans le sillage d'une impulsion laser courte et intense, la vitesse de phase de l'onde plasma dans le sillage d'une impulsion laser auto-modulée, la canalisation relativiste d'impulsions laser de durée de l'ordre de la période plasma, la dynamique ionique dans le sillage, le déferlement. Enfin on a simulé 3 expériences de propagation d'onde laser et d'accélération d'électrons.

Voici les principaux résultats de la thèse: La réduction de la vitesse de phase de l'onde plasma dans le cas d'une impulsion laser auto-modulée ne joue que dans le cas d'un canal préformé pour le guidage de l'onde laser. On a trouvé des structures self-similaires pour décrire le guidage relativiste d'une impulsion courte dans un plasma. On a démontré la propagation auto-guidée d'impulsion initialement gaussiennes de quelques périodes plasma. On a montré que la force pondéromotrice de l'onde plasma excitée par l'impulsion laser forme un canal et le déferlement dans ce canal a été analysé en détail. Les efficacités de l'accélération d'électrons dans le champ laser et dans l'onde plasma ont été comparées. Le décalage en fréquence d'une sonde se propageant dans le sillage plasma a été étudié dans des conditions correspondant à des expériences actuelles.

Mots clés: impulsions ultra-courtes, impulsions ultra-intenses, interaction laser-plasma.